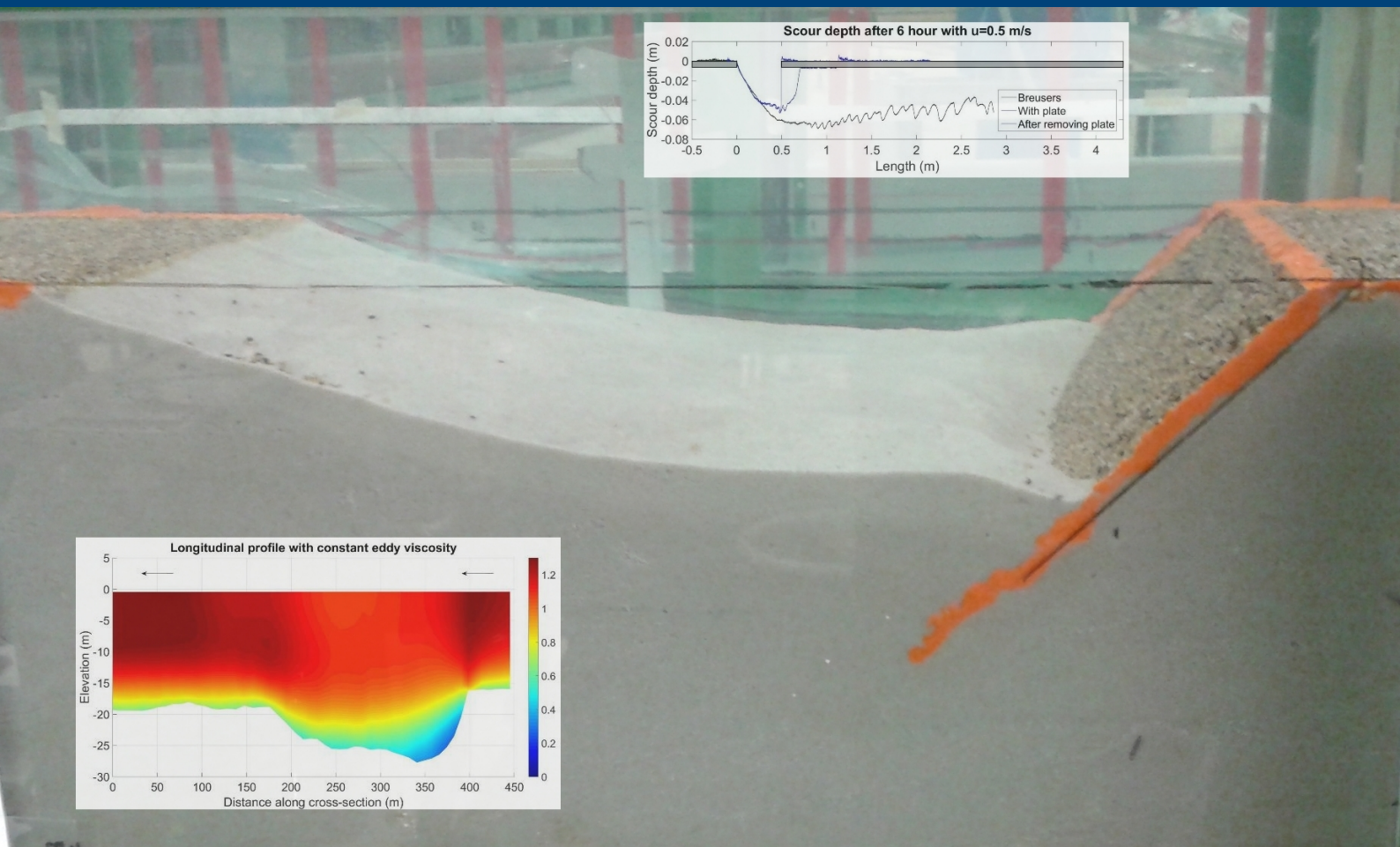


Development of scour in non-cohesive sediment under a poorly erodible top layer

Graduation thesis



J.A. (JOS) VAN ZUYLEN

Development of scour in non-cohesive sediment under a poorly erodible top layer

in partial fulfillment of the requirements for the degree of

Master of Science
in Civil Engineering

at the Delft University of Technology

To be presented in public on Monday the 22th of June 2015,
11:00h in lecture room F.

Author:

J.A. (Jos) VAN ZUYLEN

Student number:

1505092

j.a.vanzuylen@gmail.com

Committee:

Prof. dr. ir. W.S.J. Uijtewaal

Dr. ir. C.J. Sloff

Dr. ir. R.J. Labeur

Dr. ir. E. Mosselman

Dr. ir. H. Talstra

Company:

TU Delft, Chairman

Deltares, TU Delft, Supervisor

TU Delft

Deltares, TU Delft

Svašek Hydraulics

Supported by:

Deltares
Unit ZWS
Department of River Dynamics
and Inland Waterways Transport
Boussinesqweg 1
Delft

Svašek Hydraulics

Schiehaven 13 G
Rotterdam

Educational institute:

Delft University of Technology
Faculty of Civil Engineering
Department of Hydraulic
Engineering
Stevinweg 1
Delft

Preface

It is strange how life events can pass without noticing it changed your life. My life changed during a vacation to the province Friesland in May 1996. We visited several highlights of the province, but a visit to the 'Afsluidijk' had a large impact. The visitor centre displayed a film about the construction of the dam and while I was watching I said 'This is what I want to do when I am older'. Since that moment I was always interested in the Dutch waterworks and now I almost finished my master track in the field of Hydraulic Engineering.

First of all I want to thank my committee for their support. They gave the freedom to define my own path within the research. Since this type of scour was not researched before, it was hard make a clear approach plan. The tips and comments of Maarten van der Wal and Ymkje Huissmans during the set-up of the laboratory experiments are greatly acknowledged.

Leading the experiments demanded a lot of skills I did not knew I had. Coordinating the work during various stages of the experiments and making the final call in last minute changes, increased my confidence. The assistance of Jos Muller during the execution of the experiment was very much appreciated.

Further I want to thank Svašek, for the opportunity to simulate the scour problems with FINEL3D. The change of work environment gave me new energy. I want to thank Harmen Talstra and Sanne Poortman for their guidance while modelling with FINEL3D.

Furthermore, I want to thank Deltares for the opportunity to carry out my research within their facilities. Their knowledge and experience is greatly acknowledged.

Last, I want to thank my family and friends, especially my parents, for their unconditional support.

's-Gravenhage, June 2015

J.A. (Jos) van Zuylen

Summary

The river branches of the Rhine-Meuse delta in the South-Western part of The Netherlands flow over a poorly erodible bed layer consisting of clay and peat. These rivers experience a slow incision of this top layer. However, the closure of the Haringvliet (in 1970) increased the erosion of the top layer. As the poorly erodible layer becomes thinner, it sometimes breaks and the easily erodible sand layer below becomes exposed. This results in scour holes which are up to 15 m deeper than the average river bottom. These holes pose risks to the stability of adjacent flood defences. In this research the processes of the development of the scour hole were investigated.

Predictions of the development of current scour holes are based on various empirical scour formulas in combination with experience in the Dutch estuaries. The Breusers formula for scour has been developed to calculate the scour depths behind a sill with a protection. Although this formula neglects the influence of the poorly erodible layer downstream of the scour hole, this is currently the best approach.

Another disadvantage of these empirical formulas is the lack of physical background. This limits its applications and cannot be used in river simulation programs. These programs are used to simulate the behaviour of the flow and morphological development over time. However, these models are not able to give satisfying results at scour holes.

To gain insight in the flow conditions at a scour hole a physical model investigation has been carried out. The erosion resistant layer was represented by steel plates which were placed on top of a mobile bed. At the location where this cover ended, the sand was unprotected and a scour hole was formed.

The experiments with a scour hole of fixed length showed the development of scour in several stages. From the start of the experiment, sand was transported and the scour hole was formed directly behind the upstream edge. The development of scour followed the description of Breusers. Downstream of the scour holes, dunes were formed which slowly travelled further downstream. These dunes were disturbed by the edge of the plates downstream of the scour hole.

The scour hole quickly increased in depth, while a steep upstream slope was formed. The gentle downstream slope slowly moved further downstream as the scour hole developed. Once the slope reaches the edge of the downstream plates, several behaviour stages at the downstream edge determined the undermining. Due to the undermining,

the sediment transport had changed from bed-load to suspension. This decreased the development of the scour hole.

The experiments further showed that small return currents were able to smoothen disturbances at the bed. In the experiments with a flow from the reverse direction (tidal flow), the scour hole was even able to redistribute the sand over the slopes.

The extensive undermining of the experiments was never observed in the field. The steel plates in the experiments are much stiffer than the poorly erodible layer in the field, which will probably fail due to the undermining. The poorly erodible layer can fail in 2 ways. The erosion resistant layer starts to crumble and the unprotected length increases. This would lead to scour holes which rapidly develop and eventually lower the entire bed. During the second failure possibility, the poorly erodible layer fails by deformation. The layer covers the slopes and protects the non-cohesive grains similar as a falling apron.

After the results of the physical model were analysed, a next step was made by implementing these results in a computational model. The solver FINEL3D (Svašek Hydraulics) was used to simulate the flow in the scour holes. Since no field data of the flow velocities were available, a 2DV model of the experiments was made. This model was tested with four turbulence models: constant eddy viscosity, Bakhmetev mixing length, $k - L$ model and $k - \epsilon$ model. These simulations showed large variations in the flow fields. The model for constant eddy viscosity appeared to give the best fit for the flow field in the scour holes.

A last step was made by using the results of the 2DV simulations and implementing these into a 3D model of the Oude Maas and Spui. Steady state solutions of ebb and flood flows were simulated (due to tidal influence the direction of the flow reverses). The models showed similar distributions as observed in the 2DV simulations.

The shear stresses at the bed were calculated based on the computed flow velocities. These shear stresses show high peaks at the edges of the scour holes. This indicates that the edges of the scour hole are protected by the clay/peat layer, since the shear forces are larger than the critical shear stress of the non-erodible grains.

Although the simulations were not modelled with tidal conditions, this simulation showed that the poorly erodible layer bounds the dimensions of the scour hole. The results indicate that the poorly erodible layer deforms and protects the slopes of the scour hole. This means that this deformation is able to stop the development of scour and stabilize the slopes indicating that other stabilization measures are not necessarily needed. Monitoring of the current scour holes should be sufficient guarantee safety for nearby structures.

However, it does not prove the hypothesis that the poorly erodible layer stabilizes the slopes like a falling apron, but does not disprove this hypothesis either. Further research of this layer should be carried out in order to validate the hypothesis.

Contents

Preface	i
Summary	ii
List of Symbols	vii
1 Introduction	1
1.1 Introduction	1
1.2 Problem description	3
1.3 Objective	3
1.4 Research questions	3
1.5 Approach	4
1.6 Structure of the content	5
2 Field data & review of literature	6
2.1 Introduction	6
2.2 Field data	6
2.2.1 Overview of the area	6
2.2.2 Scour hole definition	7
2.2.3 Berenplaat Scour Hole	8
2.2.4 Schuddebeursedijk Scour Hole	9
2.2.5 Poortugaal Scour Hole	11
2.2.6 Soil parameters	12
2.2.7 Prototype situation	12
2.3 Hydraulics & sediment transport	13
2.3.1 Introduction	13
2.3.2 Sediment transport	13
2.3.3 Stability of grains	14
2.3.4 Breusers formula	15
2.3.5 Scour & morphology	22
2.4 Geotechnical aspects	23
2.4.1 Stability in the scour hole	23
2.4.2 Transport of non-cohesive grains	23

2.5	Recapitulation	24
3	Physical Model	25
3.1	Introduction	25
3.2	Model set-up	25
3.3	Results	26
3.3.1	Calibration of the experiment	26
3.3.2	Main experiments	28
3.4	Analyses	36
3.4.1	Comparison	36
3.4.2	Breusers formula	38
3.4.3	Flow velocity in the scour hole	40
3.4.4	Influence of the length of the scour hole	41
3.4.5	Angle of the upstream slope	43
3.5	Discussion	43
3.5.1	Influence of the poorly erodible layer in the field	43
3.5.2	Tidal influence	44
3.6	Recapitulation	45
4	Numerical model	47
4.1	Introduction	47
4.2	2DV models	48
4.2.1	FINEL3D	48
4.2.2	Model set-up	48
4.2.3	Turbulence closure models	49
4.2.4	Results	51
4.2.5	Analyses	53
4.2.6	Discussion	54
4.3	3D model, Scour holes in the Oude Maas and Spui	56
4.3.1	Model Set-up	56
4.3.2	Results	58
4.3.3	Analyses	59
4.4	Recapitulation	61
5	Discussion	63
5.1	Development of scour	63
5.2	Managing the river	63
5.3	Future prospective	64
5.4	Eastern Scheldt	65
6	Conclusions & recommendations	66
6.1	Conclusions	66
6.1.1	Conclusion towards the objective	66
6.1.2	Conclusions towards the research questions	67

6.2	Recommendations	70
6.2.1	Practical applications	70
6.2.2	Recommendations for further research	70
Bibliography		78
A Figures of scour holes		81
B Extra literature		83
B.1	Tidal influence on the system	83
B.2	Coanda effect	85
B.3	Geotechnical aspects	86
B.3.1	Failure mechanisms	86
B.3.2	Upstream slope of the scour hole	87
B.3.3	Critical failure length	88
B.4	Transport of non-cohesive grains	89
B.4.1	Introduction	89
B.4.2	Abrasive erosion	89
B.4.3	Erosion of fragments	91
C Flow conditions in the Oude Maas and Spui		92
D Set-up of physical model		95
D.1	Introduction	95
D.2	Scaling rules	95
D.3	Model set-up	98
D.3.1	Bottom roughness	98
D.3.2	Work plan	100
D.3.3	Measurement instruments	104
E Scour formula for suspended sediments		106
E.1	Introduction	106
E.2	Analyses	106
F Figures of the 2DV models		108
F.1	2DV model of physical model investigation experiment 17	108
F.2	2DV model of physical model investigation experiment 20	111
G Figures of the 3D numerical model		113

List of Symbols

Symbol	Definition	unit
a	Weir height	m
$c_{1\epsilon}$	Empirical coefficient $k - \epsilon$ model	-
$c_{2\epsilon}$	Empirical coefficient $k - \epsilon$ model	-
c_d	Dissipation coefficient	-
c_f	Friction coefficient	-
c_μ	Empirical coefficient $k - \epsilon$ model	-
c'_μ	Empirical coefficient $k - L$ model	-
C	Chézy roughness coefficient	$\text{m}^{0.5}/\text{s}$
C_0	Chézy roughness coefficient of bed protection	$\text{m}^{0.5}/\text{s}$
	Cohesion	N/m^2
C_D	Model coefficient	-
C_f	Fatigue rupture strength of clay	N/m^2
d_{50}	Median grain diameter	m
d_a	Size of detaching aggregates	m
D	Particle grain diameter	m
D^*	Dimensionless particle grain diameter	-
f_C	Roughness function related to bed protection	-
Fr	Froude number	-
g	Acceleration of gravity, 9.81	m/s^2
h	Water depth	m
h_0	Initial water depth	m
	Tide average flow depth	m
h_e	Corrected water height above the weir	m
h_k	Water height at above the weir	m
h_{se}	Equilibrium depth	m
H	Energy height	m
i	Gradient of the river bottom	-
k	Turbulence kinetic energy	m^2/s^2
k_s	Nikuradse roughness	m
k_{s-clay}	Equivalent roughness of the poorly erodible layer	m

Symbol	Definition	unit
K	Coefficient	$m^{2.3}/s^{3.3}$
l_m	Mixing length	m
L	Length (of bed protection)	m
L_s	Failure length	m
m'	Coefficient of the weir	-
n_-	Scale between prototype and model	-
N_g	Number of grid points	-
P	Turbulence generation term	m/s
q	Discharge per unit of width	m^2/s
r_0	Relative turbulence	-
Re	Reynolds number	-
s	Velocity height	m
S	Sediment transport volume per unit of time and width	m^2/s
S_{ij}	Velocity gradient tensor	1/s
t	Time	s
$t_{1,u}$	Characteristic time for tidal component	s
t_1	Characteristic time	s
	Time αu_0 exceeds u_c during flood tide	s
t_2	Time αu_0 drops below u_c during ebb tide	s
t_3	Time αu_0 exceeds u_c during ebb tide	s
t_4	Time αu_0 drops below u_c during flood tide	s
T	Part of tidal period where $\alpha u_0 > u_c$	s
T_1	Part of tidal period where $\alpha u_0 > u_c$	s
T_2	Part of tidal period where $\sqrt{\alpha u_0^2} > u_c$	s
u	Flow velocity in longitudinal direction	m/s
\bar{u}	Mean velocity	m/s
\bar{u}_0	Mean velocity at t=0	m/s
\bar{u}_c	Critical velocity	m/s
u_*	Bed shear velocity	m/s
$u_{*,c}$	Critical bed shear velocity	m/s
v	Flow velocity in transverse direction	m/s
w	Flow velocity in vertical direction	m/s
w_s	Fall velocity sediment	m/s
x	Distance along the horizontal axis	m
y_m	Scour depth at the deepest point	m
	Scour depth for a given time	m
$y_{m,e}$	The maximum scour depth in the equilibrium phase	m
z	Vertical coordinate measured upwards from the bed	m
z_b	Bed level	m

Symbol	Definition	unit
α	Amplification coefficient	-
β	Angle of the upstream scour slope	°
β_a	Average slope angle before instability	°
γ	Coefficient of Breusers method	-
γ_1	Sliding erosion slope angle after instability	°
γ_2	Sliding deposit slope angle after instability	°
Δ	Relative density	-
Δt	Time step	s
Δx	Spacial step	m
ϵ	Dissipation rate of turbulent kinetic energy	m/s
κ	Von Kármán constant	-
ν	Kinematic viscosity	m ² /s
ν_v	Vertical eddy viscosity	m ² /s
ρ_w	Density of water	kg/m ³
ρ_s	Density of sediment	kg/m ³
σ_k	standard deviation	-
σ_k	Empirical constant of the $k - L$ model	-
σ_ϵ	Empirical constant of the $k - L$ model	-
τ	Shear stress	N/m ²
τ_c	Critical shear stress	N/m ²
ϕ	Angle of repose	°
ψ_c	Shields parameter	-

Chapter 1

Introduction

1.1 Introduction

The Rhine and Meuse rivers branch out into a deltaic area in the South-Western part of The Netherlands. The outflow to the sea is by two main river branches: the Nieuwe Waterweg (North) and the Haringvliet Estuary (South). After the construction of the Haringvliet Sluices (1970), the tidal flows in the area have been significantly changed. The sluices have stopped the tidal flow in the Haringvliet and only sluice during peak river discharges. However, the tidal wave still enters the area at the Nieuwe Waterweg. This resulted in higher flow velocities in the branches connecting both estuaries. A map of the area is shown in Figure 1.1.

The river has a heterogeneous bed which consists of an erosion resistant clay/peat layer on top of a sand layer. The rivers experience a general incision, which has increased due to the higher flow velocities. The erosion resistant layer becomes thinner and sometimes locally breaks, exposing the more easily eroded non-cohesive sand layer. Suddenly, scour holes are formed, see Figure 1.2. The development of scour holes poses risks to adjacent flood defences. The steep slopes of the scour holes may lead to instability due to sliding or liquefaction. If these processes appear in front of flood defences, it may cause failure of the structure.

SLOFF *et al.* (2012a) give a general description of the scour problems in the Rijnmond Area. They investigated the effects of scour and the relation to the morphology. The software packages used (Sobek and Delft3D) were suitable to calculate the morphological development over time into detail. However, rapid deviations such as the development of scour holes were difficult to simulate. Various simulation methods were used to model the scour holes which led to different results (SLOFF *et al.*, 2012b). Knowledge of the scour processes is needed to validate and improve the results of these models.

Although extensive research on scour problems has been carried out in the second half of the twentieth century, none of these investigated scour under cohesive layers. Knowledge of combinations of non-cohesive and cohesive soils was limited since it is hard to simulate them in physical models. Most scour problems relate to structures

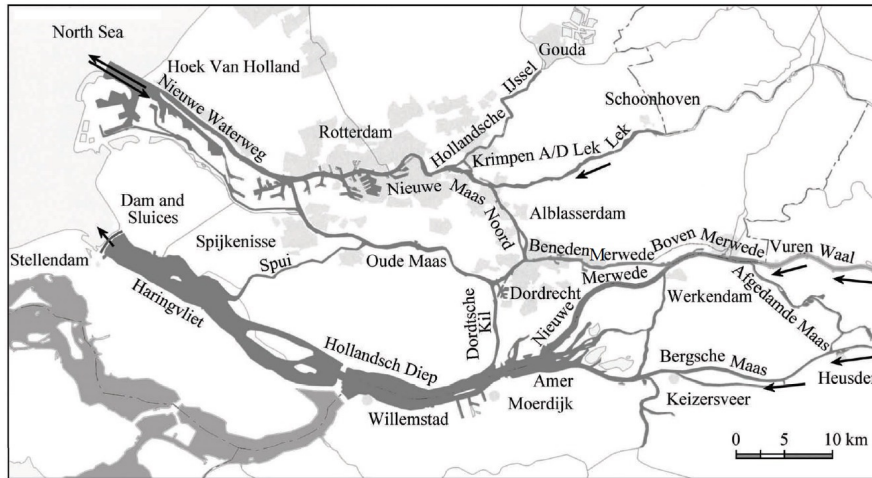


Figure 1.1: Map of the Rijnmond Area (SLOFF *et al.* 2012a).

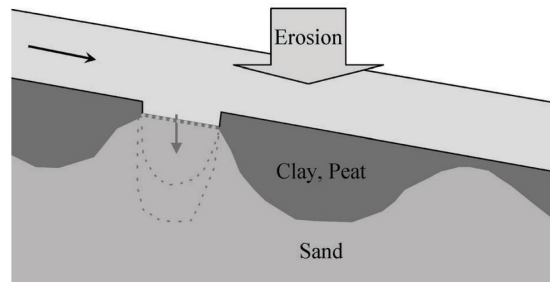


Figure 1.2: Schematic presentation of the interaction between the erosion resistant layer and the sand bed below (SLOFF *et al.* 2012a).

(local scour) at sandy locations. If needed, the methods to indicate local scour for non-cohesive soils were used on cohesive soils.

The scour holes are usually formed by a mix of causes. The bed of the branches experiences general incision. However, this does not explain why the scour holes are formed at their specific location. Changes in local conditions (thinner layers, constructions, etc.) lead to the failure of the top layer. The cause of further development the scour holes is unknown. Some scour holes are stable, while other continuously develop. Furthermore, reason why the scour holes aren't filled by sediment is also unknown.

This research was carried out within the KPP project ('Kennis Primaire Projecten') of Deltares which is commissioned by Rijkswaterstaat (RWS). During this research a river management plan and a simulation model of the Rijnmond Area have been developed.

1.2 Problem description

The knowledge to describe the development of scour under a poorly erodible top layer is limited. Figure 1.2 shows the development of a scour hole. Once the top layer is broken the depth increases. As a consequence the slopes of the hole steepen. Instability of these slopes lead to the failure of the top layer and consequent growth of the horizontal extent of the scour hole.

Literature such as HOFFMANS AND VERHEIJ (1997) has summarized the results of scour research. It describes a number of standard situations for scour, mainly near structures, but not for scour holes with a limited length. Although none of the situations describe the given problem, predictions are made with a most likely reference situation. A combination of these predictions and experience from the Dutch estuaries is used to indicate the development of the scour holes. However, these empirical relations and expert judgment cannot be implemented in computational models. Presently scour holes are often poorly (or not) included in morphology models.

The probability of failure of flood defences should be low to guarantee the safety of flood prone areas. The formation of scour holes near the flood defences increases this failure probability. The formation and development of the scour holes has to be investigated to indicate the risks.

1.3 Objective

The first objective is to obtain a better understanding of the development of the scour holes. The poorly erodible layer limits the length of the scour hole, but its influence on the development of scour is unknown. The interaction between the poorly erodible layer and the scour hole will be investigated. Comparison of existing knowledge and calculation methods with the scour holes in the field, will give the set-up of the experiments. The second objective is to implement these results within a computational model to be able to describe the development of the scour holes in the field.

1.4 Research questions

As a guideline to fulfil the objective, the following research questions are formulated.

1. How does the scour hole develop after the initial hole has formed?
2. Which methods are available to calculate the scour and to what extent are they applicable for the problem?
3. How does the velocity field react to the scour hole?
4. What is the influence of the poorly erodible layer on the development of scour?

5. What is the influence of the scour hole on the poorly erodible layer and does this describe the development of the scour hole?
6. What is the influence of the tide on the development of the scour holes?
7. Which turbulence model represents the flow velocity in the scour hole best?
8. What do the shear stresses in a numerical model tell about the development of scour?

Scope of the research

It is impossible to include all the scour hole related problems within this master thesis. Therefore some boundaries to the scope of this thesis were set. The problem focusses on the natural scour. This means that the following related subjects are not treated.

- Scour due to structures such as bridge piers and groynes.
- Effects of propeller wash (jet flow of the passing ships).
- Other ship related damages to the bottom; anchors and spud poles.
- Stabilisation methods.

1.5 Approach

The research can be split into 3 phases. Each phase has a different aim to investigate the problem.

Before the problem was investigated, field data were gathered to describe the scour holes in the area. The scour holes were simplified to a prototype situation which captures the problem.

Thereafter, the scour process was compared with known scour processes from the literature. Several theories were explained and tested in order to find the similarities. All deviations were analysed and described. A combination of these theories and experience from the field lead to a judgmental description of the scour problem.

Experiments by physical model investigation were carried out in the laboratory of TU Delft. Scour holes with a limited length were investigated to validate the proposed scour processes. The geometry of the scour hole (length, depth and slopes) and the flow regime were observed in the experiments. An attempt was made to investigate the influence of the tide on the development of scour. The physical model investigation started on November 3rd and finished on December 4th. During this month several experiments were executed to investigate various hypotheses.

During the third phase, the last research questions were answered. 2DV simulations were carried out to test several turbulence models to describe the flow field. Since no field measurements were available, the flow velocities from the experiments were used to validate the computational simulations. The results of the 2DV simulations were used in the set-up of a 3D model of the Oude Maas and Spui. The computational simulations were made with the solver FINEL3D (Svašek Hydraulics).

1.6 Structure of the content

This report has been divided into three parts which analyse the problem. Chapter 2 first investigates the data from the field. It defines 3 scour holes in the Rijnmond Area to represent the scour problem. These three scour holes are combined into a prototype situation. The second part of this chapter analyses the present methods to calculate the parameters of the scour hole (depth, angle upstream slope, etc.). Chapter 3 describes the physical laboratory experiment and the computational simulations are discussed in chapter 4. A short discussion is in chapter 5. The conclusion and recommendations are in chapter 6.

Chapter 2

Field data & review of literature

2.1 Introduction

The previous chapter introduced the problem of scour under the poorly erodible layers. This chapter discusses the theoretical approach to investigate this problem. Several scour formulas are explained to analyse the development of the scour holes. But none of these empirical formulas is made for this type of scour and the results cannot directly be used to indicate the characteristics of the scour hole. A qualitative judgment of the formulas is made to estimate the scour process of the given problem.

But first the scour holes in the field are described to clearly define the researched scour problem.

2.2 Field data

2.2.1 Overview of the area

The delta in the Rijnmond Area (Figure 1.1) consist of multiple river branches with interconnections. These branches receive water from the Rhine and Meuse River in the East and flow to the sea in the West. The rivers discharge to the sea at the Nieuwe Waterweg. At high water levels in the rivers the Haringvliet Sluices are opened to increase the discharge to the sea.

The rivers experience intertidal conditions, which even reverses the flow direction in these branches. During ebb the river discharge dominates the flow branches. The velocity in the rivers is between 0.8 and 1.8 m/s. During flood tide the sea enters the area and reverses the flow direction. The corresponding flow velocities are between 0.5 and 1.6 m/s. A salt wedge enters the Nieuwe Waterweg raises the salt concentration in the connecting river branches.

The profile of the river bed is the result of thousand years of discharge of the rivers in the area. During the ages the sediments were deposited creating sandy parts in the

generally clay and peaty subsoil. Morphological evolution of the river branches caused a heterogeneous subsoil. Layers of sand, peat and clay can be found with various thickness.

2.2.2 Scour hole definition

General description

The problem of the scour in the area has been introduced without describing what a scour hole is. In practice there is no clear definition of a scour hole (size, etc.). The dictionary gives:

- *Scour*: Of water or a watercourse make a channel or pool by flowing quickly over something and removing soil or rock
- *Hole*: A hollow place in a solid body or surface.

Combining these two definitions gives: a hollow place at the river bed which has been dug out by the force of the water flow. However, it is not that easy to define a scour hole in a river which experiences general incision.

Field description

Bathymetry maps of the river branches in the Rijnmond Area were made from multi-beam measurements (a map of these rivers is shown in 1.1). These maps were analysed with the software package ArcMaps. The multibeam measurement started in 2005 and are available in a 5 x 5 m² raster. The measurements of the Oude Maas between 2007 and 2013 are available between in a 1 x 1 m² raster. Data before 2005 was measured in a range of 100 m and the area between the measurements was interpolated. This data was not used because the accuracy (3 - 4 measurements in a scour hole) is too low.

The bathymetry maps show multiple scoured sections, but not all these sections describe the same type of scour process. A first distinction was made by the length of a scour hole. The maximum length of a scour hole is around 300 m (scoured sections with longer dimensions are often channels or combinations of scour holes). Within the KPP project of Deltares (HUISMANS *et al*, 2014) the holes have been divided into 2 categories:

- Scour with a length smaller than 200 m.
- Scour with a length larger than 200 m.

The scour holes are divided in these categories, because most scour holes smaller than 200 m are the younger scour holes, whereas older scour holes were able to develop in length. In this thesis report, attention is paid to both types of scour holes because they represent different stages of the development.

Secondly, a qualitative description of the cause of scour was made. All scour processes which are caused by structures such as groynes and bridge piers were not further

investigated.

The next section discusses three scour holes in the Oude Maas and Spui, which are shown in Figure 2.1. These scour holes were selected, since these scour holes represented both young and older scour holes and are located near each other. In the explanation the flow towards the sea is used to describe the up- and downstream elements. Nevertheless, due to the tide the flow changes in direction which makes that these terms not always correspond with the direction of the flow.

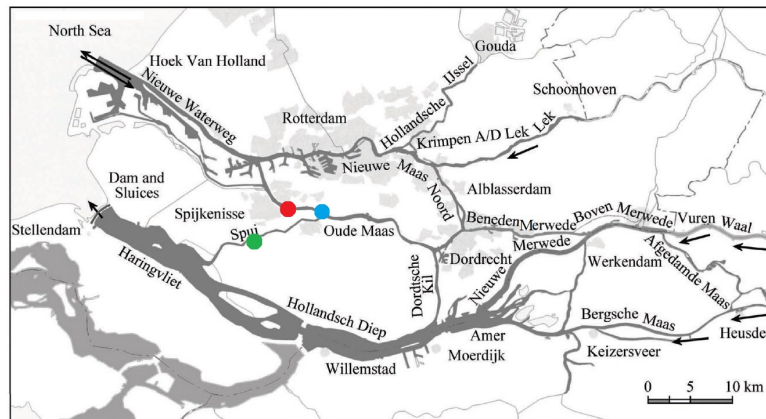


Figure 2.1: Map of the Rijnmond Area including locations of the scour holes (SLOFF *et al.* 2012a). The blue dot is the Berenplaat (Oude Maas), red Poortugaal scour hole (Oude Maas) and green Schuddebeursedijk (Spui).

2.2.3 Berenplaat Scour Hole

The Berenplaat Scour Hole is located in the Oude Maas at the West side of the confluence with Spui, North of the Berenplaat. The length of the hole is about 200 m, and its depth 28.3 m-MSL (the average river bed is at 16.5 m-MSL). Figure 2.2 shows a depth contour of the scour hole in 2013.

This is one of the newer scour holes in the area. The first time it appeared in the measurements, was around 2005. Figure 2.3 shows the rapid development of the length (10 to 60 m a year) in the longitudinal direction and much slower in the transverse direction. It also shows that the growth in the upstream direction is about 2 - 3 times larger than in the downstream direction. Figure 2.4 shows a longitudinal profile of the scour hole. The scour hole was about 100 m long and the maximum depth was 27.8 m-MSL in 2007. The length has increased to 250 m while the maximum depth increased 0.5 m in 2013. The downstream slope of the scour hole in 2013 has an averaged steepness of 1:40. The upstream slope is much steeper with a steepness up to 1:5. Note: the scour hole might be caused by the confluence/bifurcation (depending on the direction of the

flow).

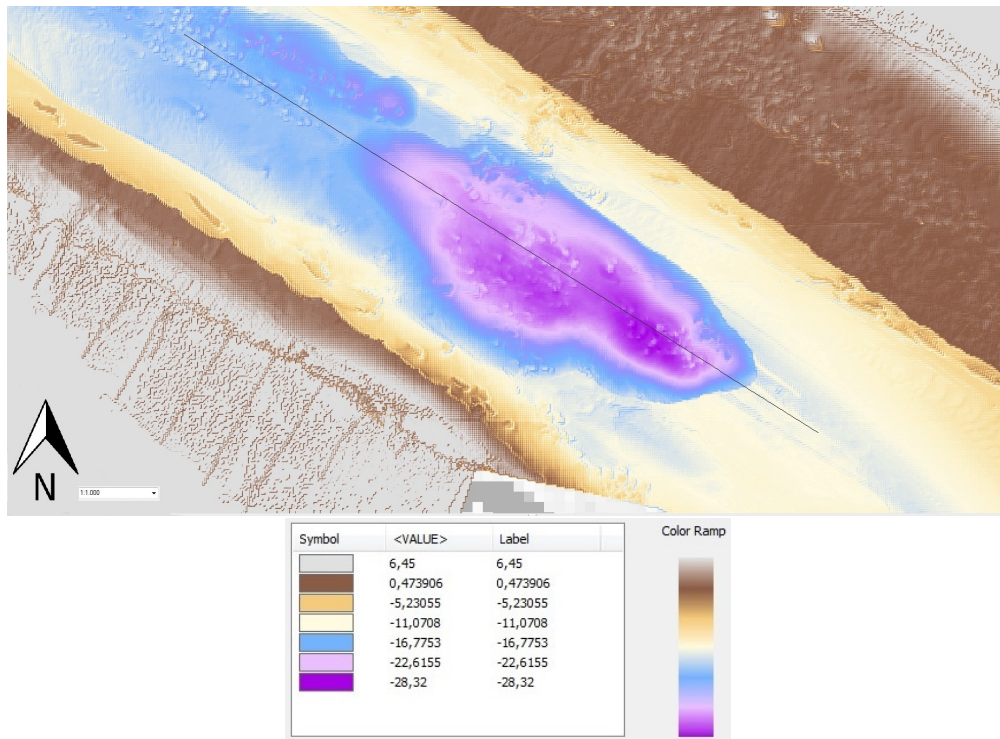


Figure 2.2: Multibeam sounding of the bathymetry of the Berenplaat Scour Hole in 2013. The black line is the location of the longitudinal profile (1:1000). The depth is in m MSL.

2.2.4 Schuddebeursedijk Scour Hole

The Schuddebeursedijk Scour Hole is located in the Spui River to the West of Nieuw-Beijerland at Schuddebeursedijk. The scour hole is the third of four scour holes in a row (counted from upstream to downstream). The first two holes merged into a large channel with a length of 900 m. Directly after a higher bar at the end of this channel is the Schuddebeursedijk Scour Hole located. The flow regime and shear stress in this scour hole were investigated by SLOFF *et al.* (2012b). This report describes the difference in the results for various types of vertical grids in Delft3D.

The scour hole is older and relatively stable over time, see Figure 2.5. The top view of the scour hole shows a symmetrical oval shape. The gradient of the upstream slopes is 1:5 and downstream 1:8. A large flat section of 120 m is located in the middle of the scour hole. The depth of this flat section hardly developed between 2007 and 2012 suggesting that the scour hole extended until another poorly erodible layer was reached. The depth of the scour hole is 16 m-MSL while the river bed is at 7 m-MSL. The scour hole is deeper than the water depth. The expected cause of the scour is the local disturbance

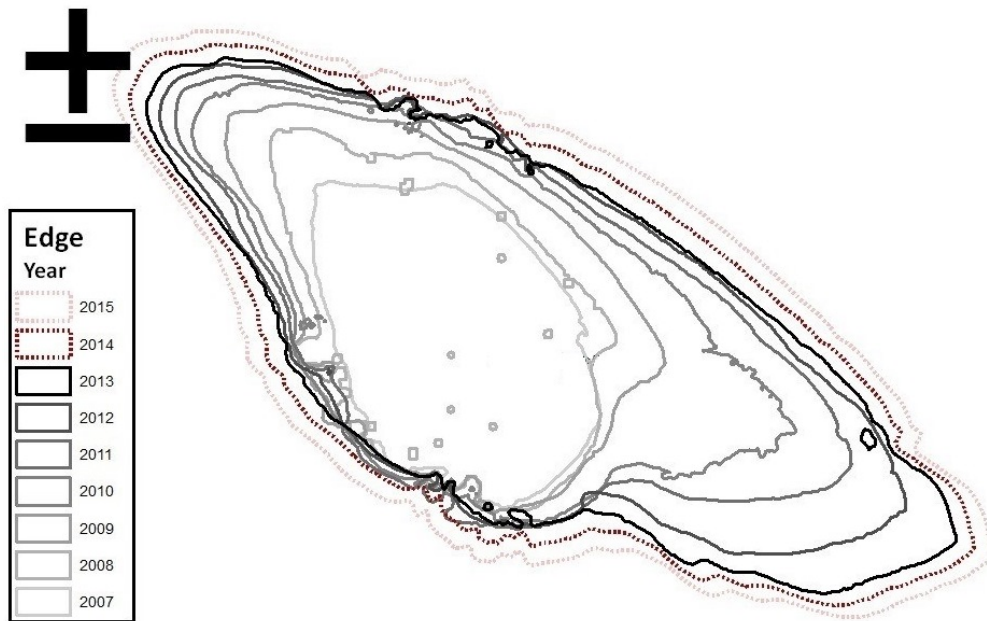


Figure 2.3: Longitudinal profile of the Berenplaat Scour Hole, where the left is downstream and right upstream.

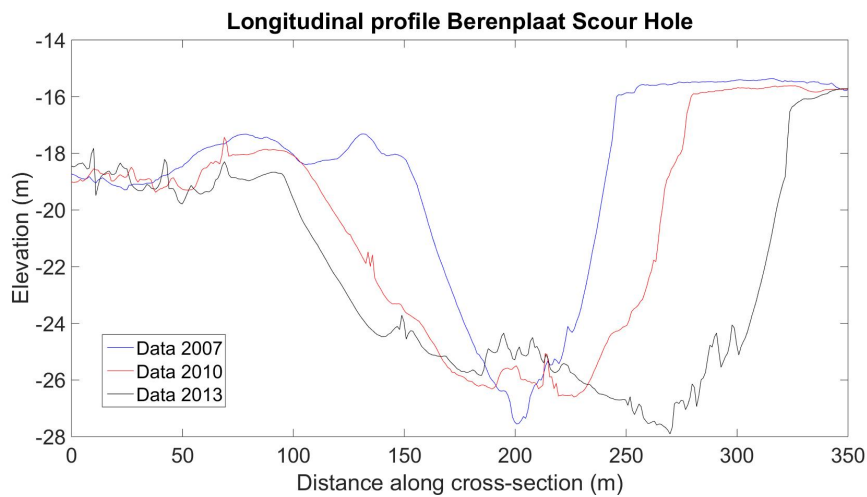


Figure 2.4: Longitudinal profile of the centre of the Berenplaat Scour Hole, where the left is downstream and right upstream.

at the end of the channel.

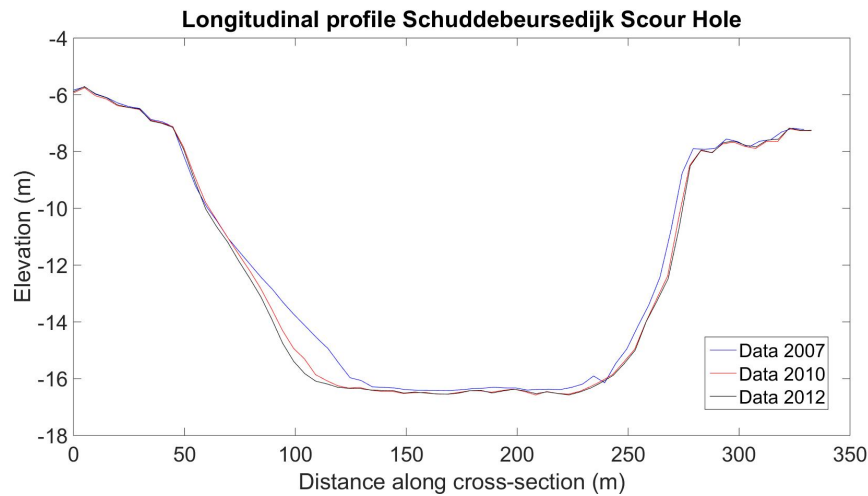


Figure 2.5: Longitudinal profile of the Scuddebeursedijk Scour Hole, where the left is downstream and right upstream.

2.2.5 Poortugaal Scour Hole

The Poortugaal Scour Hole is located in the Oude Maas South of the city of Poortugaal and North-West of the Berenplaat. It is located in the deeper part of the Oude Maas (18 m-MSL). A scoured channel that follows the outer bend of the river is located upstream of the scour hole. The location of the hole is near the crossing of the main stream from bend to bend. However, the scour hole is not in line with the channels.

Figure 2.6 shows the longitudinal profile of the scour hole. The slopes of the scour holes have the same gradient as the Berenplaat Scour Hole (about 1:5 upstream and 1:40 downstream). A bat upstream of the scour hole, stopped the development of scour in upstream direction (high peak at the right side of the figure). However, the scour hole has developed in the downstream direction, increasing the depth and the steepness of the upstream slope. The deepest point has moved upstream. A top view of the scour hole is shown in Appendix A

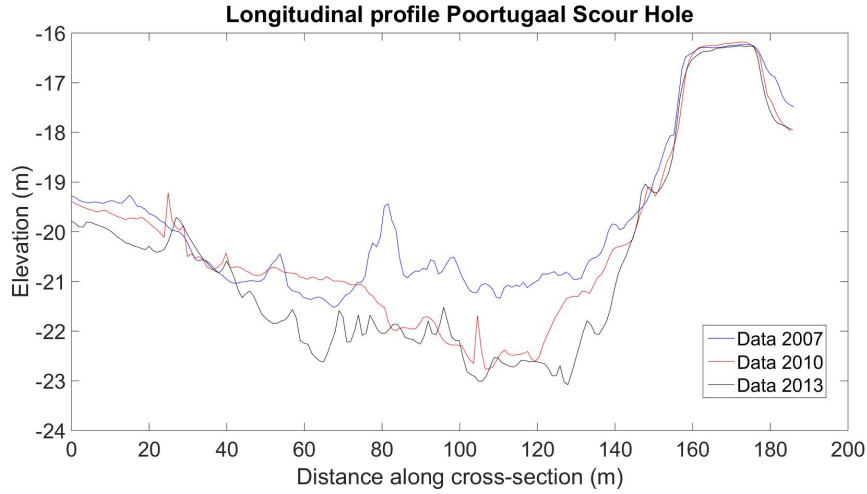


Figure 2.6: Longitudinal profile of the Poortugaal Scour Hole, where the left is downstream and right upstream.

2.2.6 Soil parameters

The soil parameters from the field followed from the report of SLOFF *et al.* (2012a). These parameters are used in the calculations to determine the depth of the scour holes.

Table 2.1: Soil parameters.

	d_{50} (μm)	ψ (-)	τ_{crit} (N/m^2)
Holocene sand	175	0,076	0.15
Pleistocene sand	350	0,054	0.3
moderately soft clay			1.8
hard consolidated clay			18.8

2.2.7 Prototype situation

A simplified model of the Berenplaat Scour Hole was made to test calculation and simulations of the scour holes. The scour hole has a length of 250 m which is bounded by the poorly erodible layers, see Figure 2.7. Since no data of the subsoil was available, the poorly erodible layer was assumed to be thick enough to stabilize the edges. Further, the sand layer was assumed to be homogeneous, for calculations the values for the 'Pleistocene' sand were used.

The river bed was at 16.5 m-MSL and the deepest point of the scour hole was 28.3 m-MSL. For simplicity a water level of 0 m+MSL at the surface was assumed. During the river dominated flow the flow velocity was 1.6 m/s and the reversed flow (tide dominance) was 1.4 m/s. More information about the flow conditions can be found in Appendix C.

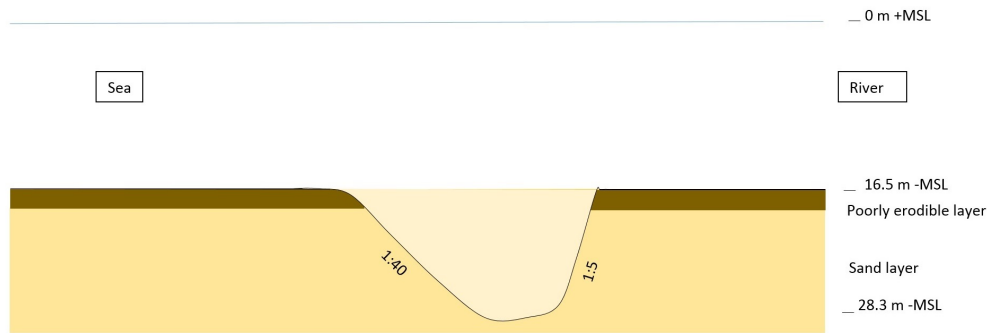


Figure 2.7: Longitudinal profile of the Poortugaal Scour Hole, where the left is downstream and right upstream.

2.3 Hydraulics & sediment transport

2.3.1 Introduction

The formation and development is in principle nothing else than erosion. Special circumstances lead to extensive local erosion. The theory behind most methods to calculate scour is based on the same principles. The first subsection explains the basic principles of sediment transport. This is followed by a description of the Shields equation, which describes the initiation of motions for particles.

The Breusers equation in the next subsection uses both theories to calculate the maximum depth of the scour hole. This is a general equation to describe scour. Within the formula several empirical parameters should be used to solve the equation. These parameters resulted from several experiments for a number of standard scour problems. An analyses of these situations/parameters is made and applied on the prototype situation. The last subsection shortly describes the relation between scour and the river morphology.

2.3.2 Sediment transport

Before the specific problem will be investigated, the basics of sediment transport are explained. The sediment transport is described by the equation of Exner.

$$\frac{\partial z_b}{\partial t} + \frac{\partial S}{\partial x} = 0 \quad (2.1)$$

$\frac{\partial S}{\partial t}$	Sediment transport per unit of time and width (m^2/s)
$\frac{\partial t}{\partial t}$	Time (s)
$\frac{\partial x}{\partial x}$	Distance along horizontal axis (m)
$\frac{\partial z_b}{\partial z_b}$	Elevation of the bed (m)

The equation describes that a gradient in transport leads to a change in bed level, see Figure 2.8. A distinction in the scour process (lowering of the bed level due to a net outflow of sediment) is made between two situations; live-bed and clear-water scour. During live-bed scour the outflow of sediment is larger than inflow. Clear-water scour is a special situation of live-bed scour, without the inflow of sediment. Clear-water scour is found downstream of locations with a lack of erodible material or a lack of transport capacity. The bed of the river branches consists of a cohesive peat/clay layer. The amount sediment in the river is limited and the scour is therefore comparable with clear-water scour.

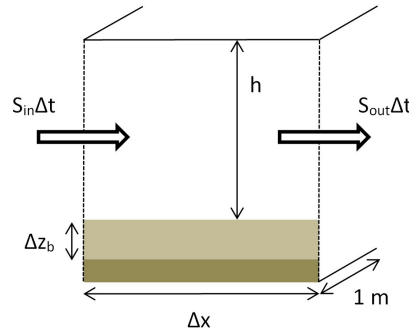


Figure 2.8: Control volume for deviation of sediment balance.

2.3.3 Stability of grains

Shields (SCHIERECK, 2012) proposed a formula for the initial movement of grains in 1936. The critical bed shear-stress, which is the load induced by the flow, is given as:

$$\tau_c = \rho_w u_{*,c}^2 \quad (2.2)$$

$u_{*,c}$	Critical bed shear velocity (m/s)
ρ_w	Density of water (kg/m^3)
τ_c	Critical shear-stress (N/m^2)

This load is derived by the mass of the grain (resistance). According to Shields, the mobility parameter is:

$$\psi_c = \frac{u_{*,c}^2}{\Delta g d_{50}} = \frac{C^2 \bar{u}_c^2}{\Delta d_{50}} \quad (2.3)$$

C	Chézy resistance ($\text{m}^{0.5}/\text{s}$)
d_{50}	Median grain size (m)
g	Acceleration of gravity, $g = 9.81 \text{ m/s}^2$
\bar{u}_c	Mean critical velocity (m/s)
Δ	Relative density given by $\frac{\rho_w - \rho_s}{\rho_w}$ (-)
ρ_s	Density of sediment (kg/m^3)
ψ_c	Shields parameter (-)

The Chézy coefficient given as:

$$C = 18 \log \left(\frac{12h_0}{k_s} \right) \quad (2.4)$$

h_0	Initial water depth (m)
k_s	Equivalent Nikuradse roughness, for hydraulically rough flow: $k_s = 3d_{90}$, hydraulically smooth flow $k_s = 2d_{50}$

The critical mean velocity for a uniform flow (logarithmic velocity profile) over a hydraulically rough bed and a width that is much larger than the depth, is given by:

$$\bar{u}_c = 2.5 \sqrt{\psi_c \Delta g d_{50}} \ln \left(\frac{12h_0}{k_s} \right) \quad (2.5)$$

The formula describes that grains start to move once the load induced by the flow is higher than the resisting shear forces. This process depend on multiple of variables; the shape, mass, placement, etc., which differ for every grain. It is impossible to determine this for every grain. Shields described a broad belt at which the grains start to move. This was refined into 7 stages of bed movement in 1969 by Delft Hydraulics, see Figure 2.9.

2.3.4 Breusers formula

Breusers proposed an empirical formula to calculate the depth of a scour hole in the second half of the twentieth century. This formula is applicable for several scour problems and can be adjusted to the problem by empirical parameters. The scour under a poorly erodible layer is best represented by the scour behind a bed protection, see Figure 2.10. This reference situation includes a sill upstream of the scour hole. A sill height of $D = 0 \text{ m}$ is used for the prototype situation. This reduces the sketch in Figure 2.10 to lower picture. The poorly erodible layer is entered as the bed protection of the formula. A difference between this approach and the prototype is the poorly erodible layer downstream of the scour hole.

The next subsections describe a number of aspects of the Breusers formula. First the equilibrium depth (final situation) is discussed. The second subsection discusses the

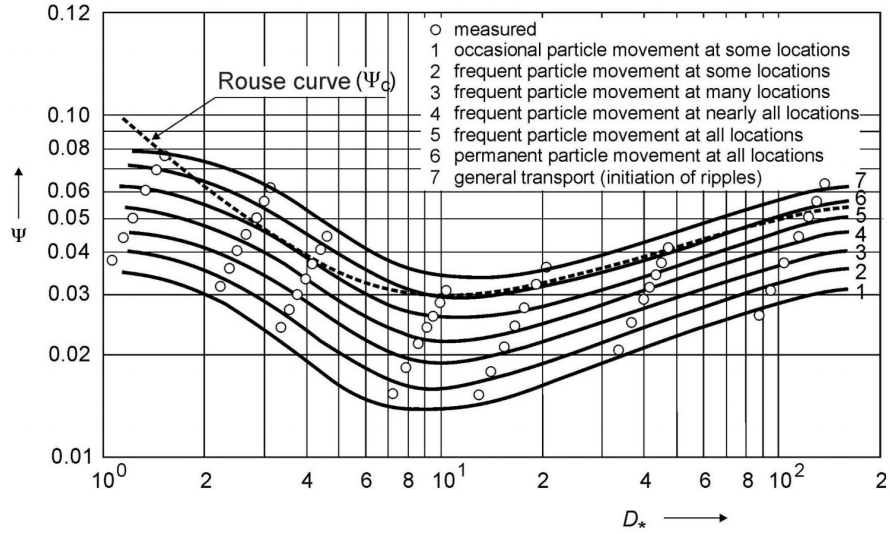


Figure 2.9: Shields diagram, adapted by Breusers, with $D_* = d_{n50} (\Delta g / \nu^2)^{1/3}$ (HOFFMANS AND VERHEIJ 1997).

turbulence factors which determine the initiation of movement. Thereafter a formula which describes the development of scour over time will be described. The last section discusses deviations of the formula with the prototype situation.

Equilibrium depth

For engineering purpose, the most important parameter of the scour hole is the depth. The depth and location of this deepest point determine the risks to nearby structures. The equilibrium depth is the depth of a developed scour hole. The formula for equilibrium scour behind a bottom protection is given by:

$$\frac{h_{se}}{h_0} = \frac{0.5\alpha\bar{u} - \bar{u}_c}{\bar{u}_c} \quad (2.6)$$

h_{se}	Equilibrium depth (m)
\bar{u}	Mean velocity in front of the scour hole, Q/A (m/s)
α	Amplification factor for the velocity (-)

The amplification factor adds a factor to the velocity to include turbulent processes. An amplification factor of $\alpha = 5$ is initially assumed, which is on the safe side (SCHIERECK, 2012). With equations 2.3 and 2.4, the equilibrium depth is $h_{se} = 104$ m. The rough calculation gives an equilibrium height of 6.5 times the water depth. This large factor is mainly caused by the amplification factor. The amplification factor is investigated in the next subsection.

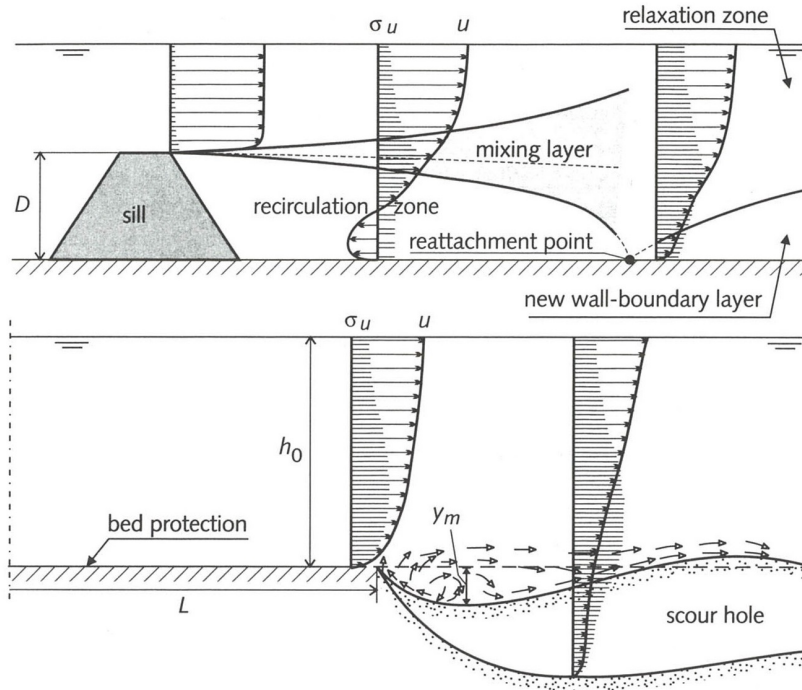


Figure 2.10: Schematization of reference case with sill, including flow pattern (HOFFMANS AND VERHEIJ 1997).

Amplification factor

Research in the past resulted into multiple methods to derive the amplification factor α . The basic idea is given by:

$$\alpha = a + br_0 \quad (2.7)$$

Where r_0 is the relative turbulence. This term includes the local turbulence in the scour hole. However, at locations where the velocity is zero, for example at a reattachment point, the relative turbulence goes to infinity. For those cases the turbulence is included as an addition to the velocity and not as multiplier.

The Scour Manual (HOFFMANS AND VERHEIJ, 1997) uses the relation found by Jorissen and Vrijling (1989);

$$\alpha = 1.5 + 5r_0 \quad (2.8)$$

The relative turbulence intensity r_0 is determined by the formula of HOFFMANS (1993).

$$r_0 = \sqrt{0.0225 \left(1 - \frac{D}{h_0}\right)^{-2} \left(\frac{L - 6D}{6.67h_0} + 1\right)^{-1.08} + 1.45 \frac{g}{C^2}} \quad \text{for } L > 6D \quad (2.9)$$

C	Chézy coefficient of bed protection ($\text{m}^{0.5}/\text{s}$)
D	Height of the sill (m)
L	Length of bed protection (m)

The formula was developed to calculate the turbulence effects of the approaching flow. The length of the bed protection has to extend beyond the reattachment point of the sill. The prototype has no sill in front of the scour hole ($D = 0$ m) and the formula is simplified to:

$$r_0 = 1.21 \frac{\sqrt{g}}{C} \quad (2.10)$$

The Chézy value of the poorly erodible clay layer is given by:

$$C = 18 \log \left(\frac{12h_0}{k_{s-clay}} \right) \quad (2.11)$$

k_{s-clay} The equivalent roughness of the poorly erodible layer (m)

The equivalent roughness is the roughness of the soil upstream of the scour hole. A roughness height of 0.5 m for example, corresponds with an amplification factor $\alpha = 1.96$. The equilibrium depth is then $h_{se} = 30.5$ m, which is much smaller than the first estimation. The equilibrium scour depth is now 2 times the water depth, but still much deeper than the depth in the field. This might be caused by the limited length.

Time dependent formula

In the previous subsections the equilibrium scour hole has been analysed. This section investigates the initiation and development of the scour hole. Initially the scour depth $y_m = 0$ m, which is similar to the initial water depth. The velocity is higher than the critical velocity and the grains start to erode. As the depth increases the flow velocity decreases (assume $u = Q/A$ with $Q = \text{constant}$), but the turbulence may increase. Thus initially the scour hole develops rapidly which decreases over time.

The same research which resulted in the formula for the equilibrium depth gave a formula for the development of scour. Again the same reference situation was chosen; scour behind a sill ($D = 0$ m) with bottom protection (HOFFMANS AND VERHEIJ (1997), see Figure 2.11.

$$\frac{y_m}{y_{m,e}} = 1 - \exp \left[\ln \left(1 - \frac{h_0}{y_{m,e}} \right) \left(\frac{t}{t_1} \right)^\gamma \right] \quad (2.12)$$

t	Time (s)
t_1	Characteristic time (s)
y_m	The scour depth for a given time (m)
$y_{m,e}$	The maximum scour depth in the equilibrium phase (m)
γ	Coefficient (-)

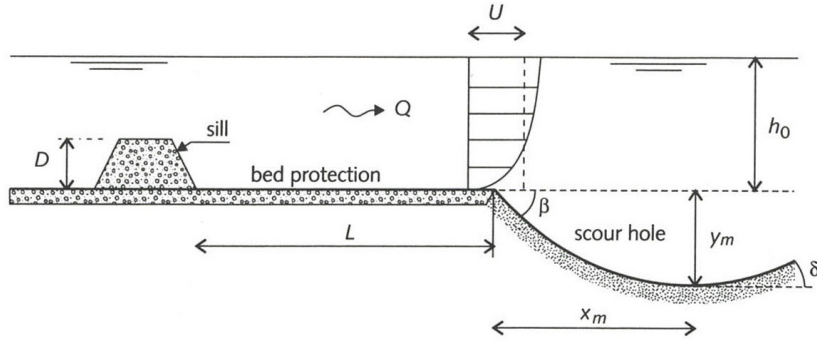


Figure 2.11: Sketch of scour hole including used parameters (HOFFMANS AND VERHEIJ 1997).

For $t < t_1$ the formula can be simplified to:

$$y_m = h_0 \left(\frac{t}{t_1} \right)^\gamma \quad (2.13)$$

The coefficient γ is estimated by the relation between the scour depth and the time factor plotted on a log-log scale. Table 2.2 gives an overview of the results from experiments to indicate γ . A value of $\gamma = 0.5$ was chosen, which corresponds with a three-dimensional problem in the development phase.

Table 2.2: Coefficient γ , HOFFMANS AND VERHEIJ (1997).

Investigator(s)	γ	Flow condition
Breusers (1966)	0.38	Two-dimensional
Mosonyi & Schoppmann (1968)	0.27 - 0.35	Two-dimensional
Dietz (1969)	0.34 - 0.40	Two-dimensional
Van der Meulen & Vinjé (1975)	0.4 - 0.8	Three-dimensional

The characteristic time is based on the time that a certain volume of sediment is transported shown in Equation 2.14.

$$t_1 = \frac{K h_0^2 \Delta^{1.7}}{(\alpha \bar{u} - \bar{u}_c)^{4.3}} \quad (2.14)$$

K Coefficient ($\text{m}^{2.3}/\text{s}^{3.3}$), t_1 in hours

The coefficient α is calculated with Equations 2.8 and 2.10. The coefficient K differs depending on the results of the investigator. Generally a value of $K = 330 \text{ m}^{2.3}/\text{s}^{3.3}$ is applied (De Graauw and Pilarczyk in 1981 HOFFMANS AND VERHEIJ 1997). This value is valid for a rough bed.

Combining formulas 2.13 and 2.14 results in the general formula:

$$h_s = \frac{(\alpha \bar{u} - \bar{u}_c)^{2.15}}{18\Delta^{0.85}} t^{0.5} \quad (2.15)$$

A calculation of the development of the scour depth for the prototype is shown in Figure 2.12. The logarithmic curve shows a rapid increase of scour depth at in the first hours. Thereafter the development slowly decreases. At the end of the graph the formula seems to reach a straight line; suggesting a linear increase of scour depth. The exact behaviour after $t > t_1$ is unknown. The line in the graph is in conflict with the equilibrium depth of subsection 2.3.4. Physical sense suggest that at some point due to deepening, bed shear stresses at the bottom of the hole are expected to drop below the critical shear stress, and no further erosion can occur.

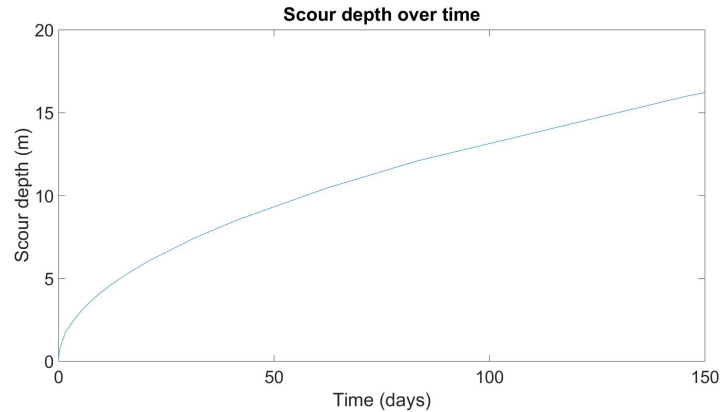


Figure 2.12: The scour depth over time.

Note: If this report refers to the Breusers equation, this means the time depended formula.

Analysis of the Breusers formula

The Breusers formula is thus able to give the scour depth during the development of scour. However the reference situation differs from the prototype. Some of these parameters are further analysed in this subsection.

Poorly erodible layer downstream of the scour hole If the length of the scour hole is bounded, this depth will probably not be reached. The same scour depth within shorter length results in steeper slopes, see Figure 2.13. The sediment transport formula describes the transport as a combination of suspended and bed load. The resisting forces of the bed load increases once the slope is steeper. Thus if the scour hole is bounded, the depth is assumed to be less than is calculated with the Breusers equation.

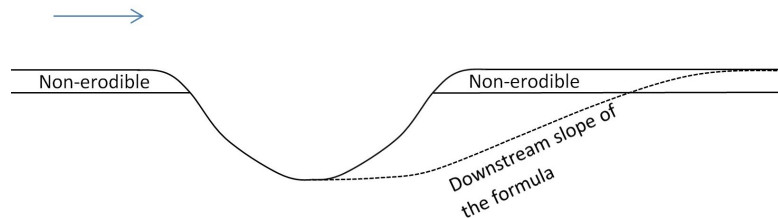


Figure 2.13: Influence of the poorly erodible layer on the length on scour hole.
The formula calculates the depth for a different geometry.

Tidal influence The Breusers formula calculates the scour depth based on a constant velocity. However, the prototype is located in an intertidal river. The flow velocity changes and even reverses in direction. The Scour Manual (HOFFMANS AND VERHEIJ, 1997) gives a simplified approach for non-steady flows. This is further analysed in Appendix B of which the results are shortly summarized below.

The tidal flow raises and decreases the flow velocities at the scour hole. A scour hole develops in the periods of the higher flow velocities, while the flow velocities are too small to cause scour during the reverse of direction. The maximum flow velocities overestimate the development of scour. However, once a reduction factor is added to the maximum flow velocity a formula with a constant flow velocity is able to capture this movement, see Figure Appendix B.2.

A scour hole normally has a steeper upstream slope than downstream. Change of flow direction gives a steep downstream slope and this decreases the sediment transport by bed load. The new upstream slope is expected to steepen, while the new downstream slope becomes gentle. The geometry of the scour hole is assumed to change during a reverse in flow direction, see Figure 2.14. The net transport decreases during this adaptation to the flow.

This corresponds with results of a physical model for bridge piers. In 1999 Escarameia and May showed that the equilibrium depth along squared bridge piers is smaller at locations with a reverse in flow direction (ESCARAMEIA AND MAY 1999).

Relative turbulence The relative turbulence in the scour hole depends on the roughness of the bed upstream of the scour hole, see Equation 2.10. But, many other processes has influence on the turbulence. The formula describes a flow which separates at the



Figure 2.14: The assumed change in geometry of a scour hole while calculated with the adapted formula.

upstream edge and forms a recirculating eddy within the scour hole, see the bottom picture of Figure 2.10. However, if the slopes are less steep (rule of thumb give 1:7) the flow does not separate and follows the bed. This is explained by the Coanda principle, see Appendix B.2. This effect leads to higher, but less turbulent flow velocities at the bottom.

2.3.5 Scour & morphology

MOSSELMAN AND SLOFF (2002) described the influence of scour on the morphology and the morphology on scour. At the scour hole, the water depth is larger and the flow resistance is reduced. This leads to a converging of the flow towards the scour hole, which again gives a rise of the erosion, see Figure 2.15. Due to the increase of the length scour holes merge, creating channels and bars. The conference paper explains how observations in the field were modelled with computational models. Some physically incorrect assumptions were introduced to include scour effects in morphological models. The models were able to show the attraction of discharge, however due to the lack of physical background, the assumptions are not applicable in the morphological simulations.

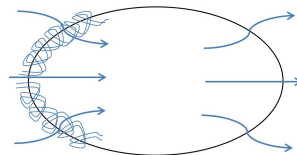


Figure 2.15: Converging flows into the scour hole.

The concepts of morphology and scour are in most studies and literature treated as two separate topics. The relation between both is ignored and therefore the effect on the scour depth is underestimated. The equations for scour are based on Breusers method and made for local situations. The empirical parameters are set by scale models, which did not include any information about the morphology.

Although no method includes the effects of the relation between morphology and scour, some assumptions have been made. In 2002 Hoffmans and Verheij proposed some equations describing the relation between local and bend scour (HOFFMANS AND

VERHEIJ, 2002):

$$h_{total} = \alpha_{bend}h_0 + \alpha_{local}h_0 = (\alpha_{bend} + \alpha_{local}) h_0 \quad (2.16)$$

$$h_{total} = \alpha_{bend}\alpha_{local}h_0 \quad (2.17)$$

Research of Mesbahi in 1992, suggested a formula where the effects are added up, equation 2.16. However, a test by Hoffmans in 1995 with a combination of bridge piers and abutments gave a result similar to the multiplication of equation 2.17. No clear relation between multiple types of scour has been found yet. Currently, such problems require engineering judgement (HOFFMANS AND VERHEIJ, 2002).

2.4 Geotechnical aspects

This section is a summary of the research to geotechnical behaviour during scour. An extended description can be found in Appendix B.3 and B.4. The first part describes the stability of the sand grains in the scour hole. The second part is about the erosion of the clay and peat.

2.4.1 Stability in the scour hole

The inner slopes of the scour hole consist of sand. Stability problems within the scour hole can cascade to failure problems of nearby flood defences. The stability depends on the forces acting on the grain. The flow velocity and mass of the other grains are the acting forces, which should be lower than the shear stresses. The porosity of the sand determines these shear forces. Depending on the shear force various failure mechanisms can be observed. A redistribution of the grains from loosely packed sand to a denser package leads to a reduction in the shear stresses. This causes a density flow and the slope fails.

This failure mechanism happens at micro scale and may lead to macro scale instability. However, another failure mechanism which can be observed is the sliding of entire sections. This is in the theory of dike stability often explained as macro instability.

The Scour Manual HOFFMANS AND VERHEIJ (1997) further describes an empirical formula which describes the stability of the upstream slope of the scour hole. With the velocity and particle parameters the angle at the upstream edge can be determined. This formula is based on the equilibrium profile of the scour hole.

2.4.2 Transport of non-cohesive grains

All explained theories describe the movement of non-cohesive grains. However the top layer consist of clay/peat fractions. Cohesion binds the particle together which increases the critical shear stress. During abrasive erosion the flow scrapes the grains off. Large forces are needed to initiate motion of the clay particles. The process is slow and depends on the properties of the medium; temperature, PH-level, etc. The heterogeneous

soil structure in combination with the various flow properties makes it hard to calculate the abrasive erosion. Appendix B.4 discusses two formulas to calculate the critical shear stress.

The clay/peat layer can also erode due to pulling off fractions (block-failure). Erosion of the sand and undermining of the top layer might form cracks. These cracks and weaker parts may lead to failure of larger lumps of the layer. Especially at the end of a layer, such as the edge of the scour hole, these processes may appear. Some dots in Figure 2.2 may suggest that fractions of the poorly erodible top layer are caught in the scour hole.

2.5 Recapitulation

During the investigation of the field data three scour holes in the area were chosen to represent the scour problem. These scour holes were simplified into one scour hole which represents the problem (prototype). The scour hole is formed between poorly erodible layers which determine the length of the scour hole. The scour depth in the field is ≈ 1 time the water depth. The scour hole is located in an intertidal area. During ebb the river discharge dominates the flow in the rivers, while during flood the direction of the flow reverses.

Although multiple scour situations are described in the literature none describes the scour of the given problem. An analyses of these standard situations was made. The scour depth was calculated with the Breusers method. The chosen standard situation describes the flow behind a sill with a bottom protection (used a sill height $D = 0$ m). The location where the bottom protection ends corresponds with the upstream slope of the scour hole, assuming the poorly erodible layer functions as a bed protection. Calculations with these formulas give larger depths than is observed in practice.

Differences between the prototype and the standard situation are:

- There is no limitation of length in the formulas which are used to calculate the scour problem, while the downstream edge of the prototype is fixed by the poorly erodible layer. The scour hole develops over a limited length which leads to steeper slopes in order to reach the same scour depth. These steep slopes decrease the transport of sediment by bed load and thus the depth of the scour hole.
- The Breusers formula calculates the scour depth with a constant flow velocity. However, large variations in flow velocity are measured during a tidal cycle. A test with an adapted formula was made to indicate the influence of these changes in velocity. This showed that the tidal effect can be included by a reduction factor to the maximum flow velocity.

Laboratory experiments were carried out to investigate the influence of the variations between the prototype and the standard situation. This is explained in the next chapter.

Chapter 3

Physical Model

3.1 Introduction

The prototype situation and the available theories of scour are described in the previous chapter. Only an indication of the dimensions of a scour hole could be made. The methods to calculate the scour are made for a couple of standard situations. The prototype differs from these standard situations, still these calculation methods were used to indicate the scour depth. The influence of differences between prototype and the known theory is discussed qualitatively. Laboratory experiments were executed to investigate the development of scour with a limited length.

3.2 Model set-up

The physical model investigation has been executed at a flume of TU Delft. The flume has a length of 14.3 m and a width and height of 0.4 m. The size of the flume limited the experiment to investigate only two-dimensional processes in the flume. An extended description of the model set-up is given in Appendix D. This section is a summary of the model set-up.

Figure 3.1 shows the set-up of the experiment. A sand bed of 0.25 m was placed to initiate scour. The water depth in the flume was 0.13 m. This directly showed one of the limitations of the flume; the height. In order to maintain sufficient measurement accuracy the water depth of physical models had to be at least 0.1 m. At the same time a rule of thumb described a scour depth of 2 times the water depth (0.26 m). Although the calculations with the time depended Breusers formula showed shallower scour holes (up to 0.13 m after 8 hours for $u = 0.7$ m/s), it was chosen to work with the 2 times the water depth. Consequently, the options to vary the water level were limited as were the variations in the calculated scour depth (after 8 hours). That is why a constant water depth was chosen. Another consequence of the high bed and the relatively small water depth were the large Froude numbers. Flow velocities up to 0.6 m/s were used to study

the development of scour, which correspond with a Froude number of 0.53. The Froude number in the field is 0.13, thus a lower Froude number was preferred.

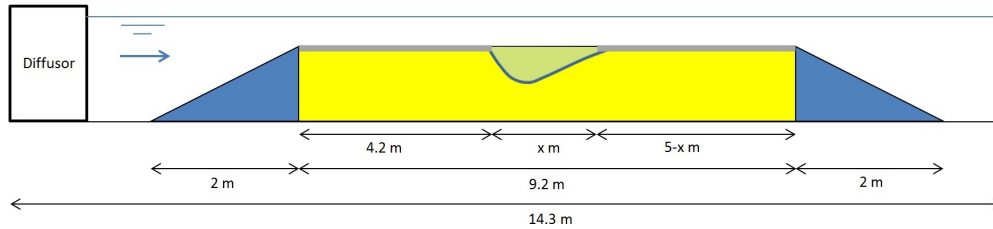


Figure 3.1: Sketch of the model set-up.

It was decided to use steel plates (5 mm thick) to represent the poorly erodible layers. The roughness was created by gluing grains on top of these plates. The decision to use steel plates resulted in a stiffer top layer than in the field. The advantage of the stiff plates was that it clearly showed the undermining. Further, the transition between sand and poorly erodible layer was hold constant over width and time. Another advantage was that the undermining was not reduced by deformation of the top layer. If this layer deforms it might behave as a falling apron.

The reason that clear-water scour conditions were investigated was based on two principles. The first principle was that clear-water scour shows a geometry which is purely caused by the flow regime. Secondly, the information of the amount of transported sediment in the field was limited and difficult to scale.

An short overview of all the experiments is shown in Table 3.1.

3.3 Results

3.3.1 Calibration of the experiment

Run 1 & 2, initiation of motion

These experiments were carried out to investigate the initiation of motion of the grains. This was visually compared with the stages of particle movement in the Shields diagram as described by Delft Hydraulics (1969), see Section 2.3.3. This experiment was executed to verify the calculated critical velocity at which sediment transport starts. Table 3.2 shows the calculated values, while Table 3.3 shows the results of the experiments.

The results of Table 3.3 were used to determine the Shields parameter. A value of $\psi = 0.04$ was found. While executing the experiment all the measurement instruments were tested. Another advantage of the experiment was that it helped to understand the principles of initiation of motion.

Table 3.1: Overview of the experiments.

Run	Velocity (m/s)	Distance between plates (m)	Description
1	0.00 - 0.37	-	Initiation of motion
2	0.00 - 0.32	-	Initiation of motion
3	0.00 - 0.60	-	Roughness
4	0.40	-	Breusers
5	0.55	-	Breusers
6	0.60	0.1	Fixed length
7	0.60	0.2	Fixed length
8	0.45	0.2	Fixed length
9	0.45	0.5	Fixed length
10	0.45	1.0	Fixed length
11	0.45	0.10 - 0.55	Movement each hour
12	0.40	0.10 - 0.45	Movement each half hour
13	0.40	0.5	Reversed flow direction
14	0.50	0.5	Reversed flow direction
15	0.50	0.5	Two day run
16	0.50	0.5	Fixed angled plate downstream
17	0.60	0.5	Fixed angled plate downstream
18	0.65	0.5	Course bed
19	0.80	0.5	Course bed
20	0.5	0.5	Fixed length

Table 3.2: Parameters of the sand.

Sand	d_{50} (μm)	D_*	ψ_c	u_c (m/s)
Silica M32	260	6.58	0.015 - 0.04	0.16 - 0.26

Run 3, bottom roughness

The influence of the friction in the flume was observed in the third experiment. The roughness of the plates generated friction which is a loss of energy. When the flow velocity decreased the value of Δh increased. With the Chézy formula the roughness of the bottom was derived for several flow velocities.

$$u = \sqrt{\frac{g}{c_f}} \sqrt{hi} \quad \rightarrow \quad u^2 = \frac{gh}{c_f} \frac{\partial h}{L} \quad \rightarrow \quad u^2 = \frac{gh \partial h}{u^2 L} \quad (3.1)$$

With this formula, the angle of the flume was determined which cancelled the acceleration/deceleration of the flow. This was used to generate a uniform flow in the flume.

Table 3.3: Flow velocity and the observed phase of motion from the Shields diagram, see Figure 2.9.

Velocity		Stage of bed movement	
m/s	Bed	Bed behind slope	
0.07			
0.16			
0.18			1
0.19	1		2
0.22	3		3
0.24	3		4
0.26	4		6
0.28	6		7
0.30	7		
0.32			

3.3.2 Main experiments

Run 4 & 5, Breusers scour hole

The set-up of these experiments is similar to the situation described by Breusers for scour behind a protection. The results of these experiments were compared with the results from the past in order to validate the set-up of the experiment. This limits the chance of error in the desired experiments.

The first 4.2 m of the sand bed were protected by steel plates (4.2 m is needed to form a fully developed flow regime). Downstream of this protected area sediment transport started to form a scour hole. The flow velocity was higher than the critical velocity and a scour hole according to the theory was formed. Downstream of the scour hole the erosion lowered the bed. The bottom friction and turbulent effects created large dunes which slowly travelled downstream.

Figure 3.2 shows the development of the scour hole over time. Within the first minutes the Breusers scour hole was formed, which further increased in size. The development of the scour hole followed the description from the Scour Manual (HOFFMANS AND VERHEIJ, 1997). It divides the development of scour into 4 phases. The first phase (initiation) is seen within the first time step of 5 minutes and is a mix of bed load and suspended sediment transport. Until 50 minutes the development phase (2) was clearly observed. The ratio between scour depth and length of the hole stays constant during this phase. Suspended transport significantly decreased due to a decrease in flow velocity (larger depth). The measurements after 3 and 7 hours showed correspondence with the second and third phase. The development of the scour hole starts to decrease and the

scour hole starts to stabilize in the third phase. Due to a short run time a stable phase (equilibrium) was never reached.

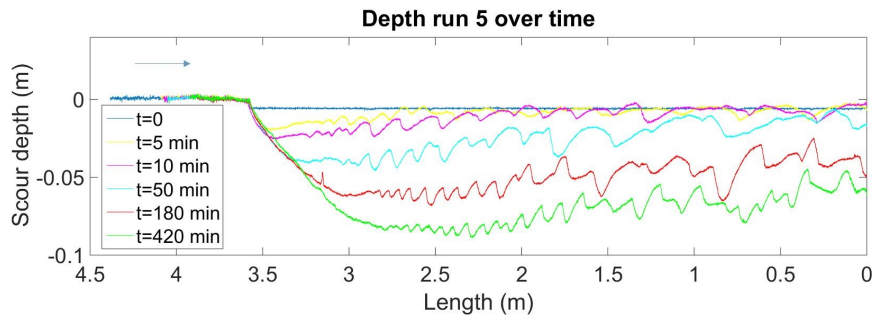


Figure 3.2: The development of the scour from run 5 over time in hours.

Run 6 - 10, scour hole with fixed length

Steel plates covered the bed downstream of the scour hole, during the experiments with a fixed length of the scour hole. This left a section of 0.10 - 1.0 m (depending on the experiment), where the sand was not covered and scour could develop. An overview of all the runs has been given in Table 3.1.

The development of the scour hole over time was described by four phases. The first phase corresponded with the first phase of the Beusers theory. The scour started directly behind the upstream plate and generated a mix of bed load and suspended sediment transport. The difference between the transport capacity and the actual transport is large at the upstream edge. Further downstream, a dynamic equilibrium situation was reached and dunes started to form. The influence of the plate downstream was limited. The sand dunes covered this edge, see Figure 3.3.

Due to wall friction and other turbulent effects the transport of sediment was irregular and dunes were formed behind the deepest point of the scour hole. These dunes slowly translated downstream and remained stable after passing the downstream edge of the scour hole, creating dunes on top of the plates.

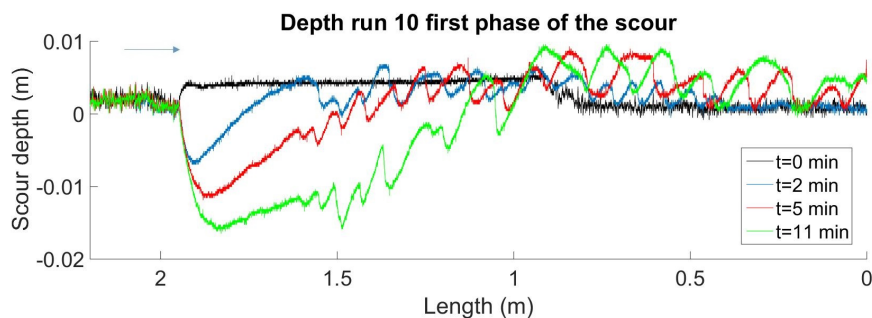


Figure 3.3: Scour of the hole in the first minutes is similar to the know Beusers development.

The scour hole still increased in depth during the second phase. The deepest point moved downstream and the angle of the upstream slope stayed constant. Consequently, the length of the scour hole increased and the downstream edge of the scour hole moved towards the edge of the plate. The dunes formed on the downstream slope were not completely able to translate over the edge of the plate, see Figure 3.4. The trough of the dune was lower than the edge. Turbulent effects initiated by the sharp edge started the undermining of the plate. However, the dune was able to fill the undermined area and the top of the dune translated over the steel plates. The graph of Figure 3.4 shows the two lines. A dune which translates over the edge is shown by the blue line (at the length = 0.95 m), where the red line shows a trough at the edge. The abrupt decrease of the depth of the red line at the edge shows the limitation of the measurement instrument. The laser measured the depth below the instrument and was not able to measure under the plate. An instant decrease of the depth (vertical line) shows the end of the plate, indicating that the slope of the scour hole ended below this edge.

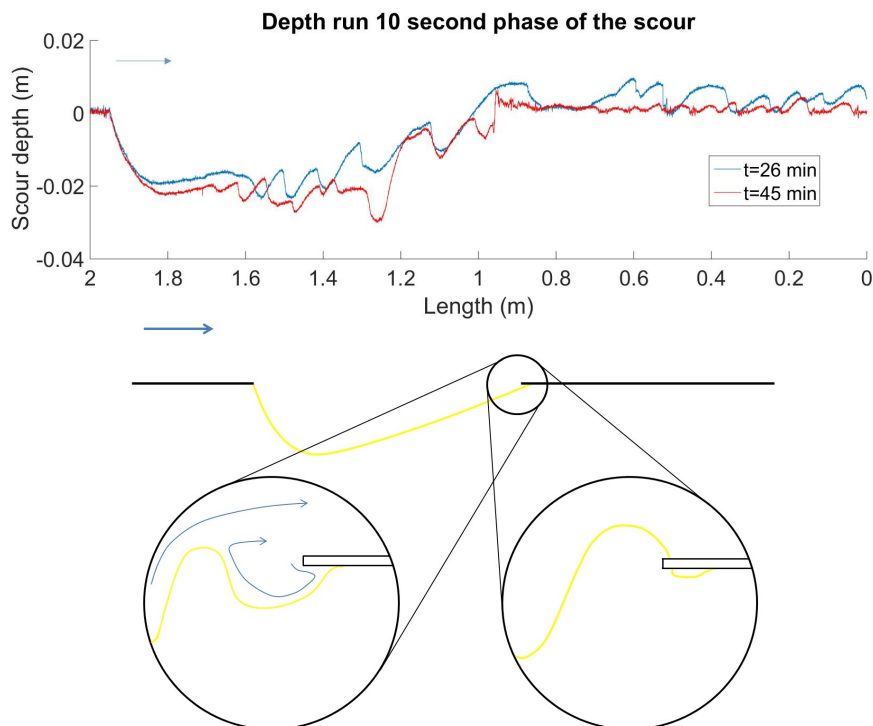


Figure 3.4: Scour during the second phase of the process dunes hit the edge of the downstream plates.

During the third phase, the top of the dune was not able to translate over the edge of the plate. However, the dunes still influenced the scour process which caused undermining. When the trough of the dune was at the edge of the steel plate the undermining was rather large. If the top of the dunes was in front of the edge, it

functioned as a ramp and directed the flow over the steel plates, see Figure 3.5. This slowed the undermining down.

Three-dimensional effects started to occur due to friction, return currents and other turbulence effects. This caused an irregular dune front and a mix of dune tops and troughs in front of the edge led to a mixture of turbulent flows under the steel plates.

Note: since the dunes never reach the edge of the steel plates, all transport was in suspension.

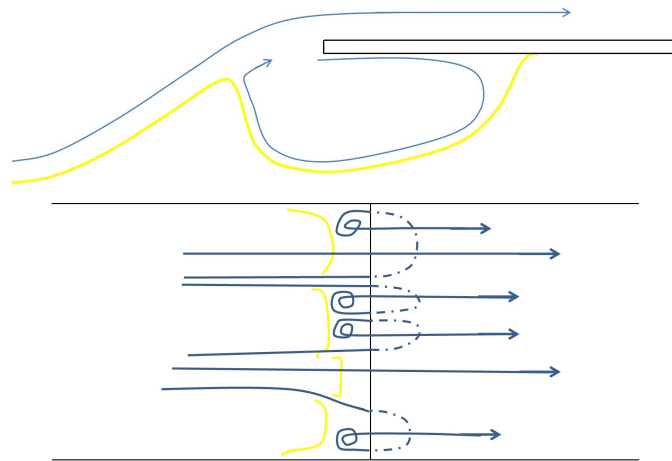


Figure 3.5: Undermining in the third phase, side and top view.

Where the dunes influenced the development of undermining in the third phase, were the dunes too low to hinder the undermining process in the fourth phase. The undermining developed rapidly in time and interacted with the scour hole. The slope and dunes between the scour hole and the undermined area decreased and disappeared in time.

The resulting velocities in the middle of the flume were, due to wall friction, higher than at the sides. A part of the flow went under the plate and hit the sand below. The mass balance tells that the flow which enters the undermined area, has to leave as well. The flow left the scour holes at the walls, creating vortexes. This flow in upstream direction was highly turbulent and changed from the left wall to the right wall and back. These vortex flows mixed with the main flow, creating whirls. This process is shown in Figure 3.6.

The sediment was dominated by suspended transport. Plumes of sediment were observed which were forced by the whirls. This changed the geometry of the scour hole. This differs with the transport in Breusers scour hole experiments, where in the middle of the flume the highest transport was due to the high flow velocities.

The depth of the scour hole still increased during this phase, but the rate of this development in depth decreased. Similarly, the downstream movement of the deepest

point decreased.

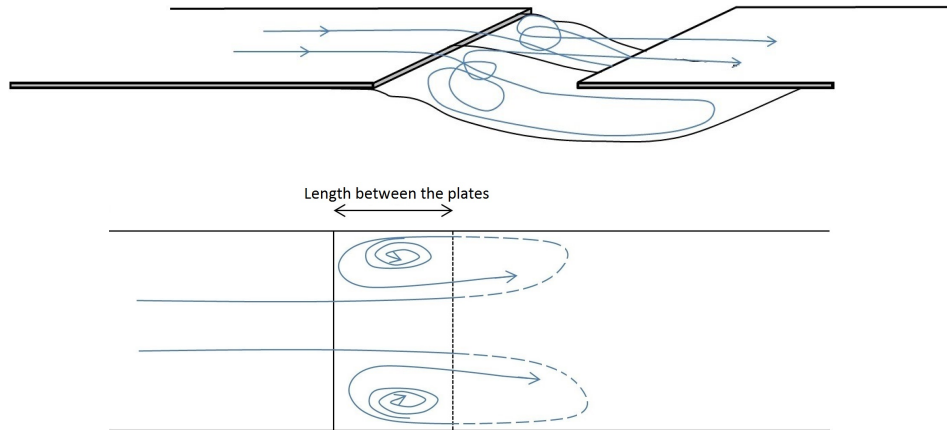


Figure 3.6: Streamlines of observed flow in the scour hole: 3D and top view.

Run 11 & 12, scour hole with an increasing length

The undermining in the previous runs was rather large. However, this amount of undermining was never observed in the field. The poorly erodible layer would fail due to this extensive undermining. Large lumps of this layer break off, which was simulated in these experiments by pulling the plates backwards. The plates were pulled backwards after each hour in run 11, while this has been done after half an hour in run 12. More criteria to move the plates were proposed in advance; for example after a certain length of undermining. But the rapid development of undermining in the first minutes made the execution hard. An entire set of measurements took at least half an hour and a quicker retreat of the downstream plate was impossible. The initial length between the plates was 0.1 m. The undermining after the first hour was rather small. As the scour hole increased in side, the reaction to the increase in size was much quicker.

The idea behind these experiments was rather logical, since the degradation of this layer results in a larger scour length. However, an increase of scour length does not change the scour process. Eventually the undermining starts all over. The observed processes did not result in new insights of this undermining and it was decided to stop these experiments.

Run 13 & 14, scour hole with reversed flow conditions

The flow velocities in the field are far from constant. The tide has a large influence on the flow velocity and even changes direction. This may have large consequences on the development of scour, however the flume can only flow in one direction. The only

solution to generate flow from the other direction is to rotate the scour hole itself 180 degrees. In run 13 and 14 the development of the scour hole under a reversed flow was investigated. Since the scour holes in the field never showed extensive undermining, it was decided to start with a scour hole without undermining.

Figure 3.7 shows the development over time. Three processes were observed in the reversed scour hole. The first process was similar as seen before; the undermining. The scour hole at the start had a sharp transition at the downstream edge. The sand was unprotected and thus directly eroded.

The second process was the redistribution of sand. The initial upstream slope was much steeper than observed in the previous experiments (and Breusers calculations). The flow separated at the upstream edge and formed a recirculating eddy at the slope, see Figure 3.8. The main direction of the flow at the bottom is upstream which transported sand upstream and decreased the steepness of the slope.

The third process describes the translation of a bar in the scour hole. The eddy which caused the undermining transported the sand upstream to the reattachment point. The mean flow velocities were lower around the reattachment point and the sand started to cumulate forming a bar. The process described in the second process takes sand from this bar. The bar slowly translated upstream as the upstream slope became gentler. During this translation the bar became smoother and vanished before it could reach the upstream edge.

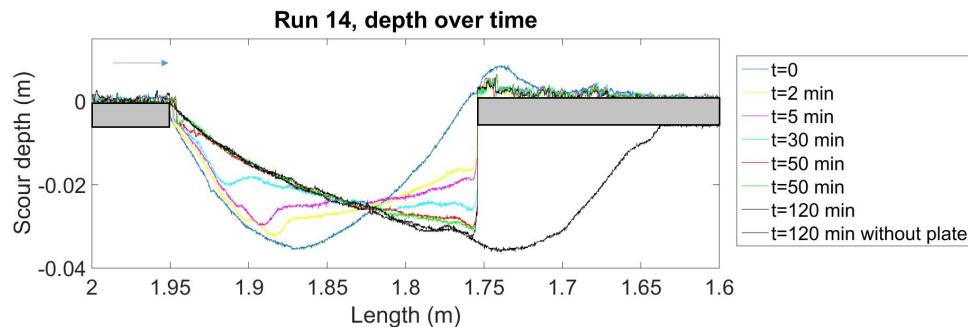


Figure 3.7: Run 14, development of the scour hole over time.

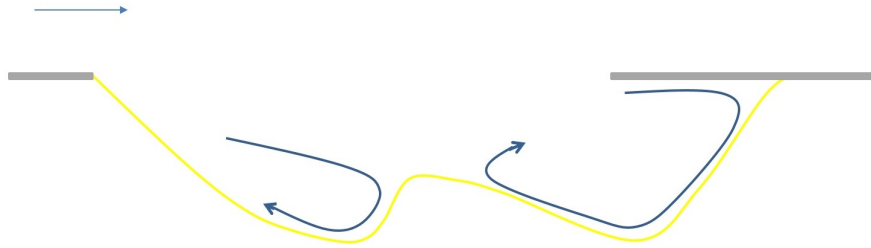


Figure 3.8: The flow line in the scour hole responsible for the redistribution of the geometry.

Run 15, two-day run

A run of two days was carried out to investigate the development of scour after a longer run time. It was assumed that the profile of the scour hole should develop in the same way as had been observed in run 7, see Figure 3.12. The longer running time showed a slow decrease of the sediment transport, but the depth and undermining length still developed.

Run 16 & 17, with a fixed downstream slope under an angle of 45 degrees

Undermining to the extent of the model was never observed in the field. To prevent undermining, the downstream slope in run 16 & 17 was protected by one of the steel plates. The steel plate was attached to the steel plates downstream and placed under an angle of 45 degrees. This is shown in Figure 3.9. This set-up represents a downstream slope which is protected by the poorly erodible layer.

Initially, the similar scour process as in the previous runs was observed. Once the downstream slope of the scour hole reached the scour hole, the dunes behind the scour hole disappeared. Instead of the dunes the plate now worked as a ramp and redirected the flow out of the scour hole. Since the plate hindered the undermining the geometry of the scour hole changed as well, see Figure 3.10. A trough was formed at the toe of the plate.

Furthermore, attraction of the flow towards the middle of the scour hole was observed. In all the experiments the velocity in the middle of the flume was higher, but turbulent flows made it hard to observe. At the sides the wall friction was higher and decreased the flow velocity. The higher flow velocities in the middle resulted in a larger scour depth. Following MOSSELMAN AND SLOFF (2002) this would attract a larger water volume, because the larger depth has a smaller bed friction on the water column.

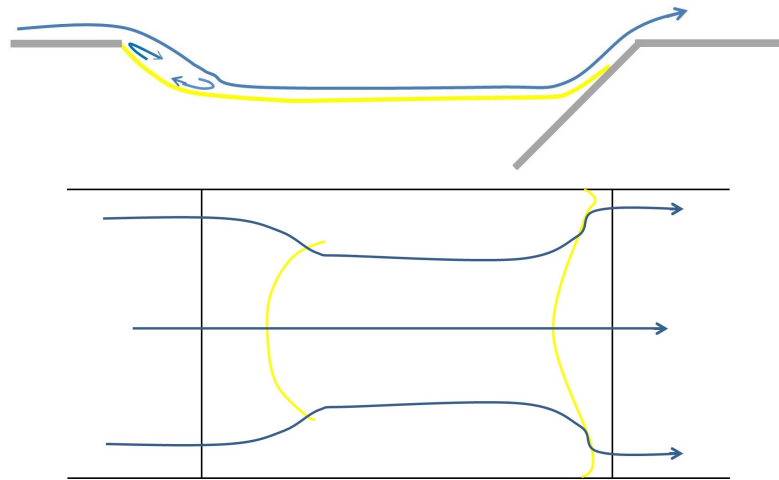


Figure 3.9: The flow in the scour hole during runs 16 & 17.

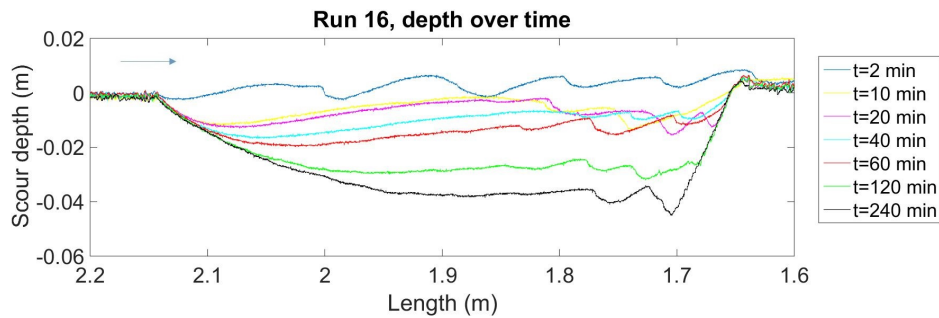


Figure 3.10: The development of the scour depth over time of run 16.

Run 18 & 19, runs with a coarser bed

The scour depth was small and the upstream slope rather gentle. A set of experiments with a coarser grain was proposed to indicate the differences. The parameters of the coarser grain are shown in Table 3.4.

Table 3.4: Parameters of the sand.

Type	d_{50} (m)	D_*	ψ_c	u_c (m/s)
Filter gravel	0.002-0.004	50-100	0.03-0.08	0.65

A disadvantage of these coarse grains was the high velocity, which was needed to initiate motion. Since the water level could not be raised, the Froude number, which was already high, was raised further.

Run 19 was stopped after a quarter of an hour. The pressure in the pores increased with the high velocity. The larger pores also increased this pressure further downstream

in the sand layer. The steel plate became unstable and the experiment was stopped.

Run 20

Run 20 was a similar runs as in experiments 6 - 10. This experiment was executed to gain more data of the flow velocity in the scour hole.

3.4 Analyses

3.4.1 Comparison

Figure 3.11 shows the results of the Breusers experiment and the fixed plates within one graph. The development of scour was in the first minutes comparable (green and red line). However, the plates downstream of the scour hole already influenced the scour process within 6 minutes. The downstream slope was steeper than in the experiments without the plates. These plates slowed down the sediment transport. After 6 hours the influence of the plates was clearly visible. The plate protected the sand layer and limited the scour length and depth. The graph also shows a similar angle of the upstream slope. Thus, the set-up of the model had no influence on the upstream slope of the scour hole.

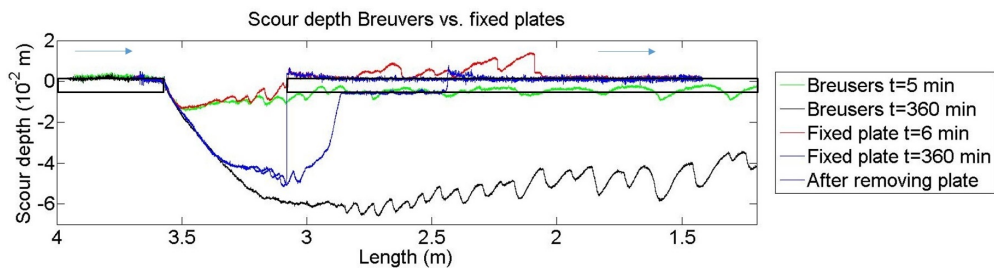


Figure 3.11: Development of the scour hole, where the results of the Breusers experiment are in the same graph as the results of the experiment with fixed plates.

Figure 3.12 shows the final measurements of two experiments. The first graph shows a scour hole with a gap between the the plates of 0.2 m (run 7). After 5 hours, the scour hole and the undermining merged into a smooth geometry. The scour hole still developed in depth and width, but the shape is assumed representative for the equilibrium situation.

The second graph shows a scour hole with a gap of 1.0 m (run 10). The dunes in the scour hole indicate that the scour hole was not as far developed as on the graph of run 7. The deepest point is in the middle of the scour hole, while this point is under the plates in run 7. This is probably caused by the state of development.

Experiment 15, which ran for 13 hours showed no other differences in the scour process than seen in run 6 - 10, see Figure 3.13. The rate of transport decreased in

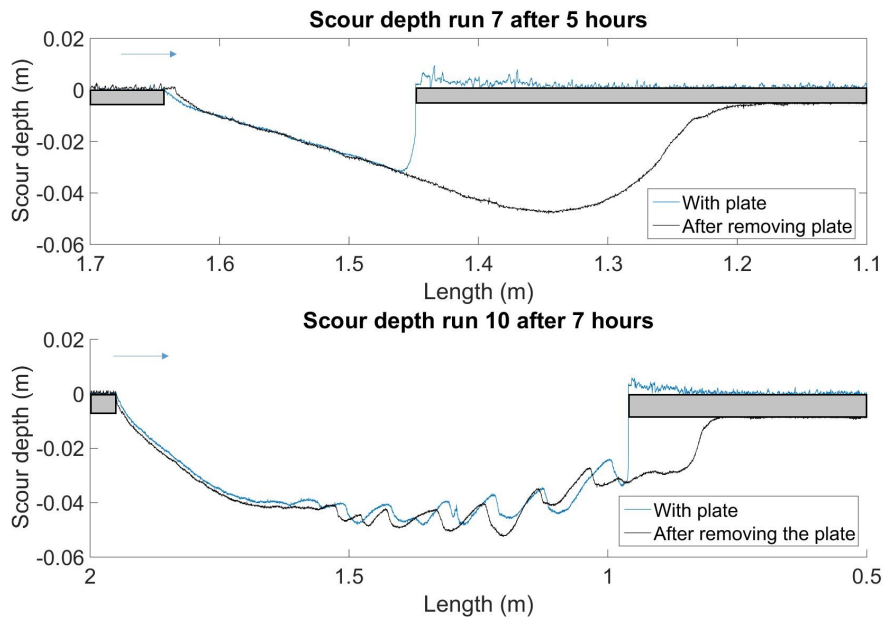


Figure 3.12: Final scour depth of run 7 and 10 at the end of the runs.

time and the shape of the scour hole became stable. All the dunes disappeared over time resulting in a smooth profile. The experiment showed large sediment plumes in the whirls forced by the return flow, even after 13 hours.

The shape of the geometry of this scour hole is comparable with the shape of Figure 3.12. The length of the scour hole seems to determine final shape of the scour hole. An initially steep gradient of the upstream edge slowly flattens. The deepest point in the scour hole is in the final situation below the plates. After 13 hours running the depth of the scour hole still increased.

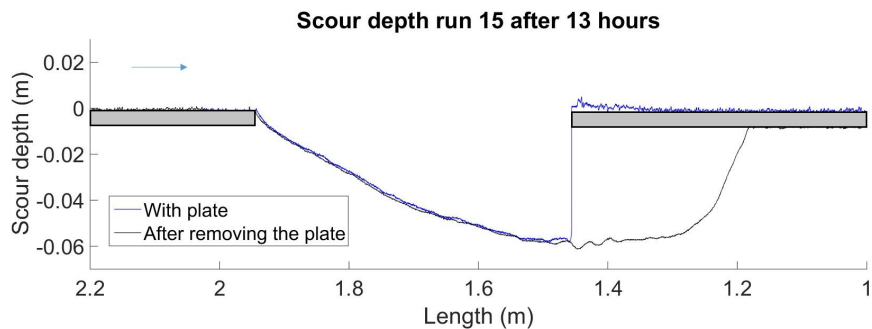


Figure 3.13: Final scour depth of run 15 after 13 hours.

Figure 3.14 shows the difference between a scour hole with a protected and unprotected downstream slope. The blue line shows the scour hole with the protected slope, while the magenta line shows the unprotected slope after 4 hours. To show the under-

mining the geometry after 6 hours with undermining was added. Again the upstream slope of both models was similar. And even the depth after 4 hours was comparable. The experiments differed in the geometry over the width. The highest sediment transport rates were found in the middle of the flume in run 16. This is logical, since the highest velocities are in the middle of the flume. However, the largest transport rates in run 20 were at the sides of the flume. The undermining causes a return flow and the generated return flow causes large turbulence effects which dominate the flow.

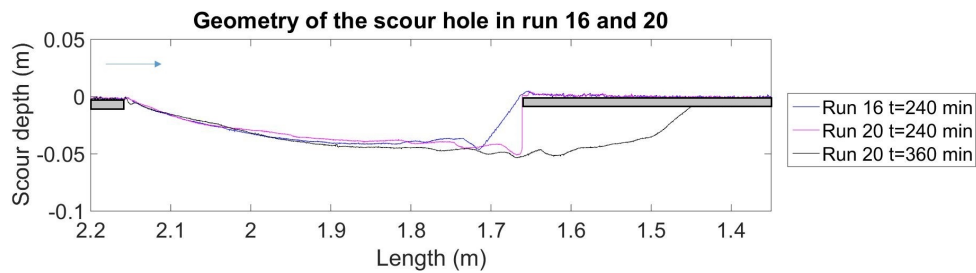


Figure 3.14: Geometry of the scour holes in experiments 16 and 20.

The runs with a coarser bed did not lead to a different result than seen with the fine sand, see figure 3.15. The scour hole could not reach large depths since the mass of the grains was larger. Increasing the flow velocities was not possible. The high velocity of run 19 even cause vibrations of the steel plates. To prevent dangerous situations the run was stopped. The porosity of the grains made the formation of dunes impossible. This led to gradual development of the scour depth in which only two phases were observed. The first phase corresponded with the first phase of finer grains. The scour hole developed without any influence of the downstream plates. Once the scour hole extended to the plates downstream, undermining started. Due to the absence of dunes this corresponds with the fourth stage of the fine sediments.

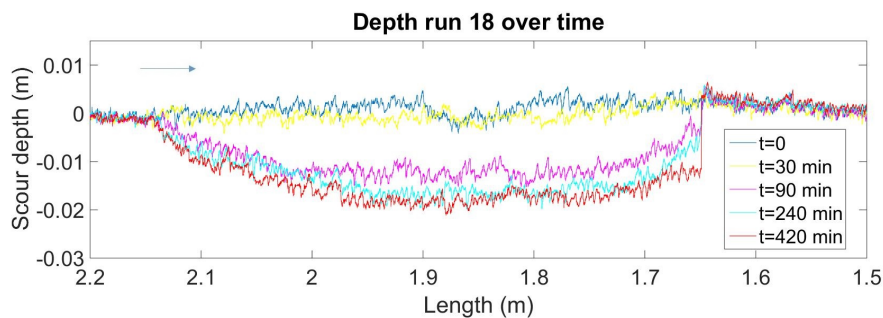


Figure 3.15: Scour depth of run 18 over time.

3.4.2 Breusers formula

Run 4 & 5 The measured depths after 7 hours is shown in Figure 3.16. The depth of both scour holes was beforehand calculated with the time depended Breusers formula,

Equation 2.13. Initially a value of $\gamma = 0.4$ was assumed. A flow velocity of $u = 0.40$ m/s gave a scour depth of $y_m = 0.035$ m (run 4) and $u = 0.55$ m/s gave $y_m = 0.088$ m (run 5). These values roughly correspond with the observed scour depths.

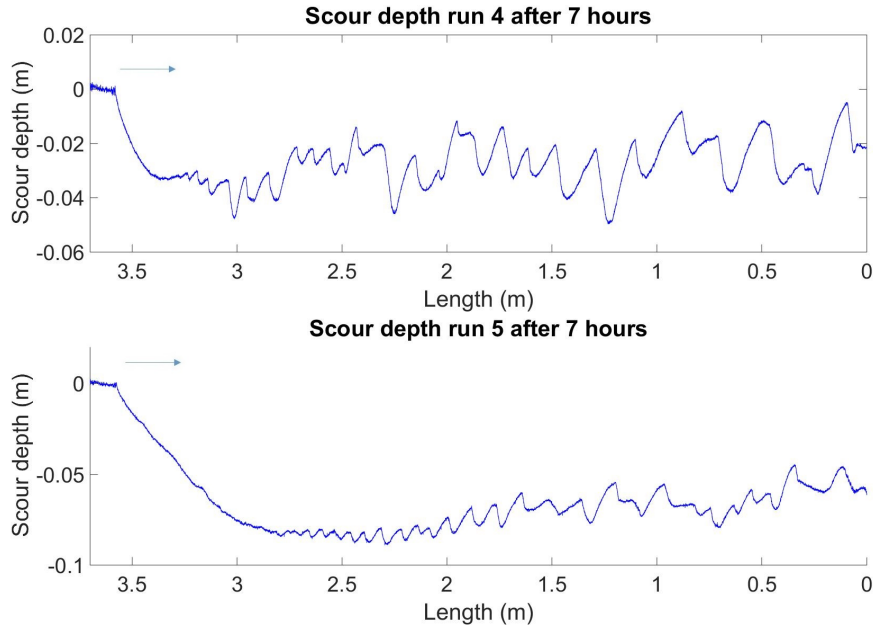


Figure 3.16: Depth at the end of the run 4 ($u = 0.4$ m/s) and 5 ($u = 0.55$ m/s).

The measured depth of the scour hole was used to determine the γ value. To obtain this γ , log-log graphs of the scour depth over the water level and the time over the characteristic time were made, see Figure 3.17. Breusers used these graphs to describe the relation between the scour depth and the time by the coefficient γ , see equation 2.13. Curve fitting gives $\gamma \approx 0.37$.

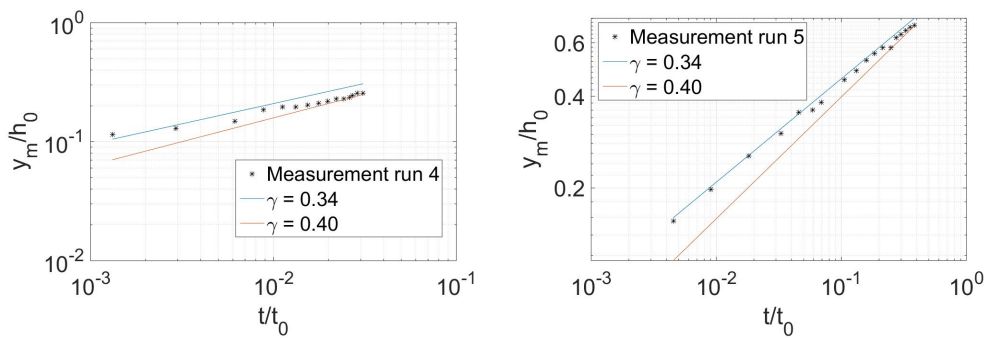


Figure 3.17: Maximum scour depth as function of time.

Run 6 t/m 10 Similarly to the previous runs, graphs to determine γ were made. Figure 3.18 shows the graphs of run 9 and 10. A value of $\gamma = 0.36$ was initially found, which is similar to the value of the Breusers scour holes. The influence of the plates downstream was thus small. The curve started to deviate from the $\gamma = 0.36$ line once the undermining started. The γ value increased and seemed to become stable around $\gamma = 0.43$. The time scale becomes larger, which means that the development of the depth decreases. In the literature the value of $\gamma = 0.36$ corresponds with two-dimensional flow conditions while $\gamma = 0.43$ corresponds with three-dimensional flow conditions. Observations of the flow regime with dye showed an increase of turbulence (three-dimensional flow condition) once the undermining started.

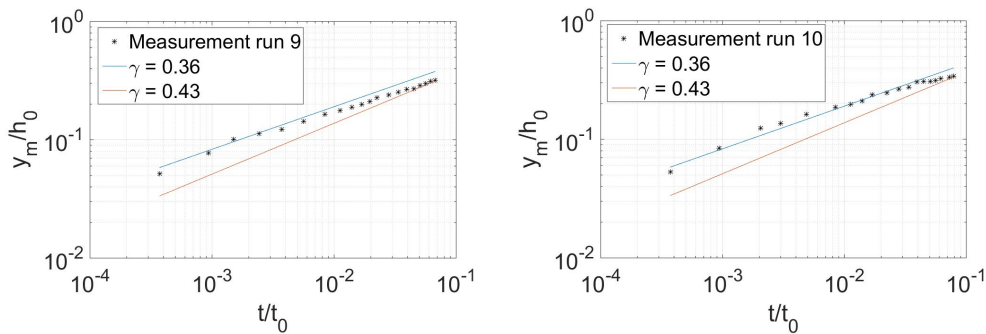


Figure 3.18: Maximum scour depth as function of time.

Translating these results back to the physics does the graphs show the initial development as if there is no limitation of the length of the scour hole. Once the scour hole extends to the plate the development is shifted back to a gentler development of scour. The new formulation ($\gamma = 0.43$) describes scour holes which is less deep. However, curve of development still followed logarithmic distribution.

The characteristic time in the Breusers formula was assumed to be a constant. However, the change in sediment transport from a mix of suspended and bed load to only suspended load changes this characteristic time. In the determination of the characteristic time the critical velocity (resistance) was subtracted from the flow velocity (load), see Equation 2.14. Grains which roll over the bed (bed load) are described as transport. Once the scour hole is undermined, the grains could not leave the scour hole without being moved upwards by the flow and only left the scour hole in suspension (large loads needed).

The decrease in scour depth which is shown in Figure 3.18, is probably caused by an increase of the characteristic time step instead of γ . A first step to include this effect in the characteristic time is described in E.

3.4.3 Flow velocity in the scour hole

Figure 3.19 shows the flow velocity in the scour hole with a fixed length of 0.5 m. A velocity profile was made each 0.1 m. The blue lines show the time averaged flow

velocity. The flow velocity at the surface was high, the decrease of flow velocity due to the increase in depth was hardly noticed at the surface. The flow velocities at the bed decreased with the increase of depth. A mixing layer was formed around $z/h_0 = 0$. The red and magenta lines show the mean velocity with 3 times the standard deviation. This shows the deviations of the velocities. Where the mean velocity is always positive these standard deviations show negative values which correspond with the tops of the return currents at approximately 0.005 m of the bed.

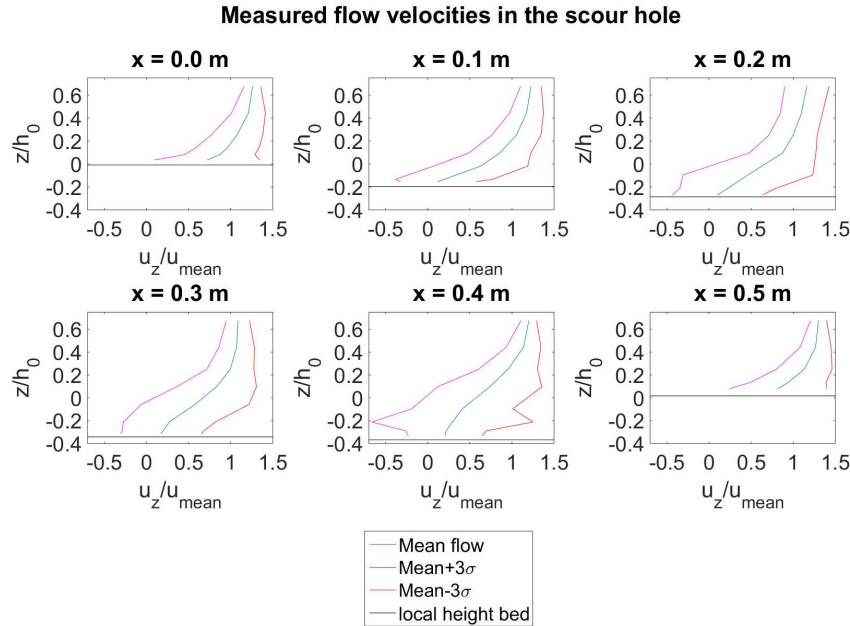


Figure 3.19: The flow velocity in a scour hole with a fixed length of 0.5 m.

The influence of the flow velocity on the development of scour is shown in Figure 3.20. The lines show the scour depth, calculated with the Breusers method (which corresponds with the values of runs 4 and 5), while the markers show the measured values. The runs differ in flow velocity. The difference between the calculated value and the measurements is in both experiments more or less similar. This indicates that the influence of the velocity on the development of scour with a limited length small is.

3.4.4 Influence of the length of the scour hole

Figure 3.21 shows the development of the scour depth over the time. The flow velocity was constant $u = 0.45$ m/s and only the length between the plates was changed. The black line gives the theoretical scour depth as calculated with the Breusers formula (without length limitations). The markers show the measured scour depths in the experiment. The shorter the length in between the plates the larger the deviation from the theoretical formula.

Figure 3.22 shows the relation between the scour depth and the length between the

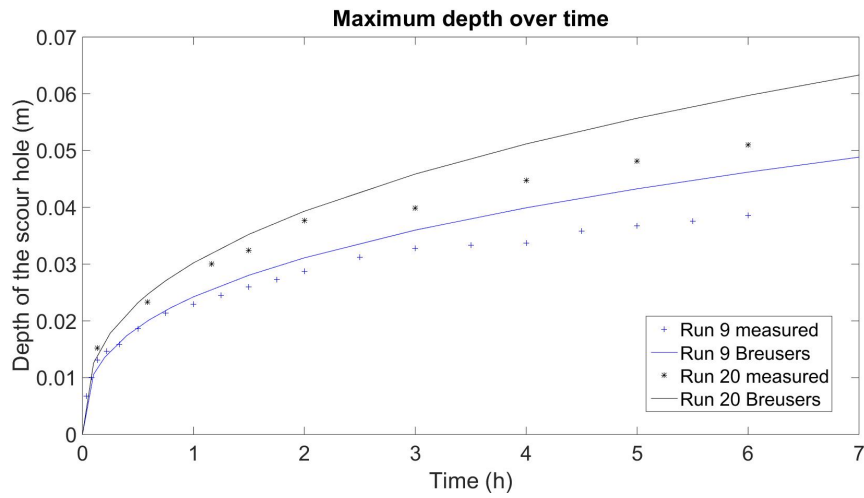


Figure 3.20: The scour depth of the experiment compared with the Breusers values. In run 9 is $u = 0.45$ m/s and run 20 $u = 0.5$ m/s, gap between the plates is 0.5 m.

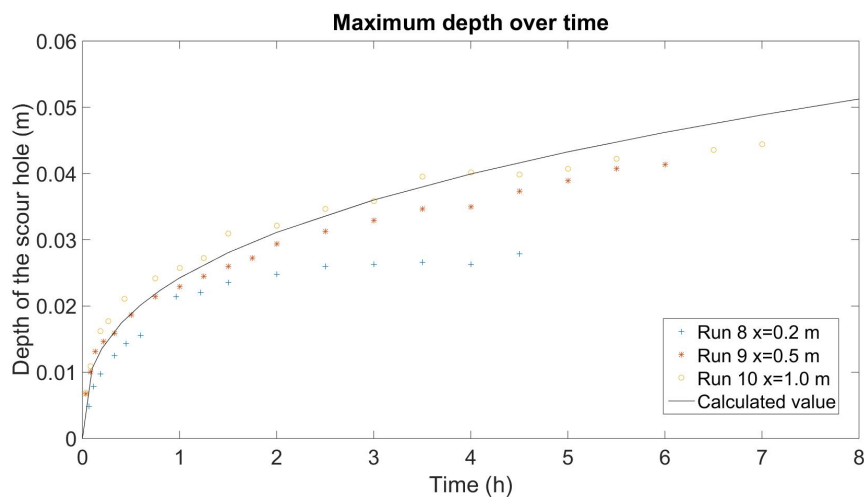


Figure 3.21: The scour depth over the time with different distances between the plates. The flow velocity $u = 0.45$ m/s.

plates. As the length of the scour hole (length between the plates) increases, the increase in scour depth decreases.

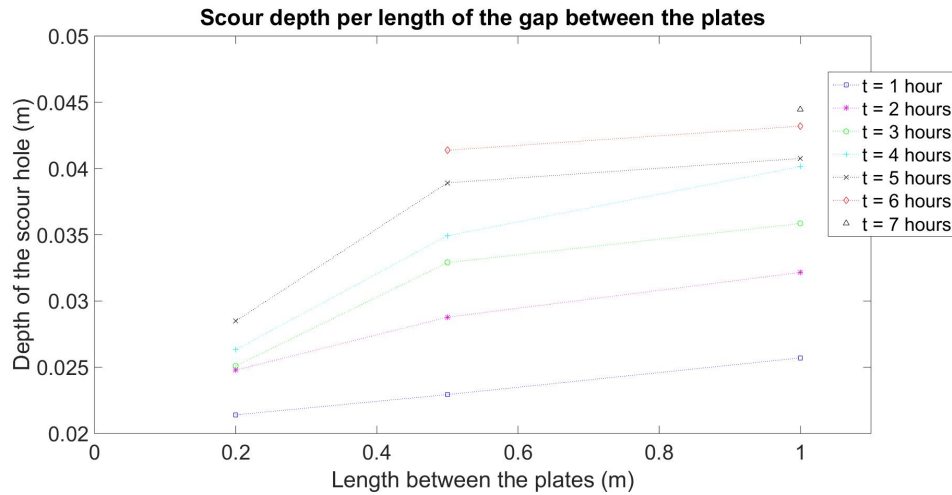


Figure 3.22: The scour depth per distance of the plates. The flow velocity $u = 0.45$ m/s.

3.4.5 Angle of the upstream slope

The angle of the upstream slope of the scour hole can be calculated with Equation B.5 of Appendix B.3.2. The formula gives $\beta \approx 11.7^\circ$ ($u = 0.40$ m/s) - 13.9° ($u = 0.55$ m/s). β is the angle of the slope at the edge of the scour hole. Deeper in the scour hole, this value slowly decreased. The calculated values of β correspond with the observed slope in the physical model.

3.5 Discussion

3.5.1 Influence of the poorly erodible layer in the field

The previous section analysed the results of the experiments. These results were compared with the known theories to describe scour. This section discusses the results in a more qualitative way to find the connections and deviations with the field.

The scour hole of the experiment with a fixed length between the plates develops in the first phase in accordance with the Breusers theory. Unfortunately, a lack of data from the prototype situation makes it hard to verify this process.

Undermining was important in all the other stages of the scour process. However, undermined sections to the extent of the model were never observed in the field. The poorly erodible layer probably fails before undermining takes place. This layer can fail in two ways. The layer could crumble and lumps of clay are eroding. This is simulated

in runs 11 and 12. These runs show that the development of the hole is pushed back, but still continues. If this happens, no equilibrium or stable condition can be found. The scour holes continuously develop in depth and eventually the entire river bed will be lowered. However, not all scour holes lead to a lowered bed. Some scour holes seem to be able to reach a stable condition. The investigated scour holes are in the category 'stable scour hole'.

The poorly erodible layer may fail as well by deformation. As it deforms this layer covers the sand below and protects it from further degradation. This type of protection is called a falling apron. As the layer deforms, the edge of the poorly erodible layer enters the scour hole and becomes part of the slopes. The transition between the sand and poorly erodible layer is within the scour hole, where the velocities are lower. Thus erosion decreases and the scour hole develops to a stable situation.

This proposition is purely hypothetical and never observed in the field, although some suggestions are found. Ideally, field measurements should be used to test these hypotheses. Field investigation of the soil structure of the slopes of the scour hole may help to verify the hypotheses. Another option to test the soil structure at the scour holes is execution by numerical models of laboratory investigations. A prediction of the soil structure, based on the shear stresses, can determine the type of soils at the edges and slopes of the scour hole.

If this theory is valid, it means that further development depends on the stability of the material of the slopes. This could be calculated with geo-technical models. A scour hole can be stabilized at the slopes instead of filling the entire scour hole.

Another proposition which explains the stabilisation of the scour holes is the variety in thickness of the poorly erodible top layer. Currently, not much is known about the poorly erodible layer. But it is probable that thicker parts alternate with thinner parts. Older river bed cut through this layer and even lowers its strength. The poorly erodible layer breaks at the thinner parts while the thicker parts limit the length of the scour hole.

3.5.2 Tidal influence

A flow from the reversed direction was introduced in runs 13 and 14. The sediment in the scour hole was redistributed and changed the steepness of the up- and downstream slope. It showed that the return currents are able to reshape the scour hole in up- and downstream direction. The transport of sediment by the river may strengthen this self-recovering ability. If material is added at one place in the scour hole, the redistribution spreads the added material over the entire hole.

Furthermore the experiments only showed undermining of the downstream slope. The reverse of flow direction causes undermining at both sides of the scour hole, which explain growth in length in both directions.

3.6 Recapitulation

A physical model investigation was carried out to study the influence of the poorly erodible top layer downstream of the scour hole. Steel plates with an added roughness are used to represent the clay/peat layer. These plates are placed on top of a sand layer and after the flow adapted to the roughness conditions the plates stop abruptly. The sand underneath is not covered anymore and the bed erodes which is the beginning of the scour hole. Since no sediment is added one can speak of clear-water scour. The investigated models are:

- A fixed non-erodible layer downstream of the scour hole. The length over which scour can develop has been varied during several runs.
- A non-erodible layer which has been moved after a certain time step.
- The influence of a two-directional flow on the geometry. An experiment with a flow from the reverse direction has been carried out. This represents the tidal flow.
- An experiment with a fixed non-erodible layer which was placed under an angle of 45 degrees.
- Influence of grain size of the erodible material by using gravel.

This gave the following results:

- Initially, the plates downstream had no influence on the development of the scour hole. The scour hole was directly formed at the end of the upstream plate and increased downstream in length. Once the fixed layer downstream has been reached, undermining of this layer started to interact with the scour hole described by Breusers.
- The undermining of the steel plate downstream generates highly turbulent return currents which determine the sediment transport. The sediment transport by bed load is stopped, while plumes of suspended sediment left the scour hole.
- The models with a fixed length approached an stable shape of the scour hole. The initially formed dunes slowly disappeared, while the deepest point of the scour hole slowly translated further downstream. The scour depth and the length of the scour hole were still developing at the end of the experiments.
- The poorly erodible layer downstream of the scour hole decreases the maximum scour depth.
- If a disturbance was added to the geometry of the scour hole the flow tended to flatten this. The dunes were formed in a scour hole and travelled in downstream direction. These dunes fill the gaps as they travel downstream. At the same time, return currents were also able to transport the grains in upstream direction.

- Experiments with a flow from the reverse direction showed that the scour hole reshaped its geometry. A bar slowly travelled upstream and increased its width while it reduced its height until it disappeared. This experiment was carried out in clear-water scour conditions which deviate from the field where sediment transport is dominant. This reduces the influence of the bar on reshaping the geometry of the scour hole.

The experiments proved that the Breusers formula overestimates the scour depth. The formula is valid for the initial development of the scour hole. Once the length of the scour hole is limited by the poorly erodible layers at the edges of the scour hole, the formula starts of to overestimate the depth.

The true behaviour of the downstream edge was not simulated in the experiment. The steel plates were too stiff which caused extensive undermining. The results suggest that the poorly erodible layer deforms once it is undermined and covers the sloped like a falling apron. This stabilizes the scour hole.

Chapter 4

Numerical model

4.1 Introduction

The observed scour process of the experiments was in the third phase simulated with a computational model. This model should be able to describe the flow, morphology and geo-technical processes. However, a program which is able to simulate all these processes is currently not available. Based on the observed scour process it was decided to focus on modelling the flow at the scour hole. Loads induced by the flow determine the morphological and geo-technical processes. Thus once forces induced by the flow are derived, these can be used as indication of the transport of sediment.

Deltares (SLOFF *et al.* 2012b) made a computational model of the entire Rijnmond Area with Delft3D. This model gave satisfying results for the overall river morphology. However, less accurate results were obtained at the scour holes. A lack of data of the flow at these scour holes made it hard to verify these local problems. A more detailed model of the Schuddebeursedijk Scour Hole has been modelled in Delft3D with two different grids (z and σ layers). These models gave entirely different flow fields, which couldn't be validated without measurements of the field. Several modelling programs were investigated to model simulate the flow at scour holes. FINEL3D has been chosen, since it was already used to simulate the flow of a scour hole in the Western Scheldt.

This part of the thesis was executed at Svašek Hydraulics, which developed FINEL3D and made the simulation of the scour holes in the Western Scheldt.

Work plan

The experiments of the previous chapter suggest that the poorly erodible layer deforms before the layer is undermined. This means that the upper parts of the slopes are protected by this layer. 3D model simulations were made to validate this assumption. The shear stresses at the scour holes were investigated to indicate the development of scour.

First, simplified models were made to verify the flow regime at the scour holes. These

2DV models simulate two experiments which were modelled with various turbulence models. The results of these 2DV models were used in the 3D model.

4.2 2DV models

4.2.1 FINEL3D

FINEL3D is a solver for fully 3D, non-hydrostatic shallow water flow and transport processes based on the Finite Element Method. It uses a triangular flexible mesh, which gives the possibility to increase or decrease the number of grid cells per section. During the research the number of grid cells was increased at the scour holes.

Several turbulence models are available in FINEL3D, of which four were tested by simulating two different laboratory experiments.

4.2.2 Model set-up

Simulations of two different laboratory experiments were made and verified by the flow conditions. Four different turbulence models were tested and compared with the measurements of the experiments. The following experiments were simulated:

- Experiment 17; scour hole with fixed downstream slope. This experiment was modelled because: the model showed low transverse velocities (those are not included in the 2DV simulations). The model further showed a larger geometrical resemblance with the scour holes in practice, than the models with undermining.
- Experiment 20; scour hole with undermining. This model was chosen to verify the flow conditions during undermining.

Computational grid

Measurements from the experiments were used for the set-up of the simulations. The final measurements of the sand bed were used as input of the bathymetry. The steel plate overhanging the undermined area (of experiment 20) was removed to measure the bathymetry. This plate was manually added in the set-up of the model.

The flume was tilted during the experiments, which was included in the models. The bottom roughness on top of the plates had a Nikuradse roughness $k_s = 0.006$ m. The sand in the scour hole had a lower roughness $k_s = 0.0006$ m.

Once the geometry had been determined, the computational grid could be created. A general grid with a triangle size of 0.01×0.01 m² was chosen. The grid size was decreased to get a higher resolution at the scour hole (point of interest). The grid size at the scour hole was 0.005×0.005 m². To create a smooth transition between the two grids a third field was introduced with a grid size of 0.008×0.008 m². The grids are shown in Appendix F.

Boundary conditions

The boundary conditions of the model were determined from the laboratory experiment. The upstream boundary condition related to the discharge of the pump. A discharge of $q = 0.078 \text{ m}^2/\text{s}$ corresponds with the average velocity of 0.6 m/s in experiment run 17. The discharge of experiment 20 was $q = 0.065 \text{ m}^2/\text{s}$ ($u = 0.5 \text{ m/s}$). At the downstream boundary the water level was set on $h = 0.13 \text{ m}$.

Courant number

The Courant number is often used to determine the time step. There is no stability criterion for momentum advection and viscosity terms, since an implicit Euler scheme is used for the momentum equations. However, an explicit pressure correction step imposes a stability criterion on the Courant number. The Courant number is given by:

$$\sigma = \frac{u\Delta t}{\Delta x} \quad (4.1)$$

At first a small Courant number was tested; $\sigma = 2$. With the smallest grid size of $0.005 \times 0.005 \text{ m}^2$ the corresponding $\Delta x = 0.007 \text{ m}$. However, the computational model became unstable at the upstream boundary. This is a known problem of the program, which is related to the application of the explicit pressure correction combined with a Dirichlet water level boundary condition, and which becomes sometimes problematic for small time steps.

A time step of $\Delta t = 10 \text{ s}$ was chosen to calculate the steady state situations of the simulations. This corresponds with a $\sigma = 857$ for experiment 17 and $\sigma = 714$ for experiment 20. Smaller time steps were tested but led to instability. These large Courant numbers are acceptable for stationary computations.

4.2.3 Turbulence closure models

Turbulence in Hydraulics (UIJTTEWAAL, 2003) describes the most common used applications in turbulence modelling. In principle, all well-posed flow problems can be solved by the Navier-Stokes equations. These equations have to be discretized on a numerical grid in order to be solved. However, the calculation time in combination with the present technology, forces the grid to be too coarse to include the smallest scale eddies. Various turbulence models have been developed to calculate the low properties on a coarser grid. These models are based on the Reynolds-Averaged Navier-Stokes (RANS) equations which smoothen the flow over the domain. The penalty is that information about the time dependent fluctuations is lost. To close the RANS equations for a coarse grid, additional equations have to be added. In this research four turbulence models were tested. The theory behind these models follows from CHRISTIAN AND CORNEY (2004).

Constant eddy viscosity

The first turbulence model is based on a constant eddy viscosity. This model can be applied if the variation of the flow field and turbulence conditions over the vertical is limited. For a flow field close to uniform channel flow, the constant eddy viscosity can be determined by taking the average value over the water depth (assuming a parabolic eddy viscosity profile and a logarithmic velocity profile):

$$\nu_v = \frac{1}{6} \kappa u_* h \quad (4.2)$$

In which κ is the Von Kármán constant (0.4) and the bed shear velocity u_* is determined iteratively by the White Colebrook equation:

$$\frac{u}{u_*} = 5.75 \log \left(\frac{12h}{k + \delta/3.5} \right) \rightarrow \delta = 11,6 \frac{\nu}{u_*} \quad (4.3)$$

This gives a $u_* = 0.043$ m/s and $\nu_v \approx 4 \cdot 10^{-4}$ m²/s for the prototype. The constant eddy viscosity to close the problem is the simplest model available. However, of all researched turbulence models, it is the most unrealistic one.

Bakhmetev mixing length model

The Bakhmetev mixing length model follows the hypothesis of Prandtl's mixing length which is used to describe the distribution of the turbulence viscosity. This viscosity is described by the mixing length l_m and a characteristic velocity based on the main velocity gradients.

$$\nu_v = l_m^2 \sqrt{\left(\frac{\partial u}{\partial z} \right)^2 + \left(\frac{\partial v}{\partial z} \right)^2} \quad (4.4)$$

Bakhmetev has described the mixing length for open channel flow by:

$$l_m = \kappa z \sqrt{1 - \frac{z}{h}} \quad (4.5)$$

Here is h the water depth and z the vertical coordinate measured upwards from the bed.

In fact, the Bakhmetev mixing length model is a special case of a k - L model (see next subsection), if in Equation 4.7 all terms are neglected except the local production and dissipation term (P and ϵ).

k - L Model

The k - L model is a one-equation model in which the turbulent kinetic energy (k) is determined by a simplified transport equation, which can be derived from the RANS equations. The k - L model determines the turbulence viscosity using the quantity k and the prescribed mixing length as given by Bakhmetev, see Equation 4.5.

$$\nu_v = c'_\mu \sqrt{k} L \quad (4.6)$$

Here is c'_μ an empirical coefficient which is determined by calibrating the model ($c'_\mu = 0.55$) and L is the characteristic length scale of the turbulent motion which corresponds with l_m . L is empirically determined by the Bakhmetev Equation 4.5 and results in a parabolic profile for the viscosity field. The transport equation to determine k is derived from the Navier-Stokes equations, see the equation below.

$$\frac{\partial k}{\partial t} + (\vec{v} \cdot \nabla)k = \nabla \cdot \left(\frac{\nu_v}{\sigma_k} \nabla k \right) + P - \epsilon \quad (4.7)$$

With σ which is a turbulence constant and is equal to 1. The buoyancy terms in this formula are neglected since the density is constant. P is the production term for k , which implies the generation of turbulence (P is always positive). This term is equal to:

$$P = \nu_v \sqrt{0.5 S_{ij}^2} \quad S_{ij} = \frac{\partial u_i}{\partial x_j} + \frac{\partial u_j}{\partial x_i} \quad (4.8)$$

Where S_{ij} is the velocity gradient tensor. The dissipation of the turbulence is represented by ϵ which is given as:

$$\epsilon = c_d \frac{k^{\frac{3}{2}}}{L} \quad (4.9)$$

Where c_d a dissipation with the value 0.16.

$k - \epsilon$ Model

The $k - \epsilon$ is a two-equation model, which uses transport equations for both the turbulent kinetic energy (k) and the dissipation rate of the turbulent kinetic energy ϵ . The transport equation for ϵ has a more empirical character than the transport equation for k (which has a physical basis in the RANS equations). The total $k - \epsilon$ model is formed by equation 4.7 and by the following two equations for ν_t and ϵ :

$$\nu_v = c_\mu \frac{k^2}{\epsilon} \quad (4.10)$$

$$\frac{\partial \epsilon}{\partial t} + (\vec{v} \cdot \nabla)\epsilon = \nabla \cdot \left(\frac{\nu_v}{\sigma_\epsilon} \nabla k \right) + c_{1\epsilon} \frac{\epsilon}{k} P - c_{2\epsilon} \frac{\epsilon^2}{k} \quad (4.11)$$

The values of the coefficients used in the $k - \epsilon$ model were; $c_\mu = 0.09$, $c_{1\epsilon} = 1.44$, $c_{1\epsilon} = 1.92$, $\sigma_k = 1.0$ and $\sigma_\epsilon = 1.3$, CHRISTIAN AND CORNEY (2004). The $k - \epsilon$ model had been calibrated in such a way that application of these standard parameter values will lead to virtually the same result for the $k - \epsilon$ model as for the $k - L$ and Bakhmetev mixing length model for a uniform channel flow situation: that is a logarithmic velocity profile and a parabolic viscosity profile.

4.2.4 Results

Simulations of the experiments show the flow velocities in the scour holes. An example of the horizontal flow velocity is shown in Figure 4.1. This simulation was made with

the constant eddy viscosity. The flow velocity upstream of the scour hole was constant and the flow started to diverge once the depth increased. The spread of the flow velocity over the depth resulted in an increase in the water level. This increased water level was clearly visible since the Froude value was relatively high.

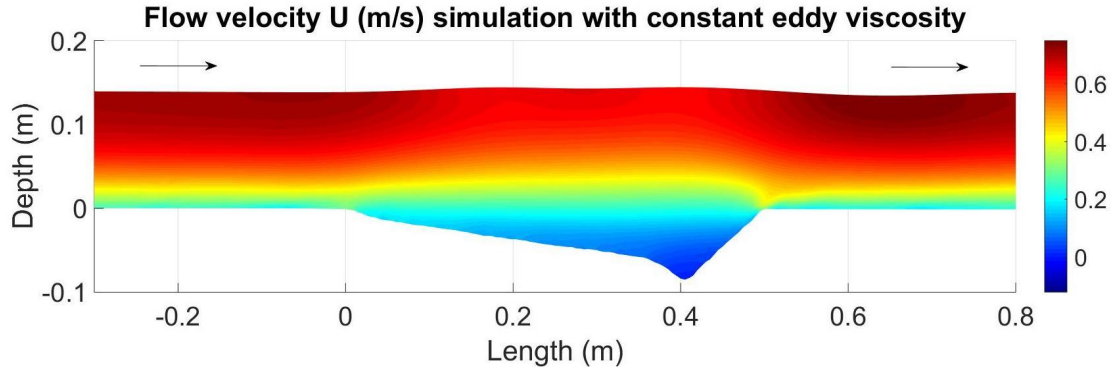


Figure 4.1: The flow velocity in the longitudinal direction of experiment 17 computed with constant eddy viscosity.

Figure 4.2 shows the velocities in the vertical direction. At the upstream slopes the velocity was slightly increased (dark blue colour). This corresponds with the spread of velocity which has been seen in Figure 4.1. At the downstream slope the velocity increased with its peak just before the edge (red colour).

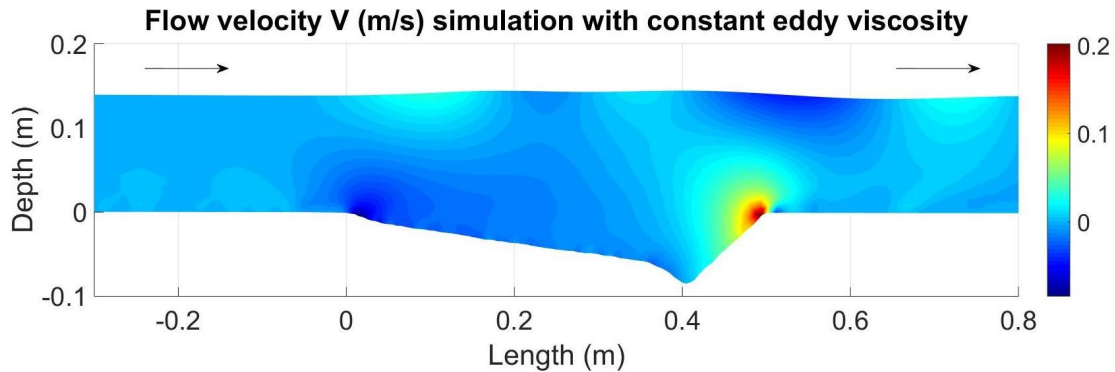


Figure 4.2: The flow velocity in the vertical direction of experiment 17 computed with constant eddy viscosity.

Experiment 20 has been modelled similarly to 17. The resulting flow velocities are shown in Figure 4.3. Although the depth of the scour hole was less deep, the velocities at the bottom were smaller. The velocity under the plates rapidly decreased due to the formed eddies. Unfortunately, it was impossible to measure the velocities below the plate during the experiments. Only visual observations of the flows below the plate were made by adding dye to the flow. This clearly showed three-dimensional turbulence structures

in the scour hole, see Figure 3.6. However, a 2DV simulation of the experiment was modelled which means that these effect could not be included.

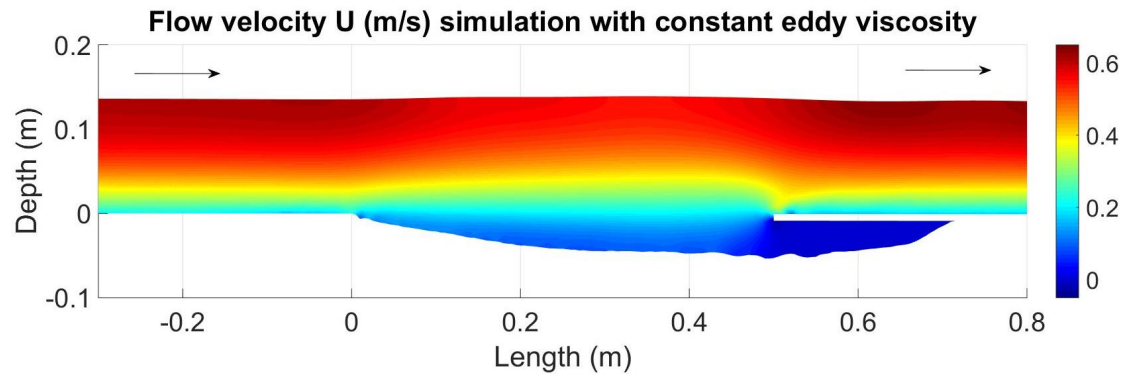


Figure 4.3: The flow velocity in the longitudinal direction of experiment 20 computed with $k - L$.

Similar simulations were made for each turbulence model. These models are compared with each other and measurements of the experiments. The Figures of these models can be found in Appendix F.

4.2.5 Analyses

As already described in the model set-up, the model was tested with multiple turbulence models. These models are compared with the measurements from the experiments in this subsection. Figure 4.4 shows the longitudinal velocity profiles of the simulations at various locations in the scour hole. The measurements of the experiments are shown as markers. There were no measurements at the surface. The measure device had to be fully submerged in the water. The highest level at which the velocity could be measured was 0.10 m above the bed.

The first graph ($x = 0$) shows the velocities at the upstream edge of the scour hole. The velocity profile is slightly influenced by the negative vertical velocity. Large variations between the turbulence models were seen. The $k - \epsilon$ model appeared to be the least accurate model which is far too diffusive.

The following graphs show the profiles in the scour hole with a step of 0.1 m. The graphs show that the constant eddy viscosity profile is the best approach of the measurements. This method fits the experiments best.

Figure 4.4 shows a similar graph for the simulations of experiment 20. Again the $k - \epsilon$ model is too diffusive and does not follow the measurements. The other models show a similar behaviour. The Constant eddy viscosity overestimates the velocity at the surface, while the Bakhmetev mixing length and the $k - L$ models show a little lower velocity at the surface. The Bakhmetev mixing length and $k - L$ model fit the results better than the constant eddy viscosity.

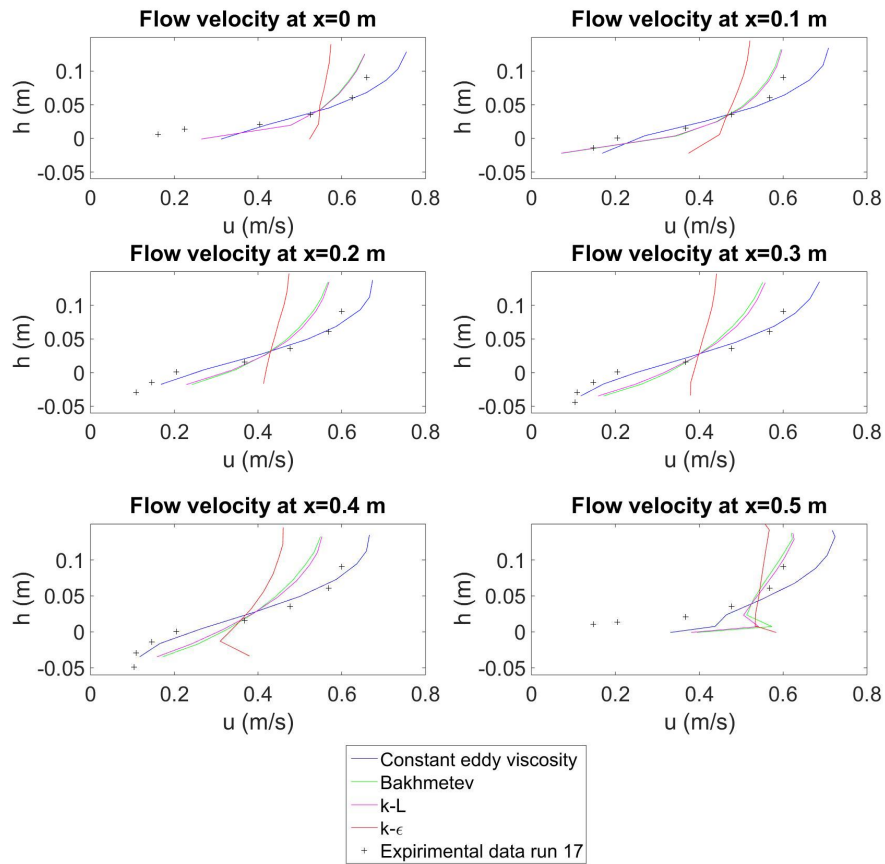


Figure 4.4: Flow velocities over the depth of the simulations and the data of the experiment 17.

4.2.6 Discussion

Experiments 17 and 20 were tested with four turbulence models. There were large difference between the turbulence models as has been observed in the previous subsection. The constant eddy viscosity is the best fit for experiment 17, while the $k-L$ model was the best for experiment 20. Comparing these scour holes with the holes in practice, experiment was assumed to 17 represents the geometry. In practice no undermining was observed, which determines the scour process in experiment 20. That is why the constant eddy viscosity is assumed to give the best solution for the scour problems.

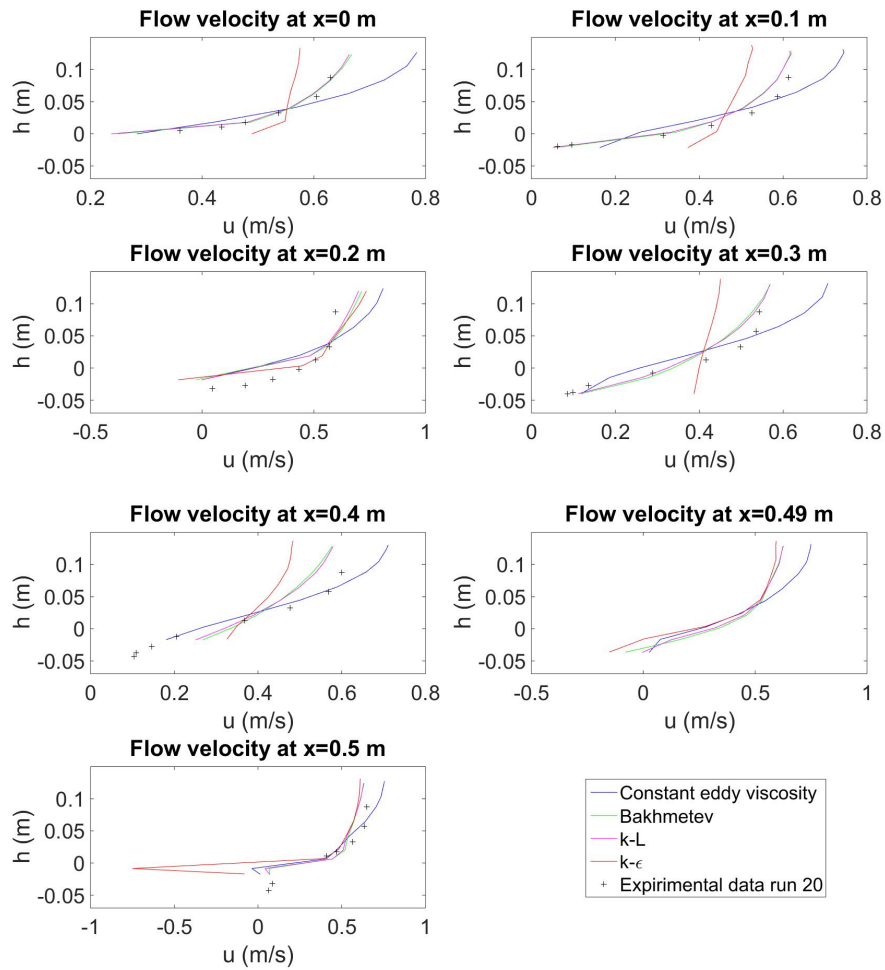


Figure 4.5: Flow velocities over the depth of the simulations and the data of experiment 20.

4.3 3D model, Scour holes in the Oude Maas and Spui

The previous section showed the dominance of the turbulence model on the flow field in a scour hole. The decision of turbulence model for the simulation appeared to be of large importance. The 'simple' models gave the most accurate results in the 2DV models, but this does not imply that these models lead to the best results in a 3D model. The four turbulence models were applied to a 3D model of the Oude Maas and Spui in this section.

It was decided to model the Oude Maas and Spui Rivers. A 3D model of the experiments should be possible, but desires a large adaptation to the modelling program. However, the advantage of modelling the experiments is the data to verify the results. Nevertheless it has been chosen to model the rivers in the field. The experiment showed different processes than observed in the field. The gained knowledge from experiments and the previous models was used to indicate the development of the scour.

4.3.1 Model Set-up

The model (see Figure 4.6) consisted the Oude Maas from its connection with the Dordsche Kil till the Spijkenisse Bridge and the Spui River. The Spui River starts at the Haringvliet Lake and conflues with the Oude Maas at Old-Beijerland. In this river stretch several scour holes can be found. In this model the focus is on the Berenplaat Scour Hole, but the Poortugaal and Schuddebeursedijk Scour Holes are also included (see Chapter 2.2).

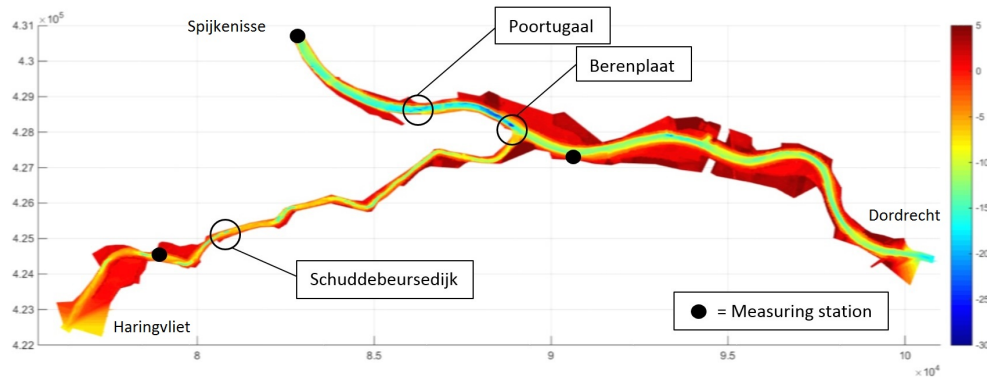


Figure 4.6: Bathymetry of the rivers in the in the model including measurements stations and points of interest. The bathymetry is a combination of the multibeam measurements and AHN maps.

Initially, the model was made to calculate the tidal flows. However, time limitations resulted in steady state simulation. This is the reason that for example the flood plains were included although they were never flooded.

First the horizontal grid was determined. This was carried out by drawing the rivers in Google Earth. This geometry was processed in Matlab to make a horizontal triangular

grid. The grid size in the rivers was $30 \times 30 \text{ m}^2$. This grid size was decreased to $7 \times 7 \text{ m}^2$ at the scour holes and the transition between these grids was made in gradual steps. Figure G.1 of Appendix G shows a detail of the grid at the scour hole Berenplaat.

Documents which contain the bathymetry, bottom roughness and number of cells over the vertical were combined within the solver. The bathymetry of the river was made from the multibeam data of 2012 while the floodplains were made with AHN maps. A constant value of the bottom roughness was determined for four sections; Spui, Oude Maas before the connection with Spui, Oude Maas after the connection and the floodplains.

The river was modelled with 6 cells over the vertical which was decreased at the shallower sections (flood plains) to 1 cell. At the scour hole the number of cells over the vertical was increased to 20, see the Figure G.3 of Appendix G. Although the floodplains in the field were dry, the cells in the model had to contain a small film of water. The height of this water film was set at $h_{min} = 0.005 \text{ m}$.

The calculations showed that the number of cells could be reduced by removing the floodplains since these were never flooded. Another reduction in the number of cells could have been made by shortening the Eastern part of the Oude Maas. There were no measurement stations and points of interest in this section.

Boundary conditions

The rivers are influenced by the tidal wave from the connection with the sea by the Nieuwe Waterweg. Due to this tidal wave the flow in the river changes in direction. The first calculations were made with constant flow conditions to set the model. The model develops to a steady state solution. The tide was never included due to time limitations. Model simulations were made for the highest difference in water levels. There is no phase error between water level and the discharge, thus the peaks in the water levels correspond with the high river velocities. During these high velocity is the development of the scour depth large. This is shown in Appendix B.2

The model was tested with two different flow conditions: ebb and flood. The boundary conditions of both situations are shown in Tables 4.1 and 4.2. These boundary conditions were formed with the water levels and velocities of Appendix C.

Table 4.1: Boundary conditions during ebb.

Location	Spui, Bernisse	Dordrecht	Spijkenisse
Boundary condition	$Q = 880 \text{ m}^3/\text{s}$	$Q = 1975 \text{ m}^3/\text{s}$	$h = -0.84 \text{ m}$
Salinity [ppm]	0.7	0.7	0.75

The chosen simulation period was 8 hours. This was sufficient to remove disturbances due to the initial conditions (about 4 - 6 hours).

The boundary conditions deviate from the situation in the field and the model cannot be taken as representative. However the main purpose of the model was to test the

Table 4.2: Boundary conditions during flood.

Location	Spui, Bernisse	Dordrecht	Spijkenisse
Boundary condition	$h = 0.39$ m	$h = 0.82$ m	$Q = 2225$ m ³ /s
	$u = -0.36$ m/s		

hypothesis of the deformed top layers which are assumed to function as a protection of the slopes of the scour hole. Although the model does not represent the field, the model is used to indicate of the assumption is valid in this model.

4.3.2 Results

Initially, the parameters of model were validated with the $k - \epsilon$ model. This turbulence model was used because it is often applied to model large river sections. Three scour holes (Berenplaat, Schuddebeurdsedijk and Poortugaal) were investigated with this model. Top views of the scour holes are shown in Appendix G.

Longitudinal cross-sections including the flow velocities were made. Figure 4.7 shows the velocities calculated with the constant eddy viscosity during ebb $\nu_v = 0.0889$ m²/s for the Berenplaat scour hole ($u = 1.6$ m/s and $h = 12$ m). This is calculated with 4.3, under the assumption of a uniform flow in front of the scour hole. This value was calculated for each scour hole and flow condition.

The model shows drop in flow velocity above the scour hole. The flow velocity in the scour hole slowly increases. Compared with the 2DV models no increase in the water levels could be observed. The larger dimensions and the lower Froude number decrease this effect.

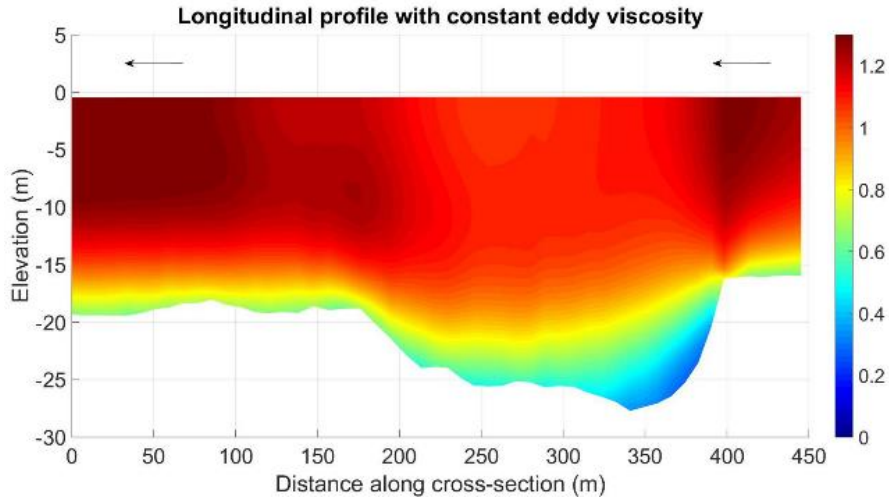


Figure 4.7: Longitudinal velocity profile of the Berenplaat Scour Hole during ebb (m/s).

Figure 4.8 shows the flow velocities during flood. The mean flow velocity during flood was lower, but the velocity profiles were comparable with the profiles during ebb. The gradual slope at the upstream side changed the spread of velocity in the scour hole. The increase of depth lowered the flow velocity. However, the diffusive spread of the velocity increased the velocities in the scour hole. The net result gave a small increase in the velocity along the scour hole. At the downstream steep slope the horizontal velocity was transformed into an increase in vertical velocity.

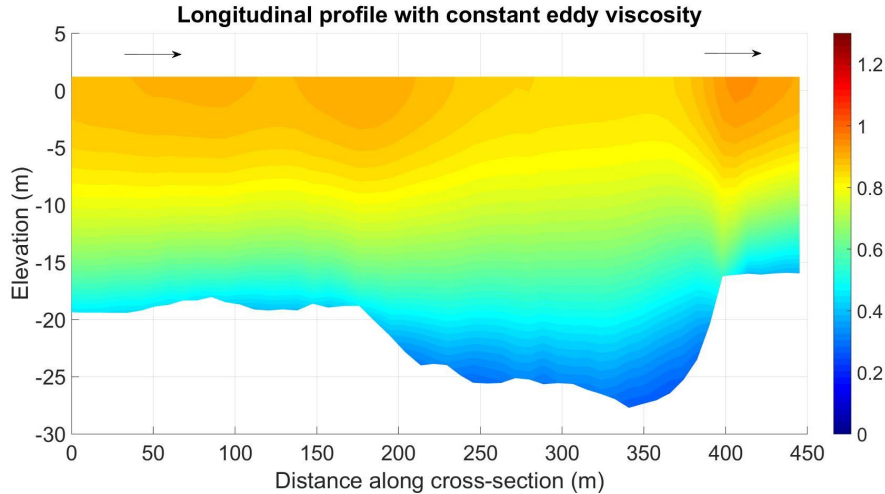


Figure 4.8: Longitudinal velocity profile of the Berenplaat Scour Hole during flood (m/s).

4.3.3 Analyses

The various turbulence models showed the same behaviour as observed in the 2DV models. The $k - \epsilon$ model was again diffusive at the scour hole. The flow velocity decreased more than 0.5 m/s at the surface, see Figure G.7 of Appendix G. The reduction in flow velocity due to bottom friction was solved within the bottom cells. This created a mixing layer between the layer of cells on top. All other cell hardly did not seem to be influenced by the bottom friction. At the upstream slope of the scour hole, the high velocity plunges into the scour hole where it directly spreads over the depth.

The Schuddebeursedijk Scour Hole shows a large difference in flow velocities between the scour hole and the normal river bed, see Figure G.11 of Appendix G. This is caused by the large increase in depth. The depth of the scour hole is 2 times of the river bed. If the velocity would directly adapt to the depth, the velocity would go down by the same factor. The simulations showed a diffusive spread of the flow velocities which decreased the velocity at the surface. The spread of the flow velocity within the scour hole is much larger than was computed at the Berenplaat Scour Hole. This is probably caused by

the flow upstream of the scour hole. A scour hole in front of the investigated scour hole influences the approaching flow.

The $k - \epsilon$ model showed a lower velocity in the scour hole, which means that the velocities at the surface were higher, see Figure G.13 of Appendix G. The flow quickly adapted to a new geometry and shows horizontal lines of the same flow velocities.

Shear stresses

The shear stresses were derived with the velocities of the bottom cells. The approach to indicate these shear stresses was made by:

$$\tau = \rho_w \cdot c_f \cdot r_0 \cdot U_c^2 \quad (4.12)$$

ρ_w	Density of water (kg/m ³)
c_f	Skin friction coefficient (-)
r_0	Relative turbulence (-)
U_c	Flow velocity in the bottom cell (m)

The Skin friction and velocity at the lowest cell were derived within FINEL3D. The relative turbulence was determined by Equation 2.10 and was ≈ 0.1 .

Figure 4.9 shows the shear stresses at the Berenplaat Scour Hole during ebb. The lower shear forces in the centre of the figure (blue circle in the main river), show the scour hole. The upstream edge of the scour hole is marked by the higher shear stresses. The red colour indicates shear stress of $\approx 2.2 \text{ N/m}^2$. The scour hole was encircled by higher shear stresses. Only at the slope to the Berenplaat, left bottom of the scour hole lower shear stresses were observed. This is caused by the confluence with the Spui River with the inner bend at this side.

Investigation of the shear stresses in the rivers with various turbulence models, showed differences in the intensity of the shear stresses at the scour hole. However, all models showed high shear stresses at the edges of the scour hole. These high shear stresses are larger than the critical shear stress of sand ($\tau_c = 0.30 \text{ N/m}^2$), indicating that the sand would erode at this location. The critical shear stress of clay ranges from moderate soft $\tau_c = 1.8 \text{ N/m}^2$ till hard consolidated $\tau_c = 15.8 \text{ N/m}^2$. The calculated shear stresses at the slopes of the scour hole are $\approx 2.2 \text{ N/m}^2$, which suggest that the clay layer would be stable while the sand erodes. This corresponds with the hypothesis that the slopes are protected by the poorly erodible top layer.

Remarks

- The red bar under the scour hole at the connection of the Spui and Oude Maas comes from a higher bar in the multibeam measurement. At this location the two maps connect. This be the cause of the bar and the high shear stresses.

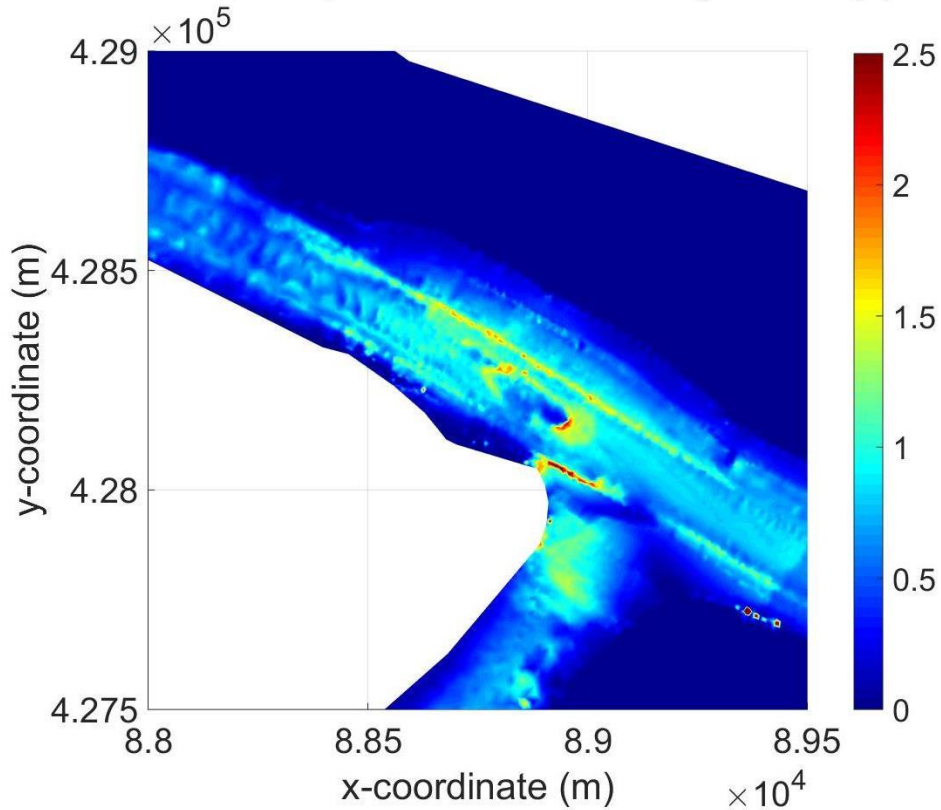
Bed shear stress Berenplaat with constant eddy viscosity (N/m^2)

Figure 4.9: Shear stress at the bottom during ebb (flow from the bottom right to top left).

- At the sides of the main channel, lines with higher shear stresses are formed. At these locations the number of cells over the depth decreased and the cells increased in height, which increased the mean flow velocity in the cell. At the sides of the main channel the differences in the shear stress follow straight lines, these were caused due to a decreases in the number of cells over the vertical.

4.4 Recapitulation

The model simulations showed large differences between the various turbulence models. Two experiments of the physical model investigation were reproduced in a 2DV model. Each of them gave a better fit with another turbulence model. A model of the scour hole with a reinforced downstream slope was best represented with the constant eddy viscosity, while a model with undermining was better represented by the $k - L$ model.

These results were used during the set-up of a 3D model of the Oude Maas and Spui River. The flow regimes in these simulations were comparable with the results of the

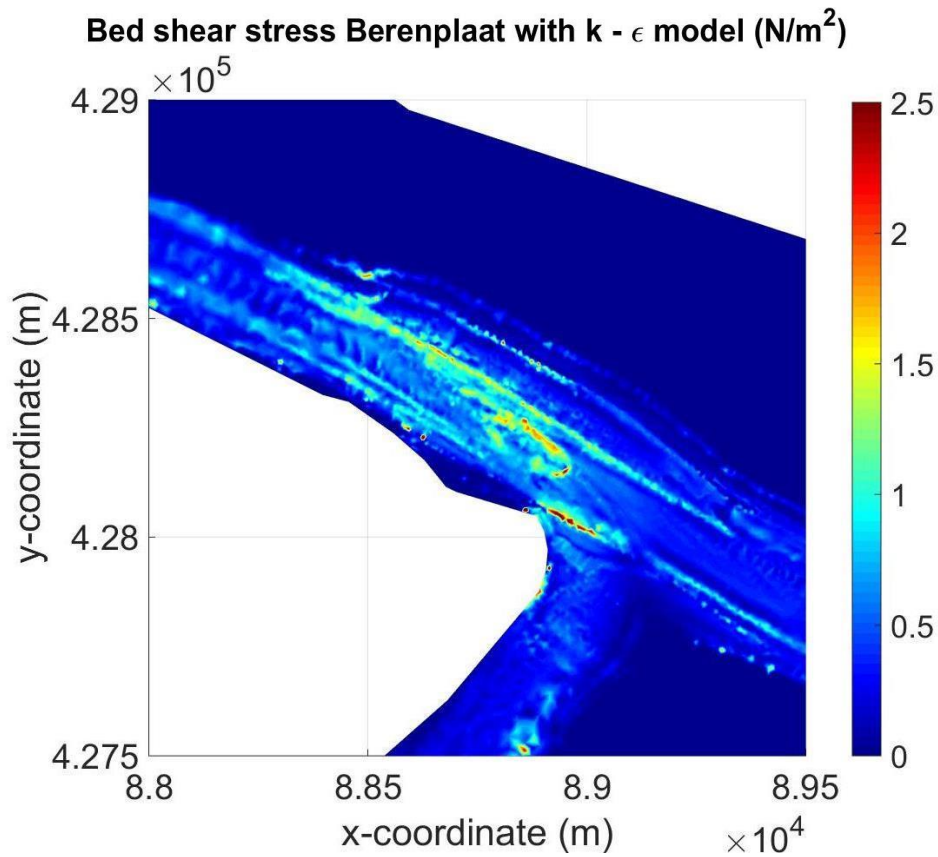


Figure 4.10: Shear stress at the bottom during ebb (flow from the bottom right to top left).

2DV simulations. Analyses of the shear stresses showed high values at the slopes and edges of the scour hole. The calculated shear stresses were higher than the critical shear stress of sand, indicating that the sand would be transported. The poorly erodible layer is able to resist the shear stresses. This corresponds with the hypothesis that edges and slopes are protected by the top layer.

A number of assumptions were made during the set-up of the model. The tide was not included; only steady state calculations with ebb and flood conditions were made. These two situations led to the highest velocities in both flow directions. Factors as salt and sediment transport were not included either. Thus, although the models gave positive result for the hypothesis, further research has to be carried out.

Chapter 5

Discussion

5.1 Development of scour

The previous chapters described the behaviour of scour holes in the models which should represent the field. However simplifications are made. The influence of these simplifications is discussed in this first subsection.

The influence of the thickness of the poorly erodible top layer was investigated. There was no data available of composition of this layer, but this may have large influences on the development of scour. A thin top layer consisting of clay with a low shear stress ($\tau_c \approx 2 \text{ N/m}^2$) will probably fail much faster by block failure than thicker and stronger clay/peat layers. In addition, the deformation of the poorly erodible layers depends on the elasticity of the top layer.

Development of scour Berenplaat Scour Hole The Berenplaat Scour Hole is characterised by a steep and gentle slope. The highest flow velocities can be found during ebb and the steep slope is than the upstream slope. Large parts of the poorly erodible top layer are deformed, following the assumption that the poorly erodible top layer stabilizes the scour hole. The gentle slope corresponds with a thinner top layer which experienced undermining (deforms easily). The steeper slope is probably formed by a thicker top layer.

5.2 Managing the river

The results of the laboratory and numerical models indicate that the undermined areas are covered by the poorly erodible layer. This layer deforms and functions as a falling apron and stabilizes the scour hole. Although field research has to be executed to validate this idea, it can help to indicate the development of the scour holes in the area. Scour holes with slopes which are stabilized by the poorly erodible top layer do not pose further risks to nearby flood defences. Similarly, it may be assumed that the deformation of the poorly erodible layer is able to stabilize the developing scour holes.

However, the stability of the scour hole depends on the poorly erodible top layer. The soil structure of this protective layer is unknown. Breakage of the poorly erodible leads to further increase of the length of the scour hole and thus threatens the stability of flood defences. It is therefore advised to maintain the monitoring of the slopes.

If measures are needed to ensure the stability of nearby flood defences, options to stabilize the slopes in correspondence with the poorly erodible layer are advised. The current scour holes show that stabilization of the slopes (up- and downstream) is sufficient to stop the development of scour.

5.3 Future prospective

So far this research only investigated scour based on measured data. The multibeam measurements of the past year were used to set the geometry for example. A model of the current scour holes was made to indicate the flow regime and the shear stresses. However, the model was just used to indicate the principle of what happens. The next subsections discuss the influence of possible future adaptations to the delta and its influence to the development of scour.

Kierbesluit

The influence of new operational schemes such as the 'Kierbesluit' at the Haringvliet Sluices changes the flows in the area. In this new management programme the Sluices are not fully closed, but maintain a small opening between the sea and the Haringvliet Lake. This improves the local fish migration. Due to this new management scheme at the sluices, a small tidal influence returns to the Haringvliet Lake. Furthermore, the concentration of salt in the Western part of the lake increases.

This change of conditions in the Haringvliet has minor consequences for the flow conditions in the Oude Maas and Spui River. The tide slightly decreases the difference in water levels and flow velocities in the branches. Nevertheless, the general incision will not be stopped and scour problems will still occur in the branches.

Deepening Nieuwe Waterweg

The Nieuwe Waterweg connects the river branches with the sea. The canal is the main entrance of the port of Rotterdam which is extensively used. As the port develops the navigation channel is deepened to allow large ships into the port. Future development of the port may deepen this canal and the flow velocities in the river branches increase. Furthermore, the salt wedge moves upstream. Consequently, new scour holes may be formed and stable scour holes may start developing.

Sea level rise

A future scenario which might have large consequences is the expected sea level rise. As described in Chapter 2 the depth of the scour hole is related to the water depth. Thus if the water level in the rivers increases due to sea level rise, the depth of the scour hole increases as well.

5.4 Eastern Scheldt

The Rijnmond Area is not the only area with this type of scour problems. The results of the experiment may therefore relate to other scour problems.

The bed in the Eastern Scheldt consists of sand. The Eastern Scheldt barrier at the mouth of the estuary protects the hinterland during high sea levels. The barrier raised the flow velocities at the mouth of the estuary. A bottom protection was placed to stabilize the bed. The end of this bed protection was stabilized with a falling apron, which should be able to follow changes of the bed. However, large flow slides increased the depth in front of the bed protection in the estuary. The length of the falling apron was already increased.

Currently, within the Delta Plan, research is carried out to the processes of the failure of this protection. The depth decreases and flow velocities increase during the ebb currents towards the sea. Undermining at the transition of the original bed and the falling apron, similar as researched within this thesis might be one of the causes of the problems. This undermining leads eventually to the failure of the falling apron.

Chapter 6

Conclusions & recommendations

6.1 Conclusions

The influence of the poorly erodible top layer on the development of scour has been researched in this thesis. The poorly erodible layer limits the length of the scour hole and thereby the geometry. These scour holes are deep and poses risks to the stability of nearby flood defences.

This research was divided in three phases. The first phase investigated the scour holes in the field and attempted to describe these hole with the literature. A physical model investigation was carried out second phase. Computational simulations were carried out in the third phase. Challenge in this research was the lack of data from the field. The velocities within the scour hole were unknown. Furthermore, no information of the soil structure in the scour hole was available. This limited the possibilities to validate the results with data from the field.

The conclusions of the research have been split in two parts. This first section describes the results towards the thesis objective. This includes the practical use of the results. The second sections describes the results towards the research questions.

6.1.1 Conclusion towards the objective

Currently, the depth of a scour hole is calculated with empirical formulas which are determined for a number of standard situations. Since none of these standard situation include the influence of the poorly erodible layer at the downstream side of the scour hole, the scour depth is indicated by a formula which calculates the depth behind a bed protection.

Steel plates were used to simulate the poorly erodible top layer in mobile bed laboratory experiments. The steel plates downstream of the scour hole were undermined, which stopped the sediment transport by bed load. Instabilities in the return currents under the plate resulted in whirls which dominate the sediment transport. The fixed

length between the plates limits the length of the scour hole and the development of the scour depth decreases. If the distance between the plates is increased (simulating block-failure of the top layer), the scour hole adapts to the new scour length. The steel plates in the experiment were too stiff and caused extensive undermining. The results of the experiments propose that the poorly erodible top layer in the field deforms and covers the slopes of the scour hole. This top layer functions as a falling apron and decreases the development of the scour hole.

Steady state computations of the scour holes in the field, showed high shear stresses at the edges and slopes of the scour hole. These high shear stresses indicated that the slopes were covered by the poorly erodible. The calculated shear stresses were higher than the critical shear stress of non-cohesive grain under the top layer. Since the slopes of the scour hole are stable the poorly erodible layer has to cover the slopes.

Both models (Physical and computational) suggest that the slopes of the scour hole are covered by the poorly erodible top layer. This layer functions as a falling apron and limits the development of scour. Thus the scour holes tend to stabilize itself and further actions to stabilize the slopes are not needed. However, the composition of the subsoil of this poorly erodible layer is unknown and local failure of weaker sections restarts the scour process. Monitoring of the development of these scour holes should be sufficient to minimize the risks for nearby structures.

6.1.2 Conclusions towards the research questions

Research questions related to the physical model

1. Initially, the scour hole develops similarly to the theory for scour at the end of a bed protection. The length of the scour hole is smaller than the gap between the poorly erodible layers, thus there is no limitation of the length.

Once the length of the scour has grown to a similar length as the gap between the plates, the scour process starts to deviate from the known scour processes. The scour hole still increases in depth, but the growth in length is hindered by the steel plates. The length of the scour hole extends below the plates and these are undermined. This stops the transport by bed load. The return currents transport the sediment upstream. Instabilities of these return currents causes whirls which transports the sediment. Large plumes of sediment are stirred up and leave the scour hole.

The dunes in the scour hole slowly vanish and the profile is becoming smoother. The deepest point moves further downstream and eventually is below the steel plates. Although the experiments were too short to investigate if an equilibrium can be reached, this smooth profile is assumed to be representative for the final situation.

2. The limited length of the scour hole decreases the development of the scour depth. Comparison of the experiments with the empirical Breusers equation showed an increase in the time factor once the undermining starts. This relation is clearly visible in the graphs which show the maximum scour and time factor on log-log scale. The graphs show a clear deviation from the line which describes the development of scour. As the undermining starts, the characteristic time increases. The characteristic time currently depends on the critical mean velocity which is determined by Shields. However this does not take the mode of transport into account. After the undermining starts, the sediment is transported in suspension instead of a combination with bed-load. A function for the suspended transport has to be included instead of the critical shear stress.
3. The experiments showed a logarithmic velocity profile in the approaching flow. At the scour hole the velocity decreases while the depth increases. The decrease in flow velocity at the surface is small and the scour hole is hardly noticed. The mean velocity in the scour hole is decreased to 10 - 20 % of the flow velocity upstream. However, the turbulence has increased and velocity peaks larger than the velocity of the approaching flow. These peaks also reach negative flow velocities.

To indicate the turbulent structures of the flow regime, dye was added. This showed small return currents (about 0.005 m) at the bottom of the scour hole. This method was also used to indicate the flow regime below the steel plates. The flow tend to flow over the plates, but under the plates two eddies were formed. An eddy grows over time until pressure differences cause a vortex to leave the scour hole. The released vortex follows the wall and mixes with the flow in the scour hole. This results in a large whirl which transports a plumes of sediment.
4. The poorly erodible layer downstream of the scour hole limits the length of the scour hole. The scour hole undermines the plates to increase in length. This limits the sediment transport to suspension. The development of the scour and the scour depth are decreased. The experiments show that the shorter the gap, the larger it's influence on the development of scour.
5. Undermining forms a hole under the poorly erodible layer. The support of the non-cohesive grains below this layer is lost and the turbulent forces are increased. The steel plates of the experiment were still and able to cope with these forces, but the clay layer is assumed to fail.
 - (a) Experiments with an increasing length between the plates (simulating crumbling/block-failure of the poorly erodible layer) showed a continuously development of the scour hole and the corresponding undermining. The downstream plate was moved backwards during the experiment to increase the length of the gap. After each retreat the plates, the development of undermining repeated. The scour hole never reaches a stable length and seems to grow to an infinite length.

- (b) The scour holes in the field become stable. However, undermining to the extent of the physical model was never observed. The poorly erodible layer in the experiments was simulated by a steel plate which is much stiffer than the poorly erodible layer in the field. This proposes a different failure mechanism: deformation of the poorly erodible layer. As the scour hole develops, the poorly erodible layer deforms. It covers the slope and protects the non-cohesive grains from further erosion. This process is comparable with the behaviour of falling apron.
6. Experiments with a flow from the reverse direction showed that the scour hole reshaped its geometry. Since the flume was not able to flow from two directions, the scour hole was reversed. The biggest difference was the steep upstream slope. Once the experiment started, a bar was formed. The bar received its grains from the downstream formed scour hole by return currents and distributed these grains over the upstream slope. This bar slowly travelled upstream and increased its width while it reduced its height until it disappeared. With sufficient material the scour hole is create an upstream slope with its original angle.

This experiment was carried out in clear-water scour conditions which deviate from the field. This reduces the influence of the bar on reshaping the geometry of the scour hole.

Research questions related to the computational model

7. (a) First, two 2DV models were made and these were tested with several turbulence models. The results of these simulations were compared with the measured flow velocities of the experiments. The constant eddy viscosity was the best turbulence model for a scour hole with a protected downstream slope (no undermining).
- (b) The flow in the 2DV model of a scour hole with the undermining was best simulated by the $k - L$ model. The constant eddy viscosity overestimated the flow velocities.
- (c) Undermining to the extent of the physical models was never observed at the scour holes in the field. These scour holes were better simulated by the scour hole with the protected slope. This suggest that the constant eddy viscosity model would be the best turbulence model to simulate the flow in the scour holes of the 3D model.
8. The 3D model of the Oude Maas and Spui River shows high shear stresses at the slopes and edges of the scour hole. These stresses are larger than the critical shear stress of the non-cohesive grains. If these grains would be located at slopes and edges, they would erode. However, field measurements show stable slopes, which indicates that these slopes consists of other materials. This result corresponds with the proposition that the poorly erodible layer fails by deformation.

6.2 Recommendations

Although the scour problem has been analysed with multiple approaches, each of them slightly touched the entire problem. Due to the limited time available to carry out this study, concessions had to be made. Furthermore, field measurements of the flow velocities and the composition of the subsoil were limited. This section discusses some needs for research and recommendations. These are ordered by the type of research.

6.2.1 Practical applications

- This report describes the an orientation into the development of scour under a poorly erodible top layer. This process is analysed by three different approaches. The results of this investigation indicate that the poorly erodible top layer is able to stop the development of scour. It is proposed that deformation of the poorly erodible top layer is able to stop the development of scour and functions as a falling apron.

The poorly erodible top layer is able to stabilize the scour hole in the area. However, this depends on the composition of this layer. This indicates that currently stable scour holes are not likely to start developing. Furthermore, currently developing scour holes will be stabilized by the poorly erodible top layer. Monitoring is needed to ensure the stability of the top layer and stability of the scour holes. Only if the stability of current structures is endangered measurements are needed.

6.2.2 Recommendations for further research

Field research

- The experiments showed that the limited scour depth results in undermining of the steel plates. Undermining to the extent of the experiments was never observed in the field and this thesis proposed that deformation of the poorly erodible layer was the cause. Numerical simulation were made in order to test this proposition, which indicated that the slopes were covered by the poorly erodible layer. However, these results followed from models which were not validated. Field data of the composition of the subsoil at the slopes is needed to validate this proposition.
- Similarly, the velocities in the scour holes were never before measured. The models were made with the available field data, but the results were only checked by interpretation of the physics. Field measurements of the flow velocities in the scour hole are needed to validate the models.

Physical experiments

- The physical model experiments were executed in a flume with a small width and height. The flume dimensions were sufficient for this reconnaissance research, but it is recommended to increase the dimensions of the flume in future research. This

decreases the Froude Number and thereby scaling effects. Furthermore, 3D effects can be analysed by increasing the width of the flume.

- The steel plates formed a sharp edge which caused extensive undermining. These steel plates represented poorly erodible layer. However, the poorly erodible layer in the field is not as stiff as steel. A proposition in the thesis describes that the slopes of the scour hole are covered by a deformed poorly erodible layer. This layer function as a falling apron and limits the length of the scour hole. It is recommended to use deformable and flexible material to represent the poorly erodible layers in the flume experiment.
- The length of the gap between the plates was varied in the experiment. However, this is not the only parameter which determines the development of the scour hole. Other variables such as: the thickness of the layer and the shape at the edge were never investigated before. New experiments are needed to indicate the influence of these parameters.
- The computational models showed the highest vertical velocity just in front of the downstream plate ($\approx 0.01 - 0.02$ m in front of the downstream edge). During following experiments, it is recommended to measure the flow velocities at this location.
- The laboratory experiments showed that the scour process deviates from the Breusers formula. The formula calculates sediment transport without describing the type of sediment transport. The experiments showed that once the scour process starts to undermine the steel plates, the development of scour depth reduces. This report shows this decrease by an increase of γ . Although γ was used to show the decrease of development, this decrease is caused by the change in sediment transport. The critical velocity in the Breusers formula is determined by the Shields parameter, which include bed load. A basic idea for a formula which depends on the suspended transport only, is proposed in this thesis. This basic idea has to be worked out and validated before it can be used.

Computational models

- The $k - \epsilon$ model shows irregularities of the flow velocity at the bottom. It is recommended to use a grid with a constant cell height at the bottom, to prevent these irregularities.
- A 3D model of run 20 would help to further analyse the flows in the scour hole. The report only discusses the 2DV models in which the three-dimensional turbulence structures are dropped out. A fully 3D model of the flows under the steel plates could be used to investigate these complex turbulence effects in detail.
- The 3D simulations of the rivers were now tested for two tidal situations. Steady state solutions of an ebb and flood current were modelled. This model has been

used to indicate the shear stresses during the highest flow velocities. However, it is recommended to include the tidal flow before making further analyses with the model. It is further recommended to include the salt concentration in the model.

List of Figures

1.1	Map of the Rijnmond Area (SLOFF <i>et al.</i> 2012a).	2
1.2	Schematic presentation of the interaction between the erosion resistant layer and the sand bed below (SLOFF <i>et al.</i> 2012a).	2
2.1	Map of the Rijnmond Area including locations of the scour holes (SLOFF <i>et al.</i> 2012a). The blue dot is the Berenplaat (Oude Maas), red Poortugaal scour hole (Oude Maas) and green Schuddebeursedijk (Spui).	8
2.2	Multibeam sounding of the bathymetry of the Berenplaat Scour Hole in 2013. The black line is the location of the longitudinal profile (1:1000). The depth is in m MSL.	9
2.3	Longitudinal profile of the Berenplaat Scour Hole, where the left is downstream and right upstream.	10
2.4	Longitudinal profile of the centre of the Berenplaat Scour Hole, where the left is downstream and right upstream.	10
2.5	Longitudinal profile of the Scuddebeursedijk Scour Hole, where the left is downstream and right upstream.	11
2.6	Longitudinal profile of the Poortugaal Scour Hole, where the left is downstream and right upstream.	12
2.7	Longitudinal profile of the Poortugaal Scour Hole, where the left is downstream and right upstream.	13
2.8	Control volume for deviation of sediment balance.	14
2.9	Shields diagram, adapted by Breusers, with $D_* = d_{n50} (\Delta g / \nu^2)^{1/3}$ (HOFFMANS AND VERHEIJ 1997).	16
2.10	Schematization of reference case with sill, including flow pattern (HOFFMANS AND VERHEIJ 1997).	17
2.11	Sketch of scour hole including used parameters (HOFFMANS AND VERHEIJ 1997).	19
2.12	The scour depth over time.	20
2.13	Influence of the poorly erodible layer on the length on scour hole. The formula calculates the depth for a different geometry.	21
2.14	The assumed change in geometry of a scour hole while calculated with the adapted formula.	22
2.15	Converging flows into the scour hole.	22

3.1	Sketch of the model set-up.	26
3.2	The development of the scour from run 5 over time in hours.	29
3.3	Scour of the hole in the first minutes is similar to the know Breusers development.	29
3.4	Scour during the second phase of the process dunes hit the edge of the downstream plates.	30
3.5	Undermining in the third phase, side and top view.	31
3.6	Streamlines of observed flow in the scour hole: 3D and top view.	32
3.7	Run 14, development of the scour hole over time.	33
3.8	The flow line in the scour hole responsible for the redistribution of the geometry.	34
3.9	The flow in the scour hole during runs 16 & 17.	35
3.10	The development of the scour depth over time of run 16.	35
3.11	Development of the scour hole, where the results of the Breusers experiment are in the same graph as the results of the experiment with fixed plates.	36
3.12	Final scour depth of run 7 and 10 at the end of the runs.	37
3.13	Final scour depth of run 15 after 13 hours.	37
3.14	Geometry of the scour holes in experiments 16 and 20.	38
3.15	Scour depth of run 18 over time.	38
3.16	Depth at the end of the run 4 ($u = 0.4$ m/s) and 5 ($u = 0.55$ m/s).	39
3.17	Maximum scour depth as function of time.	39
3.18	Maximum scour depth as function of time.	40
3.19	The flow velocity in a scour hole with a fixed length of 0.5 m.	41
3.20	The scour depth of the experiment compared with the Breusers values. In run 9 is $u = 0.45$ m/s and run 20 $u = 0.5$ m/s, gap between the plates is 0.5 m.	42
3.21	The scour depth over the time with different distances between the plates. The flow velocity $u = 0.45$ m/s.	42
3.22	The scour depth per distance of the plates. The flow velocity $u = 0.45$ m/s.	43
4.1	The flow velocity in the longitudinal direction of experiment 17 computed with constant eddy viscosity.	52
4.2	The flow velocity in the vertical direction of experiment 17 computed with constant eddy viscosity.	52
4.3	The flow velocity in the longitudinal direction of experiment 20 computed with $k - L$	53
4.4	Flow velocities over the depth of the simulations and the data of the experiment 17.	54
4.5	Flow velocities over the depth of the simulations and the data of experiment 20.	55

4.6	Bathymetry of the rivers in the in the model including measurements stations and points of interest. The bathymetry is a combination of the multibeam measurements and AHN maps.	56
4.7	Longitudinal velocity profile of the Berenplaat Scour Hole during ebb (m/s).	58
4.8	Longitudinal velocity profile of the Berenplaat Scour Hole during flood (m/s).	59
4.9	Shear stress at the bottom during ebb (flow from the bottom right to top left).	61
4.10	Shear stress at the bottom during ebb (flow from the bottom right to top left).	62
A.1	Multibeam sounding of the Schuddebeursedijk Scour Hole in 2013. The scale is 1:3000 and the values of the legend are in m MSL.	81
A.2	Multibeam sounding of the Poortugaal Scour Hole in 2007. The black line is the location of the longitudinal profile 2.6(1:1250). The Depth in in m MSL.	82
A.3	Multibeam sounding of the Poortugaal Scour Hole in 2013. The black line is the location of the longitudinal profile 2.6 (1:1250).	82
B.1	The development of the scour depth by the tide in the first day.	85
B.2	The scour depth due to tidal currents over time in the first week, the blue line is the calculation with the tide included and the red line is the approximation of the scour.	85
B.3	Schematized situation of attached flow.	86
B.4	Effect shear-stress on loose and dense grains (HOFFMANS AND VERHEIJ 1997).	87
B.5	Macro instability of the outer slope (WEIJERS AND TONNELJCK 2009).	87
B.6	Two-dimensional schematisation of a flow slide (HOFFMANS AND VERHEIJ 1997).	89
C.1	Water levels measured at the Spijkenisse Bridge.	93
C.2	Water levels measured at Goidschalxoord.	93
C.3	Water levels measured at Bernisse/Zuidland.	93
C.4	Flow velocities at the Spijkenisse Bridge.	94
D.1	Schale effect once the Froude requirement is not met with $s = \frac{u^2}{2g}$ (velocity height) and H the energy height, DE VRIES (1975).	96
D.2	Set-up of model at the start of run 1.	99
D.3	Comparison between Nikuradse roughness and the grain size.	99
D.4	Set-up of model at the start of run 2 & 3.	101
D.5	Set-up of model at the start of run 4.	101
D.6	Set-up of model at the start of run 6 - 10.	102
D.7	Set-up of model at the start of run 11 & 12.	103

D.8	The change of geometry; left the expected result after a previous runs, right the start position of the run.	103
D.9	Set up of runs 16 & 17.	104
F.1	Set-up of the computational grid of model run 17, with a detailed view of the scour hole.	108
F.2	The flow velocity in the longitudinal direction computed with Bakhmetev.	109
F.3	The flow velocity in the vertical direction computed with Bakhmetev.	109
F.4	Profile of the eddy viscosity computed with Bakhmetev.	109
F.5	The flow velocity in the longitudinal direction computed with $k - L$ model.	110
F.6	Profile of the eddy viscosity computed with $k - L$ model.	110
F.7	The flow velocity in the longitudinal direction computed with $k - \epsilon$ model.	110
F.8	Profile of the eddy viscosity computed with the $k - \epsilon$ model.	111
F.9	Set-up of the computational grid of model 2.	111
F.10	The flow velocity in the longitudinal direction computed with Bakhmetev mixing length.	111
F.11	The flow velocity in the longitudinal direction computed with $k - L$	112
F.12	The flow velocity in the longitudinal direction computed with the $k - \epsilon$	112
G.1	Top view of the Berenplaat Scour Hole.	113
G.2	Top view of the Berenplaat Scour Hole with the cross sections.	114
G.3	Computational grid of the longitudinal profile of the Berenplaat Scour Hole.	114
G.4	Top view of the Schuddebeursedijk Scour Hole with the cross sections.	115
G.5	Top view of the Poortugaal Scour Hole with the cross sections.	115
G.6	Longitudinal velocity profile of the Berenplaat Scour Hole ebb (m/s).	116
G.7	Longitudinal velocity profile of the Berenplaat Scour Hole during ebb (m/s).	116
G.8	Cross-section with flow velocities along the Berenplaat Scour Hole ebb (m/s).	117
G.9	Cross-section with flow velocities along the Berenplaat Scour Hole ebb (m/s).	118
G.10	Cross-section with flow velocities along the Berenplaat Scour Hole during ebb(m/s).	118
G.11	Longitudinal velocity profile of the Schuddebeursedijk Scour Hole during ebb (m/s).	119
G.12	Longitudinal velocity profile of the Schuddebeursedijk Scour Hole during ebb (m/s).	119
G.13	Longitudinal velocity profile of the Schuddebeursedijk Scour Hole during ebb (m/s).	120
G.14	Cross-section with flow velocities (m/s) along the scour hole during ebb (flow from bottom left to top right).	121
G.15	Cross-section with flow velocities (m/s) along the scour hole during ebb (flow from right to left).	121

List of Tables

2.1	Soil parameters.	12
2.2	Coefficient γ , HOFFMANS AND VERHEIJ (1997).	19
3.1	Overview of the experiments.	27
3.2	Parameters of the sand.	27
3.3	Flow velocity and the observed phase of motion from the Shields digram, see Figure 2.9.	28
3.4	Parameters of the sand.	35
4.1	Boundary conditions during ebb.	57
4.2	Boundary conditions during flood.	58
B.1	Critical depth average velocities for cohesive sediments (rough estimates), HOFFMANS AND VERHEIJ (1997).	90
C.1	Conditions at the measurement stations in the reference situations.	92
D.1	Parameters of the sand.	97
D.2	Overview of field and model values.	98
D.3	Roughness following Adihardjo (1972).	99
D.4	Overview of the indicated runs. Depending on the results of previous runs it is possible to change the scheme.	102

Bibliography

- ADIHARDJO, R. (1972) Invloed geometrie en aard van de verdediging bij tweedimensionale ontgrondingen, *report M 847-I, Waterloopkundig Laboratorium, Delft.*
- BREUSERS, H.N.C. (1966) Conformity and time scale in two-dimensional local scour, *Proc. symposium on model and prototype conformity, Hydraulic Research Laboratory, Poona.*
- CHRISTIAN, C.D., CORNEY, P.A. (2004) Three dimensional model of flow over a shallow trench, *Journal of Hydraulic Research, Vol 42, No 1, pp. 71-80.*
- DE GRAAUW, A.F.F., PILARCZYK, K.W. (1981) Model-prototype conformity of local scour in non cohesive sediments beneath overflow-dam, *19th IAHR-congress, New Delhi.*
- DE VRIES, M. (1975) Waterloopkundig onderzoek , *Lecture notes B80, Department Hydraulic Engineering, TU Delft, Delft.*
- DIETZ, J.W. (1969) Kolkbildung in feinen oder leichten Sohlmaterialien bei strömendem Abfluß, *Mitteilungen, Heft 155, Universität Fredericiana Karlsruhe.*
- DELFT HYDRAULICS (1969) Begin van beweging van bodemmateriaal, *report S159-1, Delft.*
- ESCARAMEIA, M., MAY, R.W.P. (1999) Scour around structures in tidal flows, *report SR 521, HR Wallingford, Wallingford.*
- HOFFMANS, G.J.C.M. (1993) A study concerning the influence of the relative turbulence intensity on local-scour holes, *report W-DWW-93-251, Ministry of Transport, Public Works and Water Management, Road and Hydraulic Engineering Division, Delft.*
- HOFFMANS, G.J.C.M., (1995) Scour around bridge piers and abutments, *report W-DWW-94-312, Ministry of Transport, Public Works and Water Management, Road and Hydraulic Engineering Division, Delft.*
- HOFFMANS, G.J.C.M., VERHEIJ, H.J. (1997) Scour Manual, *A.A.Balkema, Rotterdam.*

- HOFFMANS, G.J.C.M., VERHEIJ, H.J. (2002) On the Challenges of Scour Prediction, *First International Conference on Scour of Foundations, ICSF-1, Texas A&M University*.
- HUISMANS, Y., OMAHONY, T., VAN VELZEN, G., HOFFMANS, G.J.C.M. (2014) Analyse ontgrondingskuilen Rijn-Maasmonding, *Onderdeel van "Advies beheer rivierbodembodem RMM", Deltares*.
- JANSEN, P.PH. (1979) Principles of River Engineering, *VSSD, Delft*
- JORISSEN, R.E., VRIJLING, J.K. (1989) Local scour downstream of hydraulic constructions, *Proceedings 23rd IAHR-congress, Ottawa: B433-B440*.
- MESBAHI, J. (1992) On combined scour near groynes in river bends, *Delft Hydraulics/IHE Delft, M.Sc. thesis HH132, Delft*.
- MIRTSKHOULAVA, TS.YE. (1988) Basic physics and mechanics of channel erosion, *Gidrometeoizdat, Leningrad*.
- MOSONYI, E., SCHOPPMANN, B. (1968) Ein Beitrag zur Erforschung von örtlichen Auskolkungen hinter geneigten Befestigungsstrecken in Abhängigkeit der Zeit, *Mitteilungen des Theodor-Rehbock-Flußbaulaboratoriums, Universität Karlsruhe*.
- MOSELMAN, E., SLOFF, C.J. (2002) Effect of local scour on macroscale river morphology, *part of River Flow 2002, Bousmar & Zech, Swets & Zeitlinger, Lisse*
- Oxford dictionary *oxforddictionaries.com* retrieved October 17th 2014.
- SCHIERECK, G.J. (2012) Introduction to Bed, bank, and shore protection, update by VERHAGEN, H.J. *VSSD, Delft*.
- SHIELDS, A. (1936) Anwendung der Ähnlichkeitsmechanik und der Turbulenzforschung auf die Geschiebebewegung, *Mitteilungen Preussischen Versuchsanstalt für Wasserbau und Schiffbau, 26, Berlin*.
- SILVIS, F. (1988) Oriënterende studie naar grondmechanische aspecten bij ontgrondingskuilen, *Report CO-291720/12, Grondmechanica Delft, Delft*.
- SLOFF, C.J., VAN SPIJK, A., STOUTHAMER, E., SIEBEN, A. (2012a) Understanding and managing the morphology of the branches incising into sand-clay deposits in the Dutch Rhine Delta, *International Journal of Sediment Research, Vol 28, No 2, 2013, pp. 127-138*.
- SLOFF, C.J., VAN DER SLIGTE, R.A.M., HUISMANS, Y., FUHRHOP, H. (2012b) Morphological model of the Rhine-Meuse delta, *Deltares, Delft*.
- UIJTTEWAAL, W.S.J. (2003) Turbulence in Hydraulics CT5312 *Lecture notes, TU Delft, Delft*.

VAN DER MEULEN, T., VINJÉ, J.J. (1975) Three-dimensional local scour in noncohesive sediments, *Proc. 16th IAHR-congress, Sao Paulo*.

WEIJERS, J., TONNEIJCK, M. (2009) Flood defences, *Lecture notes CIE5314 Flood Defences, Tu Delft*.

Appendix A

Figures of scour holes

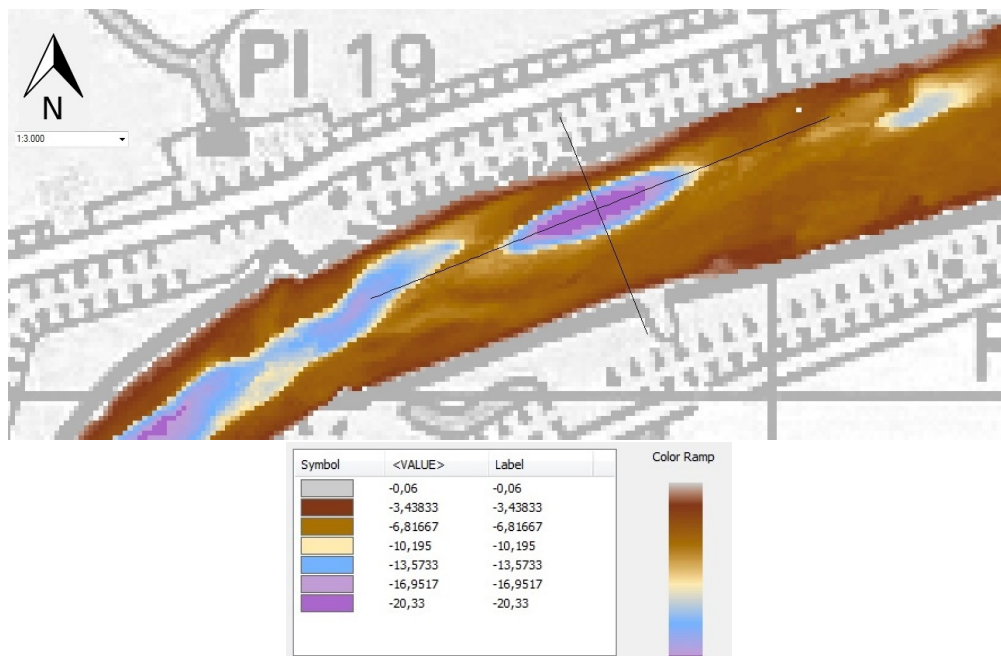


Figure A.1: Multibeam sounding of the Schuddebeursdijk Scour Hole in 2013.
The scale is 1:3000 and the values of the legend are in m MSL.

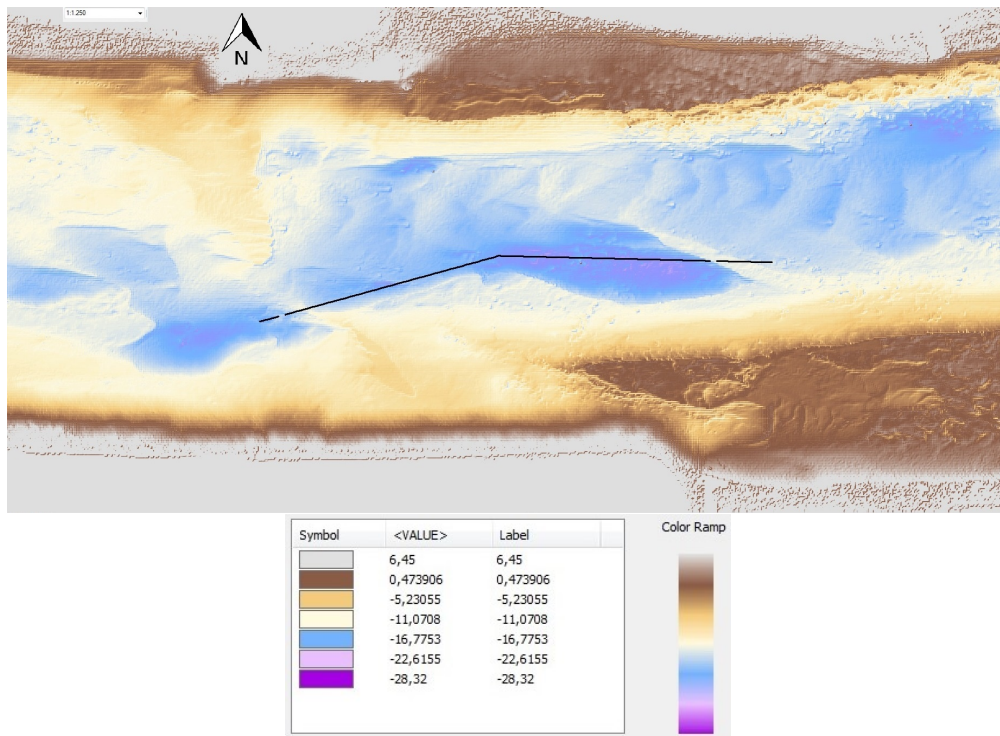


Figure A.2: Multibeam sounding of the Poortugaal Scour Hole in 2007. The black line is the location of the longitudinal profile 2.6(1:1250). The Depth in in m MSL.

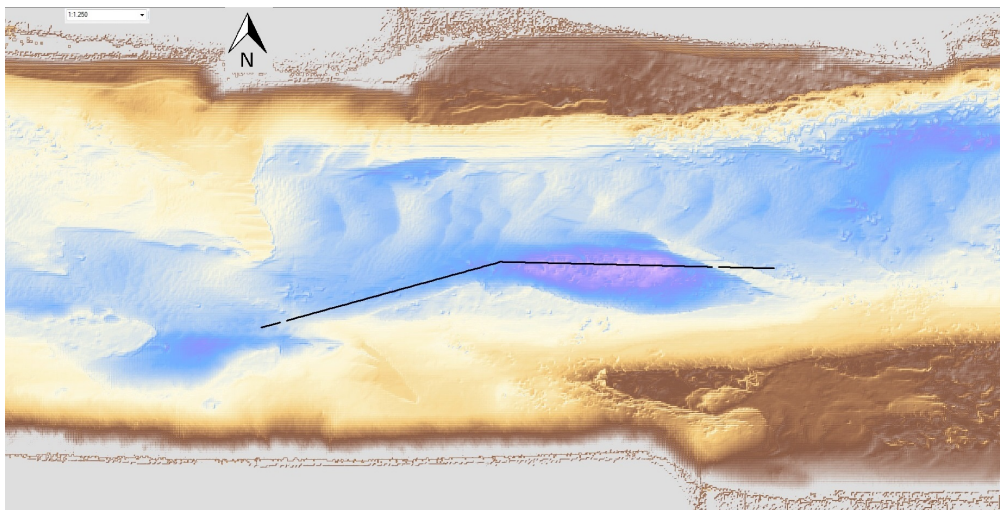


Figure A.3: Multibeam sounding of the Poortugaal Scour Hole in 2013. The black line is the location of the longitudinal profile 2.6 (1:1250).

Appendix B

Extra literature

B.1 Tidal influence on the system

The tidal flow influences the flow velocities in the river. The Breusers formula 2.13 uses uniform flow velocities to calculate the scour depth. Using the highest flow velocities would overestimate the scour depth, while the mean flow velocity neglects the influences of the tide, etc. The characteristic time for cyclic tidal flows is shown in B.1 (HOFFMANS AND VERHEIJ 1997).

$$t_{1,u} = \frac{Kh_0(0)\Delta^{1.7}}{\frac{1}{T} \int_{t_1}^{t_2} \frac{(\alpha\bar{u}_0(t) - \bar{u}_c)^{4.3}}{h_0(t)} dt} \quad (\text{B.1})$$

$t_{1,u}$	Characteristic time with tidal flows (s)
T	$t_2 - t_1$, part of period where $\alpha\bar{u}_0 > \bar{u}_c$ (s)
t_1	Time at which $\alpha\bar{u}_0$ first exceeds \bar{u}_c during flood tide (s)
t_2	Time at which $\alpha\bar{u}_0$ first drops below \bar{u}_c during ebb tide (s)

The mean flow velocity of the characteristic time (Equation 2.14) is rewritten and includes a mean component for the flood velocity. But, the formula lacks a component for the ebb velocity and does not include the reverse of flow direction. This formula resulted from a field scale model in the Brouwers Dam sluice. The incoming tide dominated the scour process. The flood flow had to pass the entire sluice, which increased the turbulence. The investigated scour hole was located at the end of the bed protection. The ebb flow originated from the estuary and the flow conditions were differed from the flood flow. This is probably why the influence of the flow from the reversed direction was never included. Both sides of the scour hole are protected by the poorly erodible top layer and the difference in the approach between the ebb and flood flows is small. To include both flow directions, the formula has been adapted into Equation B.2.

$$t_{1,u} = \frac{Kh_0(0)\Delta^{1.7}}{\left(\frac{1}{T_1} \int_{t_1}^{t_2} \frac{(\alpha\bar{u}_0(t) - \bar{u}_c)^{4.3}}{h_0(0)} dt + \frac{1}{T_2} \int_{t_3}^{t_4} \frac{(\alpha\sqrt{\bar{u}_0(t)^2 - \bar{u}_c})^{4.3}}{h_0(0)} dt \right)} \quad (\text{B.2})$$

- T_1 $t_2 - t_1$, part of tidal period where $\alpha\bar{u}_0 > \bar{u}_c$ (s)
 T_2 $t_3 - t_4$, part of tidal period where $\alpha\sqrt{\bar{u}_0^2} > \bar{u}_c$ (s)
 t_3 Time at which $\alpha\sqrt{\bar{u}_0^2}$ first exceeds \bar{u}_c during ebb tide (s)
 t_4 Time at which $\alpha\sqrt{\bar{u}_0^2}$ first drops below \bar{u}_c during flood tide (s)

Rewriting this in an Euler forward scheme gives:

$$y_{m+1} = y_m + \left(\frac{t(m+1)}{t_1} \right)^\gamma - \left(\frac{t(m)}{t_1} \right)^\gamma \quad (\text{B.3})$$

$$t_1 = \frac{Kh_0(0)\Delta^{1.7}}{\left(\frac{\alpha\sqrt{\bar{u}_0^2(m+1) - \bar{u}_c}}{h_0(0)} \right)^{4.3}} \quad (\text{B.4})$$

This formula is tested with a sinusoidal tide of 12 hours. The result is shown in Figures B.1 and B.2 by the blue line. A maximum flow velocity of $u_{max} = 1.6$ m/s was used to form the sinusoidal wave. The time step was $t = 0.5$ hours. The blue line shows large scour during the high velocity peaks and during the reverse of flow direction the scour completely stops. The red line in B.2 shows an approximation of scour by the original scour formula, with $\bar{u}_0 = 1.6$ m/s and a reducing factor for the tide. This factor is calculated by $u_{0,tide} = \eta u_{0,max}$ with $\eta = 0.60$. This approximation is sufficient for the sinusoidal wave, but has to be tested for irregular tides.

Note: The amplification factor B.2 in formula is assumed to be constant. The change of flow directions may lead to different conditions of the approaching flow. This factor assumed to be the same at both sides, because both side have the same erosion resistant top layer. Another flaw in the formula is caused due to the time factor which is calculated for each situation as if the previous were all calculated with the same t_1 . This gives an error to the decay/increase over time.

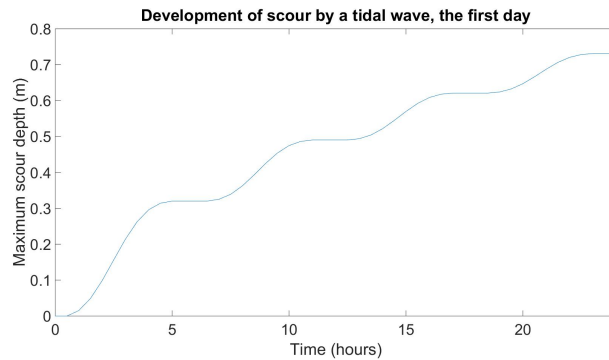


Figure B.1: The development of the scour depth by the tide in the first day.

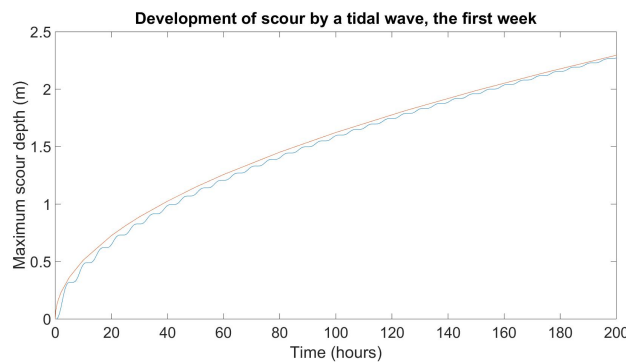


Figure B.2: The scour depth due to tidal currents over time in the first week, the blue line is the calculation with the tide included and the red line is the approximation of the scour.

B.2 Coanda effect

The flow does not seem to separate in the case of less steep slopes (rule of thumb gives 1:7) and is pulled into the scour hole. This has been described by the Coanda effect: *Deviation of a plain jet of a fluid that penetrates another fluid in the vicinity of a convex wall.*

In other words, if the fluid flows along a wall, the fluid tends to follow all deviations of the wall. This is shown in Figure B.3. At the upstream edge of the scour hole the depth starts to increase. If the transition is gentle enough the flow is able to follow the bed. The flow velocities in the scour hole are then decreased due to the increase of depth. If the transition is abrupt, the flow is not able to follow this movement. The flow separates and recirculating eddies are formed. These eddies reduce the flow velocity at the bed.

Separation of flow is not only determined by the upstream slope, also the geometry at the edge (point of separation) is important. The fluid can only follow the wall if the curvature smooth is.

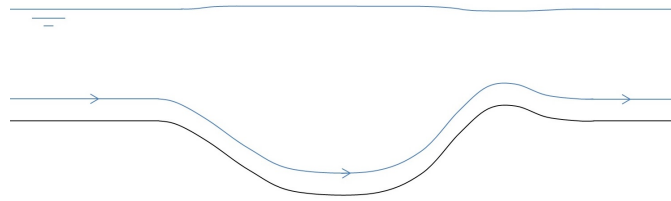


Figure B.3: Schematized situation of attached flow.

B.3 Geotechnical aspects

B.3.1 Failure mechanisms

How sand on a slope reacts when the critical load is exerted depends on how well the sand is packed. In The Netherlands one usually speaks of loosely packed sand when the porosity is larger than 40 %. If the shear-stress of the loosely packed sand is larger than the critical value, the particles tend to adopt a denser packing (see Fig B.4). This creates an over-pressure of the pore water, which diminishes the effective stress and reduces the frictional resistance. If the frictional resistance is too low the sand loses stability and slides away. The particles higher up the slope lose their support and flow down (density flow) into the scour hole, see Figure B.6. If this lack of support extends to structures or dikes this may lead to their failure. Therefore it is important to know the stability at micro-scale level.

In denser packed sand the shear-stress resistance can be much larger and it is even possible to reach vertical walls. If the shear-stress on densely packed sand is increasing the particles tend to move to a less dense packing. This creates an under-pressure which can be solved by an inflow of water. The inflow depends on the porosity. In the case that the porosity is small, steep walls are temporarily stable. The inflow of water leads to failure which is called breaching.

These processes differ from the shear failure which for dikes is often described as macro instability, see Figure B.5. A complete section of the slope fails by sliding down (often described as a slip circle). The failure is within the dike, whereas the previous are at the outer side. This phenomenon describes failure due to a higher load than frictional resistance within the slope. The failure mechanism is better known and can be calculated by methods of Bishop, etc. The advantage is that the length of the failed section can be calculated and therefore this risk can be implemented in the designs. The mechanisms of the flow slides are still not fully known and their length scale can be much larger which may endanger the constructions.

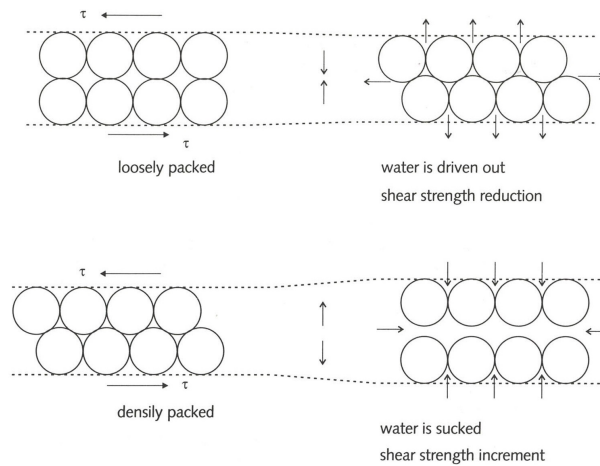


Figure B.4: Effect shear-stress on loose and dense grains (HOFFMANS AND VERHEIJ 1997).

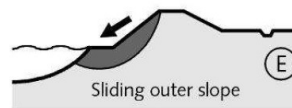


Figure B.5: Macro instability of the outer slope (WEIJERS AND TONNEIJCK 2009).

B.3.2 Upstream slope of the scour hole

The Scour Manual by HOFFMANS AND VERHEIJ (1997) includes a formula which describes the relation between the flow into the scour hole and the angle of the upstream slope. This formula is valid for non-cohesive sediments behind a hydraulically rough protection. The formula describes the final equilibrium situation, where the scour hole has grown to its equilibrium length. It is unknown if this is the same if the scour length is limited as in the prototype.

The upstream slope is defined as the slope of the upstream part of the scour hole, see Figure 2.11. This slope can due to instability grow further upstream than the end of the protection. To reach an equilibrium the slope should be less steep than the angle of repose, ϕ , which is for sand between $\phi = 30$ and 40 degrees, however steeper slopes have been observed. If the slope exceeds the critical value, shear failure or liquefaction can occur. This may lead to the loss of sediment under the protection, which in the given case may lead to the loss of the clay layer at the edge. This type of failure may repeat itself a number of times until an equilibrium is found.

The formula is based on the stability of the grains under an angle and the load due to shear-stresses. Using some empirical relations equation B.5 has been found by HOFFMANS (1993).

$$\beta = \arcsin \left(2.9 \cdot 10^{-4} \frac{\bar{u}^2}{\Delta g d_{50}} + (0.11 + 0.75 r_0) f_C \right) \quad (\text{B.5})$$

C_0	40 m ^{0.5} /s, if $C < C_0$ than $f_C = 1$
d_{50}	Median grain size (m)
f_C	Roughness function related to bed protection, $f_C = C/C_0$
r_0	Relative turbulence at the end of the bed protection (-)
\bar{u}	Depth averaged velocity at the end of the bed protection (m/s)
β	Slope angle of the upstream slope (°)

Comparing the situation of the formula with the prototype, there are certain differences. However, the theory seems applicable for the calculations of the prototype. The main difference is the limited length of the scour hole, but as long as the bed load is the governing sediment transport this should not change the geometry of a scour hole. The length is then only limiting the depth. With the clay cover instead of the protection there is not a big difference in the formation of the slopes. It only differs when shearing/liquefaction leads to the erosion of the clay layer. Calculation with the formula gives for the earlier proposed values a slope of 1:4.8. This is comparable with the upstream slope of the prototype.

The influence of the change in flow direction due to the tide is not included in the formula. A change in flow direction changes the upstream slope into a downstream slope and the other way around. Since the angle of the downstream slope is less steep the slopes should first adapt to the new flow direction before scouring. It is therefore questionable if steep slopes can be reached. In the reference situations this has never been shown.

B.3.3 Critical failure length

Silvis reported an equation to calculate the length of the upstream slope of the scour hole after failure in 1988 (HOFFMANS AND VERHEIJ 1997). The background is that with this equation the length of the protection can be estimated.

$$L_s = y_d \left(\frac{1}{2} \frac{y_d}{y_m} - 1 \right) (\cot \gamma_2 - \cot \gamma_1) + \frac{1}{2} y_m (\cot \gamma_2 - \cot \beta_a) \quad (\text{B.6})$$

L_s	Failure length (m)
y_d	Scour depth at transition of steepest and second slope (m)
y_m	Maximum scour depth (m)
β_a	Average slope angle before instability (°)
γ_1	Sliding erosion slope angle after instability (°)
γ_2	Sliding deposit slope angle after instability (°)

Equation B.6 is based on a two-dimensional storage model in which a sediment balance is made, see Figure B.6. Since the formula is made for a non-cohesive subsoil it is questionable if this formula is applicable for the situation of the prototype. The formula strongly depends on the angle of the slope of the deposited sediments γ_2 . There are no references of such a slope with a clay layer.

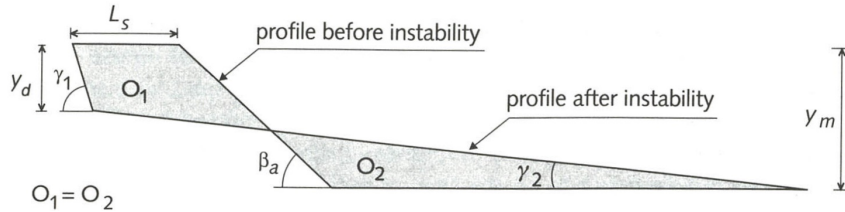


Figure B.6: Two-dimensional schematisation of a flow slide (HOFFMANS AND VERHEIJ 1997).

B.4 Transport of non-cohesive grains

B.4.1 Introduction

The transport of non-cohesive grains is discussed in section 2.3. Transport is induced by shear-stress on a single grain and the gravity (frictional force) determines the resistance. This section elaborates the effects of cohesion on the transport. This is achieved by looking at two types of erosion; abrasive and by pulling of fractions. Abrasive erosion is the slowly scraping off of sediment grains by the flow, where the other process is the instantaneously loss off lumps of material.

B.4.2 Abrasive erosion

During abrasive erosion the flow scrapes off the gains particle by particle. Clay particles are much smaller than the non-cohesive grains and therefore much easier transported. However, cohesion binds the particles, which increases the forces are needed to break the particles loose. The erosion process is influenced by a number of parameters, of which the degree of cohesion is determined by: Cation Exchange Capacity (CEC), salinity, Sodium Absorption Rate (SAR), pH-level of pore water, temperature, sand, organic content and porosity.

Due to the difficult relations between all the parameters, there are no equations or theories available which include the complete set of parameters. It is also impossible to measure the parameters continuously. Most formulas only use a constant value for the cohesion as a measure against erosion. The Breusers method for example gives a first estimate of the critical velocities. This is shown in the table B.1.

The critical velocity is rewritten as a critical shear-stress by (SLOFF *et al.* 2012a):

$$\tau_c = 0.7\rho_w (r_0u_c)^2 \quad (\text{B.7})$$

Table B.1: Critical depth average velocities for cohesive sediments (rough estimates), HOFFMANS AND VERHEIJ (1997).

Type of soil	h(m)	$\bar{u} - c$ (m/s)
Loamy sand, light loamy clay with low compaction	1	0.4
Heavy loamy clay with low density	3	0.5
Low density clay	10	0.6
Light loamy clay with medium density	1	0.8
Heavy loamy clay with low density	3	1.0
Clay of medium density	10	1.3
Light loamy clay (dense)	1	1.2
Heavy loamy clay (dense)	3	1.5
Hard clay	10	1.9

A more detailed approach is proposed by Mirtskhoulava in 1988, see equation B.8 (HOFFMANS AND VERHEIJ 1997).

$$\bar{u}_c = \log \left(\frac{8.8h}{d_a} \right) \sqrt{\frac{0.4}{\rho_w} ((\rho_s - \rho_w) g d_a + 0.6C_f)} \quad (\text{B.8})$$

C_f	Fatigue rupture strength of clay $C_f = 0.035C_0$ (N/m ²)
C_0	Cohesion (N/m ²)
d_a	Size of detaching aggregates, $d_a = 0.004$ m
g	Acceleration of gravity, 9.81 m/s ²
h	Water depth (m)
\bar{u}_c	Critical mean velocity for cohesive sediment (m/s)
ρ_w	Density of fluid (kg/m ³)
ρ_s	Density of sediment (kg/m ³)

Equation B.8 includes the parameters: cohesion at saturation and particle size. This gives a more accurate critical velocity, which is based on local bottom parameters. But the bottom in the field is heterogeneous, which means that the formula gives a detailed outcome of a specific section. The heterogeneity of the subsoil is included by a safety factor. A disadvantage of this method is that the accuracy gained by the formula is lost by the safety factor. Therefore the method by Breusers has been used for the scour of clay, see Table B.1. The method of Mirtskhoulava could be used for calculation on specific locations such as at the edge of a scour hole.

The influence of peat on the clay layer is unknown. The literature gives no concrete description these combinations. An increase in organic content generally contains increase the cohesiveness. The critical bed shear-stress is higher, which means that the transport is less.

B.4.3 Erosion of fragments

The erosion of fragments occurs undrained by pulling-off or shearing. The undrained shear strength is a measure of critical shear and can be related to the cone resistance and bearing capacity (undrained shear-stress = cone resistance/bearing capacity Nk). This cone resistance can be derived from sounding (cone-penetration tests), while the bearing capacity is estimated based on expert judgement. In the prototype area this is for holocene clay $Nk = 10$ and for stiff clay $Nk = 20$ (SLOFF *et al.* 2012a)

Erosion of fragments is especially important at the transition between clay and sand layers. If the clay has a higher critical shear-stress than sand, the erosion of sand may lead to undermining and at a certain moment a pebbles of clay break loose. This is assumed to be the main process of the degradation of the clay layer at the edges of the scour hole.

Appendix C

Flow conditions in the Oude Maas and Spui

The flow conditions in the Oude Maas and Spui River investigated in this appendix. The used data is received from the Servicedesk Data of Rijkswaterstaat and is shown in Figures C.1, C.2, C.3 and C.4. The locations of the measurement points are shown in 4.6.

The dataset to determine the water levels is relatively short and is not sufficient to determine the governing water levels and flow velocities. However, the dataset was used in calculations to understand the processes rather than to find a solution. There is no phase error between the water level and the flow velocities. A combination of the largest differences in the water levels and the flow velocities has resulted in the following conditions:

Table C.1: Conditions at the measurement stations in the reference situations.

		Spijkenisse Brug	Goidschalxoord	Bernisse/Zuidland
Ebb 12-3-2015 0:40	h (m)	-0,86	-0,47	0,14
	u (m/s)	1,6		
Flood 17-3-2015 17:10	h (m)	1,14	0,96	0,39
	u (m/s)	-1,09		

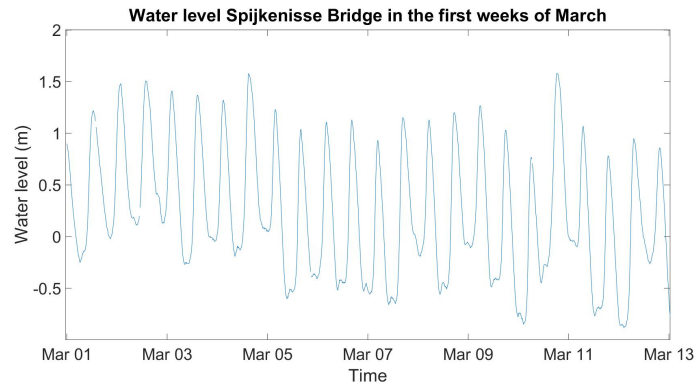


Figure C.1: Water levels measured at the Spijkenisse Bridge.

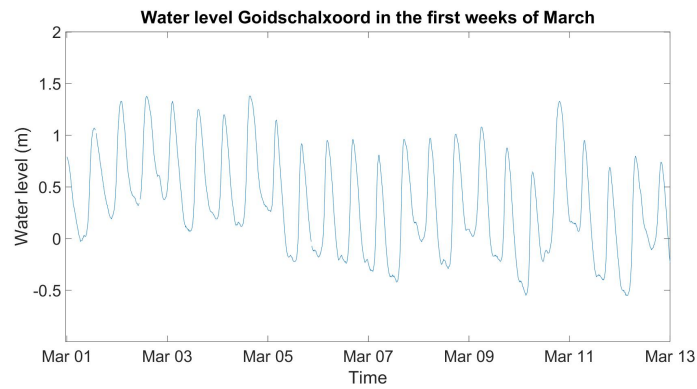


Figure C.2: Water levels measured at Goidschalxoord.

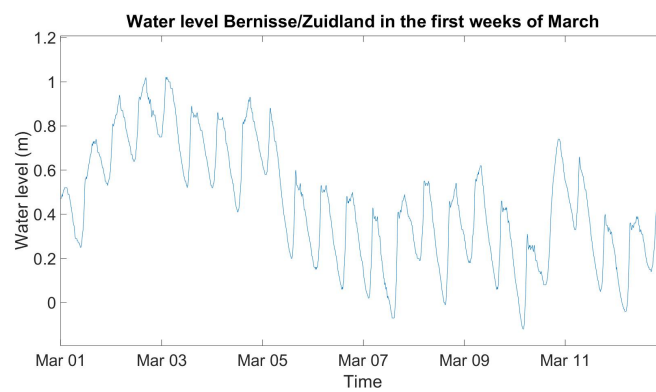


Figure C.3: Water levels measured at Bernisse/Zuidland.

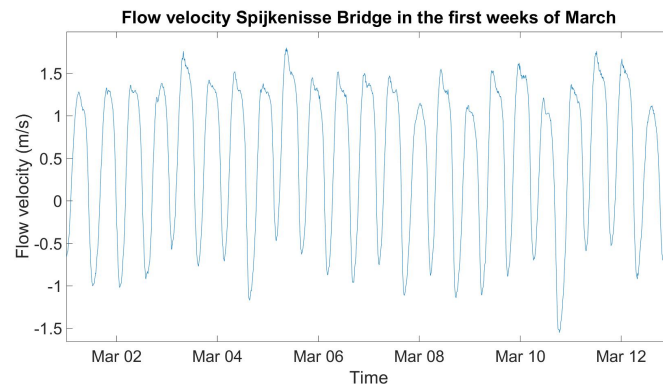


Figure C.4: Flow velocities at the Spijkensse Bridge.

Appendix D

Set-up of physical model

D.1 Introduction

Based upon the availability, time, complexity and budget it has been chosen to do the physical model investigation at a flume at the hydraulic laboratory of the faculty of Civil Engineering of the TU Delft. The available flume is 14.3 m long and has a width and height of 0.4 m. This is smaller than desired, but the advantage is that set-up time and the time in between the experiments is shorter. The width limits the experiments to investigate two-dimensional effects since the influence of the walls is rather large.

The height is another limiting factor. The water depth should be larger than 0.1 m to maintain sufficient measurement accuracy. Rule of thumb gives a scour depth of two times the water depth which means that the set-up is at least 0.3 m high. The possibility to increase the water level is thus limited and the related variations of scour depth are small as well. A constant water level of 0.13 m and a sand bed of 0.25 m was eventually chosen.

The main question to be asked is if these limitations of the flume make it impossible to answer the research questions. Most of the predefined questions may be answered, however not all can be answered with the model. The problem was that the ideas about the development scour differed. The limited time before a report had to be presented made it impossible to investigate every question and was the decision made to investigate only two-dimensional processes and use the results to define specific questions for following experiments. The physical model investigation can be seen as a reconnaissance of scour processes.

D.2 Scaling rules

All the processes of the field should ideally be included in physical model, scaled but similar to the prototype situation. Scaling means that the sizes of the model differ with the field. The scale factor is found by dividing the prototype scale by the model scale.

The similarity between prototype and model can be divided into geometry, kinematics, dynamics and morphology. The geometry is the difference in sizes, kinematic

in water flow, dynamics in the forces and morphology the development of the scour between the prototype and model. Once that the scale of the model differs from the prototype, which is the case in this research, it is impossible to find a solution that fits all the requirements and scale effects occur. To investigate the desired processes, it is important to make sure the dominating processes are scaled properly and to know the scale effects of the other processes.

Scaling Froude

When convective accelerations are important, Froude scaling has to be used. This means that in order to obtain the right energy height, the velocity and the water depth had to be scaled by Froude. This is shown below:

$$Fr = \frac{u}{\sqrt{gh}} \rightarrow \frac{n_u}{\sqrt{n_g n_h}} = 1 \quad (D.1)$$

Fr	Froude number (-)
n_u	Velocity scale (-)
n_g	Gravitational acceleration scale (-)
n_h	Depth scale (-)

The scale of the gravitational acceleration between prototype and model cannot be changed which means that the scale is 1. This concludes:

$$n_u = \sqrt{n_h} \rightarrow n_u^2 = n_h = n_s \quad (D.2)$$

Once this requirement is not met, scale effects are introduced. This means that the energy height is not only depending on the scales, but also on the parameters of the model, see Figure D.1.

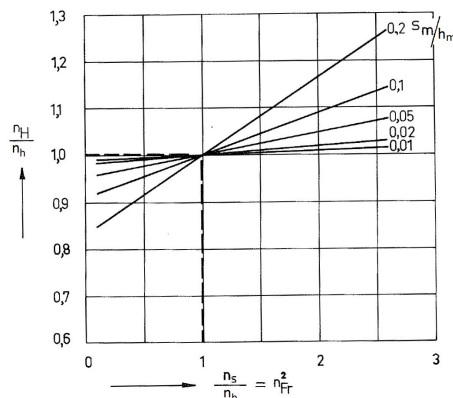


Figure D.1: Schale effect once the Froude requirement is not met with $s = \frac{u^2}{2g}$ (velocity height) and H the energy height, DE VRIES (1975).

Scaling Reynolds

When viscous forces are dominant in modelling the flow (around the determination of laminar or turbulent flow; low Re) Reynolds scale has to be used:

$$Re = \frac{uh}{\nu} \rightarrow \frac{n_u n_h}{n_\nu} \quad (\text{D.3})$$

Re Reynolds number (-)
 n_ν Viscosity scale (-)

The scale of the viscosity between the prototype and the model is 1, which concludes:

$$n_u = n_h^{-1} \quad (\text{D.4})$$

This shows that it is impossible to fulfil the Froude and the Reynolds requirement at the same time for a scale factor different than 1. As long as the model is not too small ($h < 0.1$ m) and Re stays turbulent ($Re > 2000$) it is possible to neglect the viscous effects, which means that the Reynolds scale is not a strict condition. In the scaled model with $Re \approx 5 \cdot 10^4$ this requirement is met.

Critical flow velocity

The critical flow velocity has to be determined without scale effects in order to model the physical processes correctly. Ideally Froude scaling has to be used, but the dimensions of the grains have to be scaled similarly with the geometry. This is impossible since a scale of more than 1:100 gives grains of $3 \mu\text{m}$. For the experiment sand with the following properties is available:

Table D.1: Parameters of the sand.

Sand	d_{50} (μm)	D_*	ψ_c
Silica M32	260	6.58	0.015 - 0.04

The critical flow velocity is given by:

$$u_c = 2.5 \sqrt{\psi_c g d_{50}} \ln \left(\frac{12h}{k_s} \right) \quad (\text{D.5})$$

The corresponding critical velocity lays between $u_c = 0.16 - 0.26$ m/s. This is verified in the first experiment.

Geometry of the scour hole

The Scour Manual HOFFMANS AND VERHEIJ (1997) gives the formula for the time scale according the Breusers formula:

$$n_t = n_\lambda^2 n_\Delta^{1.7} (n_{\alpha_l u_l - u_c})^{-4.3} \quad (\text{D.6})$$

Overview of parameters

An overview of all the scaled parameters is given in table D.2.

Table D.2: Overview of field and model values.

Parameter		unit	field	Scale factor	model
Water depth	h	m	16.5	126.92	0.13
Max depth hole	y_m	m	28	126.92	0.22
Max length hole	L	m	300	126.92	2.36
Max velocity	u_{max}	m/s	1.6	3.2	0.50
Min velocity	u_{min}	m/s	-1	3.2	-0.31
Critical velocity	u_c	m/s	0.55	2.12	0.26
Relative turbulence	r_0	-	0.09	1.00	0.09
Turbulence coefficient	α	-	1.94	1.00	1.94
Reynolds	Re	-	26000000	400	65000
Froude	Fr	-	0.13	0.28	0.44
Chézy	C	$m^{0.5}/s$	43	1.00	43
Bed roughness / d_{50} material plate	$k_{s,field}$	m	0.413	126.92	0.00325
Nikuradse Roughness	k_s	m	0.825	126.92	0.0065
Relative density	Δ	-	1.65	1.00	1.65
Diameter sand	d_{50}	μm	350	1.35	260
Shields parameter	ψ	-	0.054	1.35	0.040
Initiation of movement	$\alpha u - u_c$	m/s	2.554	3.60	0.710
Time	t	s	11.315	65.65	0.172

Based upon Figure D.1 is it possible to derive the scaling effect of the energy height.

$$\frac{n_s}{n_a} = 0.28 \quad \frac{s_m}{a_m} = 0.098 \quad \rightarrow \quad \frac{n_H}{n_h} \approx 0.91 \quad (D.7)$$

D.3 Model set-up

The flume is filled with sand to create an erodible bed. The height of the sand layer is 0.25 m. At both sides of the sand layer are slope constructed. These slopes diverge the water flow over the sand bed. Upstream of the model set-up is a diffusor placed to limit waves and decrease the length which is needed to have a fully developed flow regime. The set-up is shown in Figure D.2.

D.3.1 Bottom roughness

Some length was used to let the flow upstream of the scour hole adapt to the bottom friction and form a logarithmic velocity profile. This was important to have a fully de-

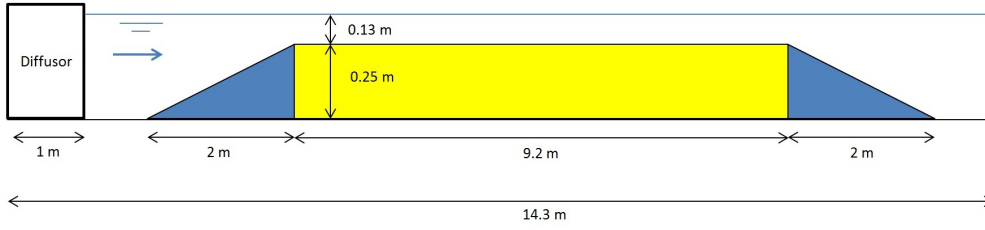


Figure D.2: Set-up of model at the start of run 1.

veloped flow regime approaching the scour hole. Following the assumptions of researches from the past, two hydraulic roughnesses have been chosen (Adihardjo, 1972).

Table D.3: Roughness following Adihardjo (1972).

Roughness description	Roughness C ($\text{m}^{0.5}/\text{s}$)	k_s (m)
Medium	42.9	$k_s = 0.025h_0$
Rough	48.3	$k_s = 0.05h_0$

The next step is transferring these Nikuradse roughness's to a more practical value. Often used examples are $k_s = 2d_{50}$ for hydraulically smooth conditions and $k_s = 3d_{90}$ for hydraulically rough conditions. Theoretical background of these values is shown in Figure D.3. This figure shows that a perfect placing of the particles gives a diameter similar to the grains similar to the roughness. When the placement is less neat it is around the 2 times the diameter and with an irregular bed and multiple grain sizes the factor only grows.

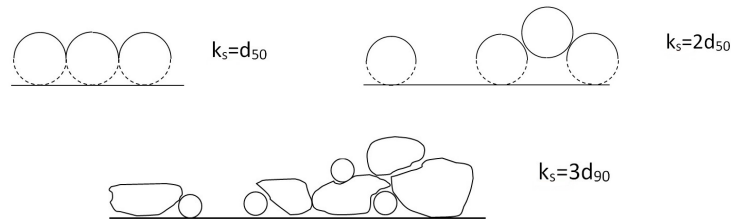


Figure D.3: Comparison between Nikuradse roughness and the grain size.

To add roughness to the poorly erodible bed it was chosen to glue grains on top of the steel plates. With above described theory grain size leading to this roughness was determined. For $h_0 = 0.13$ m and $k_s = 2d_{50}$ is the grain size for a medium bed $d_{50} = 1.625$ mm and for a rough bed $d_{50} = 3.25$ mm. However this is a calculated value and these values does not have to correspondent with the available materials. Further is as shown in Figure D.3 the placement of the grains a determining factor the roughness. A

run has to be carried out to know the roughness of the grains on the plate.

Because of the time limitation and the time needed to prepare the steel plates with the roughness, only one roughness: $d_{50} = 1.75$ mm was used.

D.3.2 Work plan

Week 1

Prepare the flume; make the slopes, fill the flume with sand and prepare the steel plates with roughness. Further all the measuring equipment has to be tested.

Week 2

Run 1 & 2: The calculated critical velocity at which the sand starts to move is verified in the first experiments. Based on the d_{50} some calculations have been made to estimate the this critical velocity. During these experiments is the initiation of sediment transport investigated. Based upon the results the model parameters can be corrected where needed. At the same time, the measurement equipment was tested.

The set-up of the model is shown in Figure D.2. The water enters the flume from the left and flows through the diffusor, which diminishes the length to reach the acquired flow conditions. Thereafter, the water level is reduced by a sill which is made to navigate the water over a sand package. The sand package was not protected during these runs and once the velocity reaches the critical velocity, the sand will erosion of sand is observed.

Run 3: The roughness of the plate is investigated in the third run. The plates with the roughness are placed on top of the sand layer, see Figure D.4. Some sand has to be removed to place the plates at the right height.

As already mentioned the goal of this experiment is to calculate roughness of the plates. This is achieved by measuring the change in water level (δh) over the construction. When the water depth, flow velocity and the length between the measuring points is known the roughness can be calculated by:

$$u = C\sqrt{hi} \quad \rightarrow \quad u = C\sqrt{h\frac{\delta h}{L}} \quad \rightarrow \quad C = \frac{u}{\sqrt{h\frac{\delta h}{L}}} \quad (\text{D.8})$$

To determine if it is possible to measure a difference in water depth between two points is this Δh calculated. With $h = 0.13$ m, $C = 42.8$ m^{0.5}/s, $L = 9$ m and $u = 0,35$ m/s a difference of $\delta h = 0.004$ m should be found, which means that the difference can be measured. Higher flow velocities lead to a larger difference between the water levels.

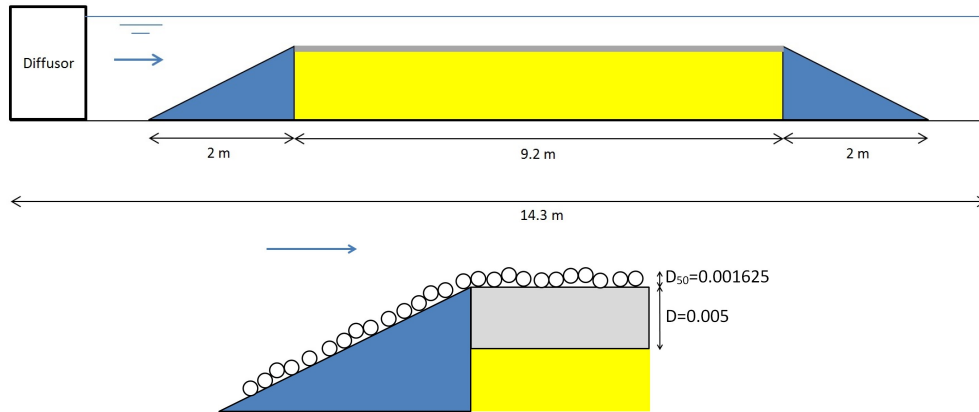


Figure D.4: Set-up of model at the start of run 2 & 3.

Based on the found results the flume can be tilted. When Δh becomes 0 due to the tilting of the flume, a uniform flow has been reached. This means that the friction and advection of the momentum equation are in balance.

Run 4 & 5: Steel plates with a length of 4.2 m are placed against the upstream slope in experiments 4 and 5, see Figure D.5. The 4.2 m has been determined by a rule of thumb ($30 \cdot h_0$), which is needed to have a uniform flow regime. For $h = 0.14$ m, which is the maximum water depth that is possible in this flume, a length of $L = 4.2$ m has been found. The experiments with only a protection upstream corresponds with the experiments of Adihardjo (1972) which can be used as reference. The run also corresponds with the scour situation which has been chosen as reference in the literature report; scour downstream a sill with a sill height $D = 0$ m and a bed protection downstream the sill. This means that the scour depth can be estimated by the Breusers equation 2.12. The difference between the experiments is the flow velocity and the roughness upstream.

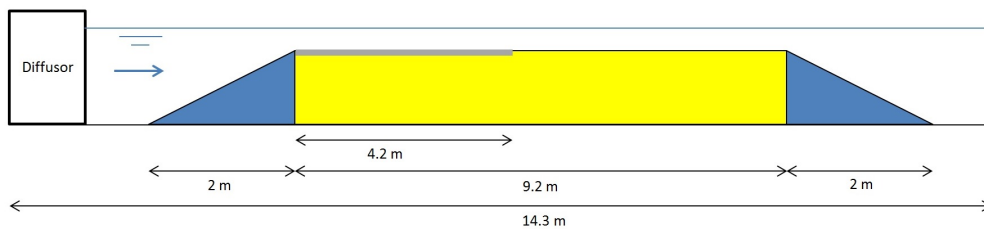


Figure D.5: Set-up of model at the start of run 4.

Run 6 - 10: During the experiment is the plate downstream of the scour hole at a fixed distance from the upstream plate, see Figure D.6. With the experiment can be determined if the available length to scour has influence on the development of the scour hole. The results of each run can be compared to the results of the runs 4 and 5. Answer

should be given if there is a difference in the gradient of the up/down-stream slope, scour depth and overall geometry. Also the question if undermining is a problem and if it is up or downstream can be answered. Further the flow velocity in the scour hole and the development of an equilibrium profile was studied.

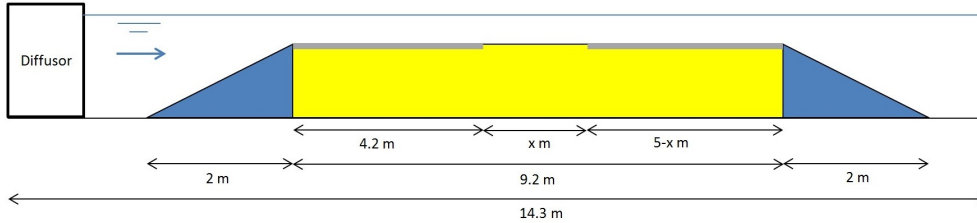


Figure D.6: Set-up of model at the start of run 6 - 10.

Table D.4: Overview of the indicated runs. Depending on the results of previous runs it is possible to change the scheme.

Run	Length scour hole (m)	Flow velocity (m/s)
6	0.1	0.6
7	0.2	0.6
8	0.2	0.45
9	0.5	0.45
10	1.0	0.45

Week 3

Run 11 & 12: The experiments of the third week depend on the results of the previous experiments (6 - 10). With the knowledge about the undermining geometry for each run it is possible to make conditions for movement of the plates. The plate is moved backwards and the scour hole has adapted to the new situation. This is roughly the principle which is expected to happen in the field. The hole is developing and slopes become steeper and eventually undermines the downstream poorly erodible layer. The undermining grows until the stiff layer fails due to erosion of lumps (movement of the plate). This gives the same geometry as in previous stages of the scour process.

Proposed conditions of moving the plate:

- Move the plates once the undermining reached a certain length.
- Move the plates once the hole reaches an equilibrium.

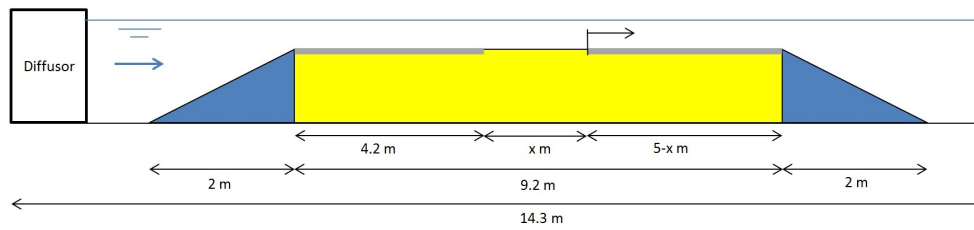


Figure D.7: Set-up of model at the start of run 11 & 12.

Week 4

Run 13 & 14 Experiments 13 and 14 are carried out with a different approach. The tidal influence on the flow in the field is simulated. This means that the flow velocity is variable over time and during a tidal cycle even reverses its direction. Problem is that the flume can only flow in one direction. The only way to solve this, is to make an artificial scour hole with a geometry which is 180 degrees rotated, see Figure D.8. This simulates the flow from a reverse direction by rotating the scour hole.

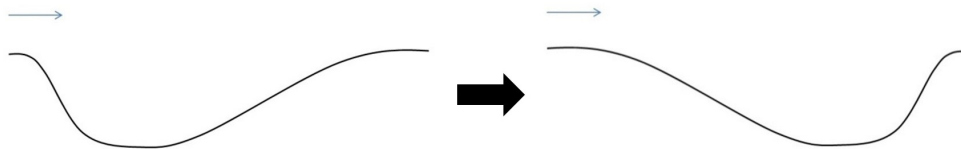


Figure D.8: The change of geometry; left the expected result after a previous runs, right the start position of the run.

Run 15 A 2 day run is carried out to investigate the final profile after a longer run time. It has been chosen to work with a 0.5 m long hole and a velocity of $u = 0.5$ m/s. The reason to perform this experiment is to gain more knowledge of the possible equilibrium profile.

Week 5

At forehand the fifth week would not be used, but during the experiments some new questions and ideas were raised. One of the unforeseen results was the large undermining. Undermining to this extend is never in the field observed and to create an experiment without undermining the downstream slope was made of an erosion-resistant layer, see D.9. A steel plate with a length of 0.20 m was place within the scour hole under an angle of 45 degrees.

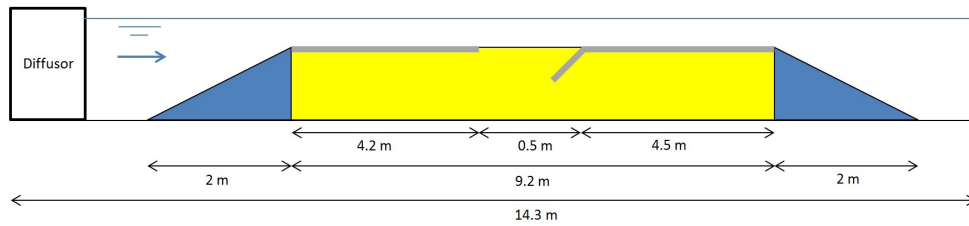


Figure D.9: Set up of runs 16 & 17.

D.3.3 Measurement instruments

Laser

The laser measures the length of its beam to the surface below. This gives an electric signal which can be translated to depth. The laser is placed in a small boat, with a bottom of transparent plastic, in order to measure the depth along the flume. It is connected to a cart above the flume which can measure the distance while rolling over the tracks of the flume. A number of pulses are generated during its rotation of the wheels. The water depth is measured during each pulse. This includes the distance to the signal.

The laser scans only measure at the surface directly below the beam. Undermining is not directly visible in the results of the scans. It has to be measured along the glass wall. When the experiment is finished it is possible to make a normal scan first and thereafter a scan of the surface after removing the plates. Comparison gives the undermining in the final state.

Video

The development over time the experiment is filmed. It makes it possible to look back at long term movements, but also to look back at abrupt movements.

Gauge needles

The water levels are determined with gauge needles. These needles have an accuracy up to a tenth of a millimetre.

ADV

The Acoustic Doppler Velocimeter sends out ultrasonic pulses which should reflect onto a particle in the water. The reflection is caught by the receivers around the pulse generator. The difference in time between the received signals comes from the movement of the particles. The flow velocity is measured by the Doppler Effect between the signals. The water depth is only 0.13 m and the instrument has measures at 0.05 m from ultrasonic sounder which has to be in the water. This limits the depth of measurements. Therefore the head of the ADV is orientated to look from the side (side looking probe) instead of from the top. Downside of this method are the disturbances which may be caused by

the ADV. The instrument has to be close at the bottom to measure the velocity at the bed.

The ADV detects particles in the water and measures this velocity. Often clay particles are added as medium. However, the suspended materials in the water may hinder the laser. Furthermore, the water of the entire water system of the laboratory becomes turbid. It was decided to use electrolysis to create air bubbles in the water. The difference in electric potential splits the water in hydrogen and oxygen. The oxygen bubbles substitute the clay particles and the water is clear. However, the electrical power supply has to be placed in front of the ADV which may influence the flow.

The ADV can work at certain ranges: ± 0.01 , 0.1, 0.3, 1, 2 and 4. The accuracy is $\pm 0.5\%$ of the installed range.

Dye

At locations the ADV cannot measure the flow velocity, dye was added to the water. It is impossible to measure the flow velocity of this dye, but it helps to analyse the flow. The dye is also used to give a general idea about the flow regime in the flume.

Rehbock weir

The discharge of the flume can be measured at two locations: a pressure meter in the supply pipes and at the Rehbock weir after the flume. The discharge will be measured with both meters, however with different accuracies and functionality they have their field of applications for specific functions. The electronic meter gives a quick readable number of the discharge, but is not that accurate. The Rehbock is therefore used during the runs with the electronic as verification and the electronic is used to set the flow.

The Rehbock weir is a sharp weir where the water level can be measured at 2 times the weir depth. This water level has to be measured as $h_k = h - h_{weir}$. With this level the discharge can be derived by:

$$\begin{aligned}
 q &= m' \frac{2}{3} h_e \sqrt{\frac{2}{3} g h_e} \\
 m' &= 1.045 + 0.141 \frac{h_e}{a} \\
 h_e &= h_k + 0.0011
 \end{aligned}
 \tag{D.9}$$

q	Discharge per unit of width (m^2/s)
m'	Coefficient of the weir (-)
h_e	Corrected water height above the weir (m)
a	Weir height (m)
h_k	Water height minus the weir height at the measure point (m)

Appendix E

Scour formula for suspended sediments

E.1 Introduction

The theory of the scour is explained in chapter 2. It elaborates the theories to calculate the parameters of the scour hole. The Breusers formula calculates the scour depth for development of scour at the end of a bed protection. The scour depth depends on the erodible material and the upstream flow conditions. However, the results of the laboratory experiments showed that the poorly erodible layer downstream of the scour hole influences the scour depth. This appendix shortly investigates the opportunity to include the difference between bed load and suspended sediments.

E.2 Analyses

The experiments showed that sediment transport by bed load was stopped when the scour hole extended under the steel plates; only suspended transport remained. The sediment transport in the Breusers formula (u_c) is based upon the Shields criteria. This criteria describes initiation of movement of the grains, but does not include the type of transport. That is why the calculated amount of scoured material larger than observed.

Furthermore, the formula only calculates the scour for a specific type of grains. Various gradations of sediments are usually found in the field. The grains with a lower mass are more easily transported and the grains with a higher resistance may remain. These larger grains protects the smaller grains.

Another factor which increases this mobility parameter is the development of slopes. The grain has to move up the slope and the load has to overcome gravity. Adding all these aspects results in a different behaviour of the scour hole. In the present formula the scour constantly increases and no equilibrium depth will be found, but with these new factors an equilibrium may be described.

The resistance of the bed is given by \bar{u}_c , see equation below:

$$\bar{u}_c = 2.5\sqrt{\psi_c \Delta g d_{50}} \ln\left(\frac{12h_0}{k_s}\right) \quad (\text{E.1})$$

d_{50}	Median grain size (m)
g	Acceleration of gravity (9.81 m/s ²)
k_s	Nikuradse roughness
ψ_c	Shields parameter

Physical model investigation showed that once suspended sediment is the only mean of transport, the initiation of movement is not sufficient to describe the sediment transport. Vertical motion is necessary to transport the grain out of the scour hole. Turbulence and gravitational forces act on the grain during the vertical transport. The gravitational force is given in the fall velocity which can be determined by (JANSEN 1979):

$$w_s = \frac{1}{18} \frac{\Delta g D^2}{\nu} \quad (\text{E.2})$$

w_s	Fall velocity sediment (m/s)
D	Particle grain diameter (m)
ν	Kinematic viscosity m ² /s

Depending on the location of the grain a certain vertical height has to be overcome to be transported out of the hole. As the scour hole increases in depth this height increases as well. This suggest that the time depended formula has to depend on the scour depth, which means that the maximum scour depth is a parameter in its own formula. The consequence is that a large scour depth decreases the rate of scour and thus a value for the maximum scour depth can be found. As already mentioned is upwards movement dominated by the turbulence in the scour hole. However it is questionable if this turbulence is correctly denoted in the formula. The Breusers formula determines the turbulence intensity at the transition from the protected bed and the erodible bed. This is based upon the idea that the structure upstream of the scour hole is the source of the turbulence. However, the physical model showed that the undermined plates downstream had a large influence on the flow regime and turbulence in the scour hole.

Due to the limited time available and the lack of data, this was not further investigated. It is recommended to investigate the turbulence and sediment transport in the scour hole more accurately.

Appendix F

Figures of the 2DV models

This Appendix contains the figures of the results of the numerical simulations of the 2DV model. The results of the models with the constant eddy viscosity can be found in the report. The results of the other turbulence models are shown below.

F.1 2DV model of physical model investigation experiment 17

The downstream slope of the scour hole was protected during run 17 of the Physical model investigation. This stopped the undermining and limited the length of the scour hole. The gap between the plates was 0.5 m and the plate at the downstream slope was placed under an angle of 45 degrees.

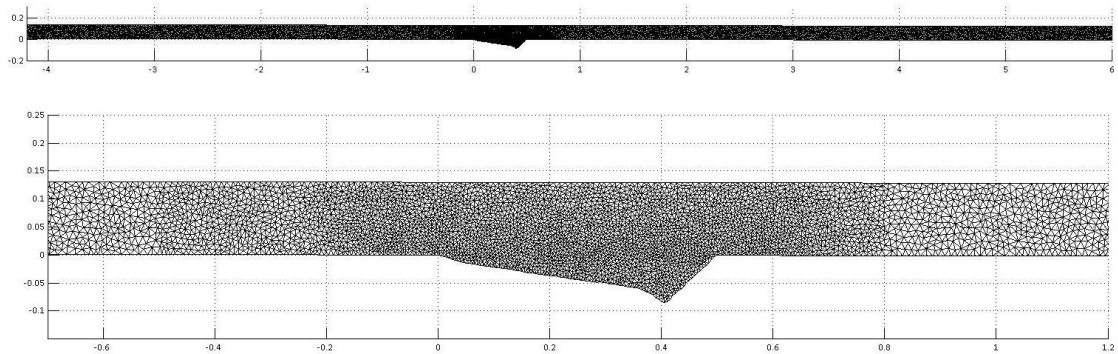


Figure F.1: Set-up of the computational grid of model run 17, with a detailed view of the scour hole.

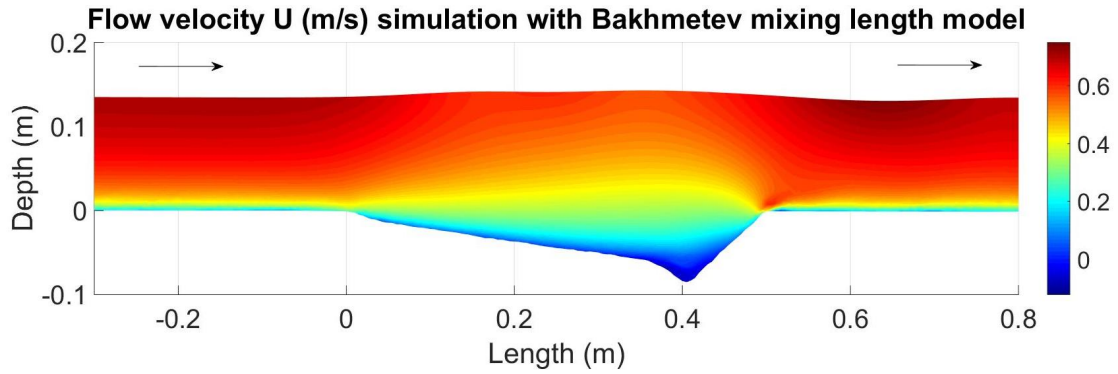


Figure F.2: The flow velocity in the longitudinal direction computed with Bakhmetev.

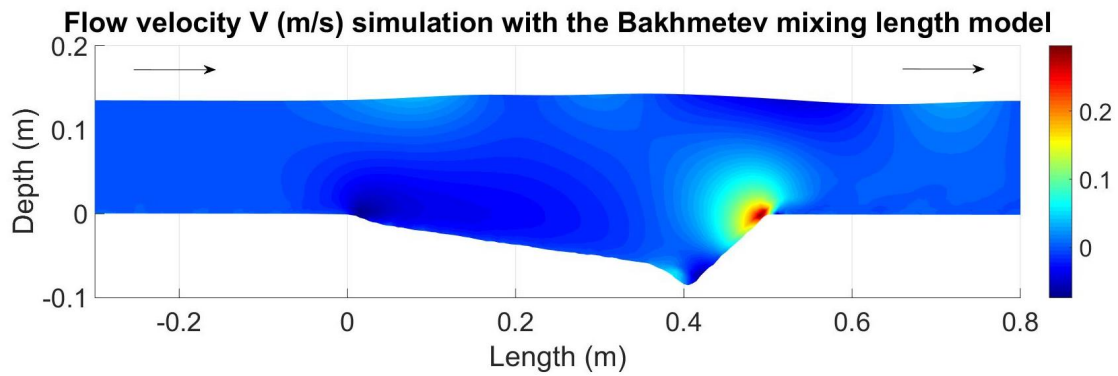


Figure F.3: The flow velocity in the vertical direction computed with Bakhmetev.

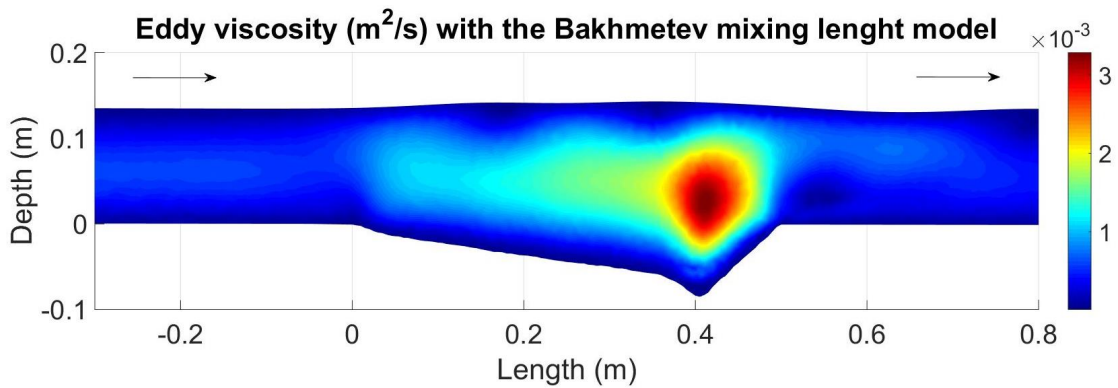


Figure F.4: Profile of the eddy viscosity computed with Bakhmetev.

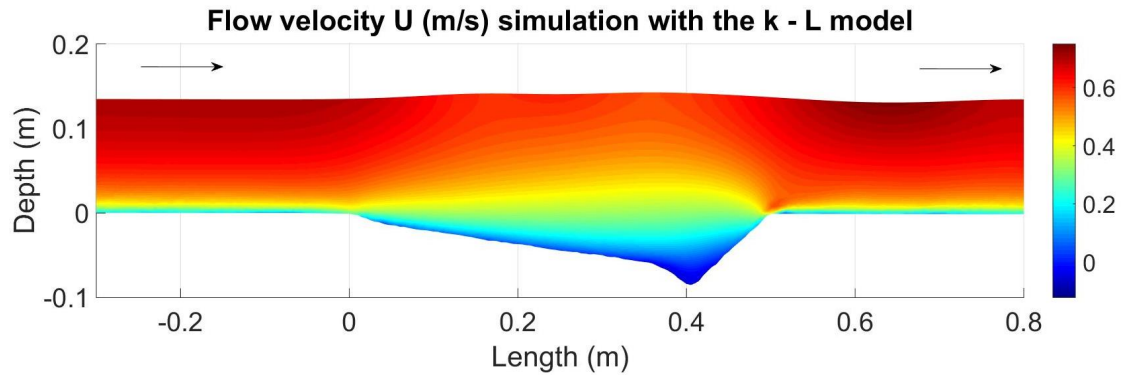


Figure F.5: The flow velocity in the longitudinal direction computed with $k - L$ model.

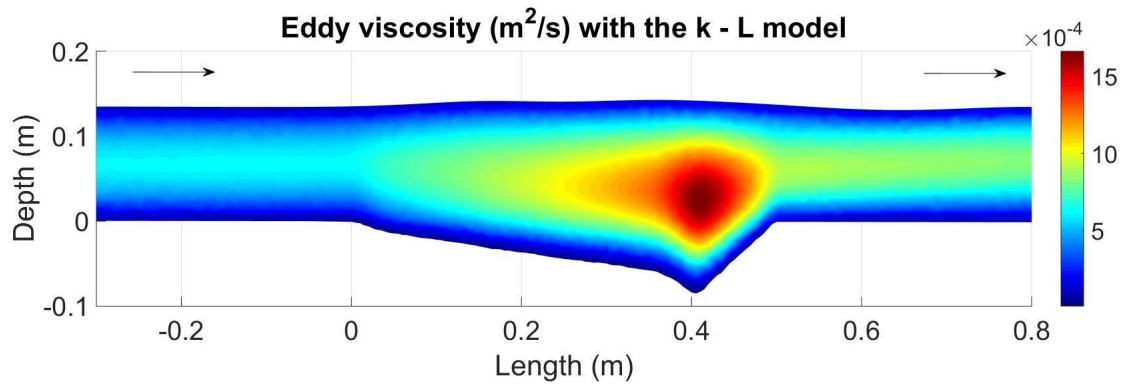


Figure F.6: Profile of the eddy viscosity computed with $k - L$ model.

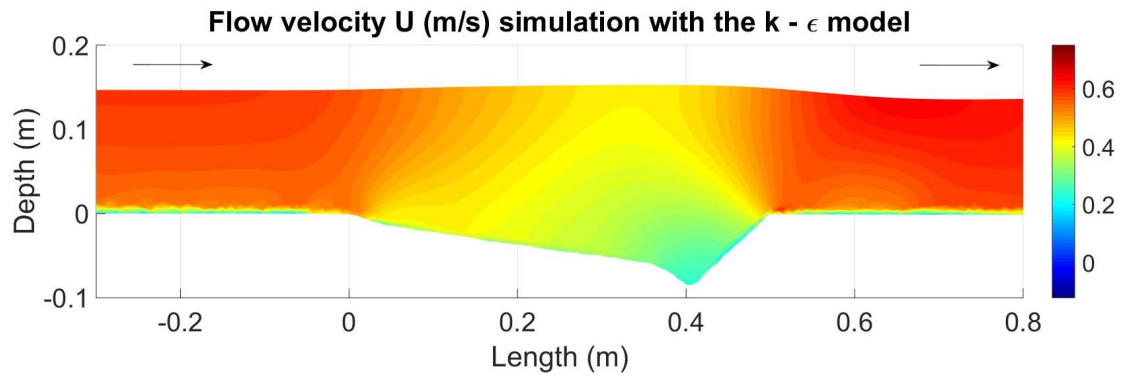


Figure F.7: The flow velocity in the longitudinal direction computed with $k - \epsilon$ model.

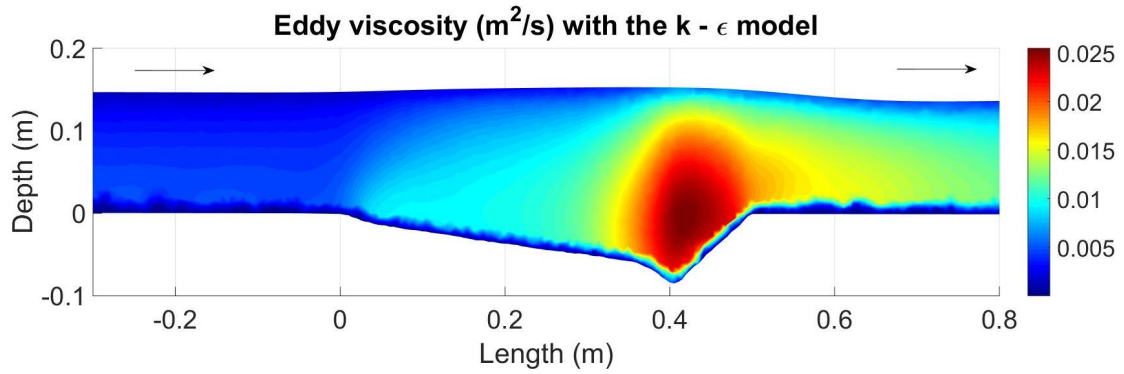


Figure F.8: Profile of the eddy viscosity computed with the $k - \epsilon$ model.

F.2 2DV model of physical model investigation experiment 20

During run 20 of the physical model investigation the scour hole had a gap of 0.5 m between the plates. The slope at the back of the scour hole was unprotected and undermined.

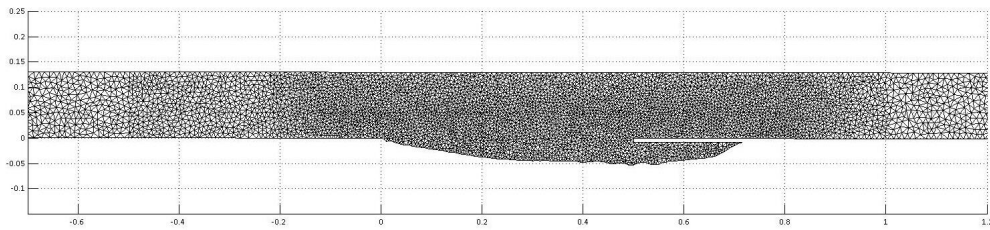


Figure F.9: Set-up of the computational grid of model 2.

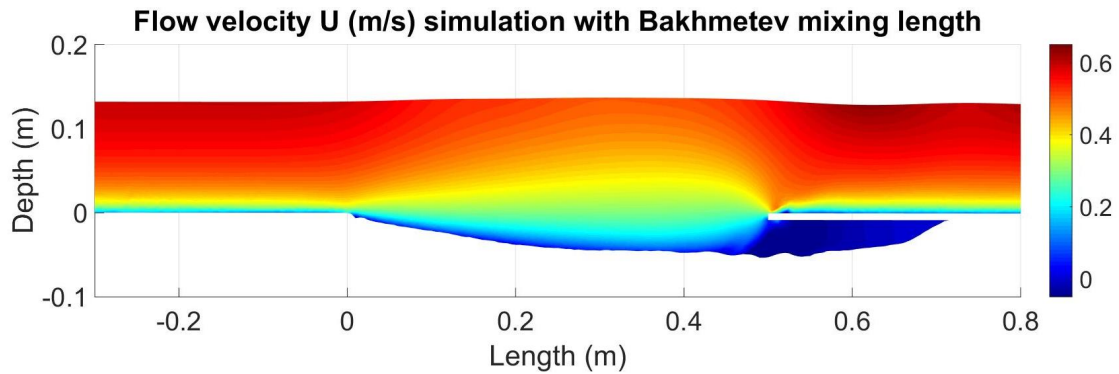


Figure F.10: The flow velocity in the longitudinal direction computed with Bakhmetev mixing length.

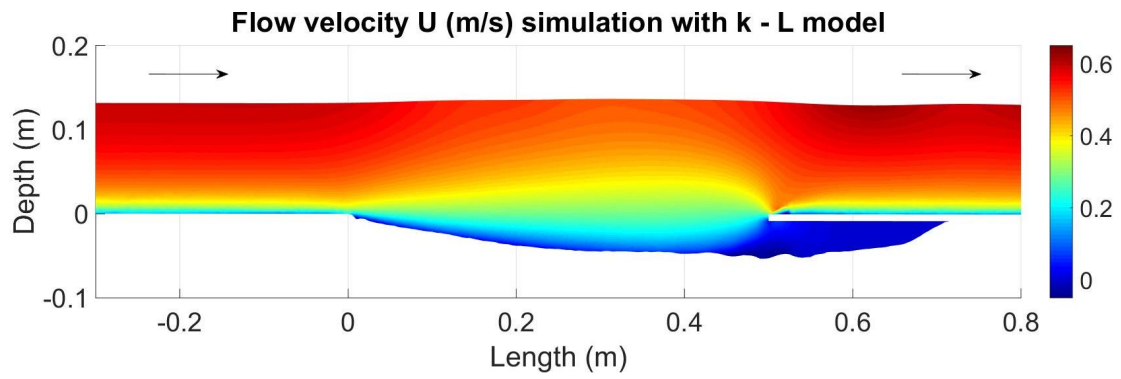


Figure F.11: The flow velocity in the longitudinal direction computed with $k - L$.

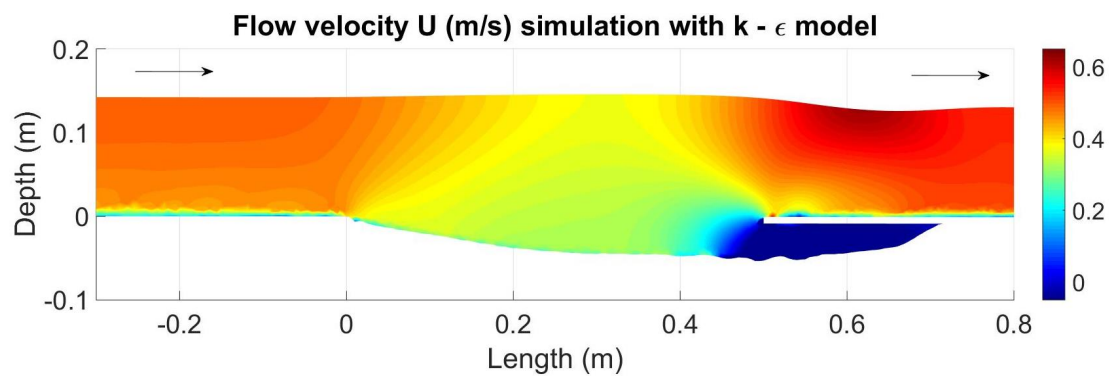


Figure F.12: The flow velocity in the longitudinal direction computed with the $k - \epsilon$.

Appendix G

Figures of the 3D numerical model

Detail scour holes

The figures in this section show a top view of the scour holes. Figure G.1 shows the decrease of cell size at the berenplaat scour hole. The colours show the water depth.

Detail of the grid at the Berenplaat scour hole including the depth (m)

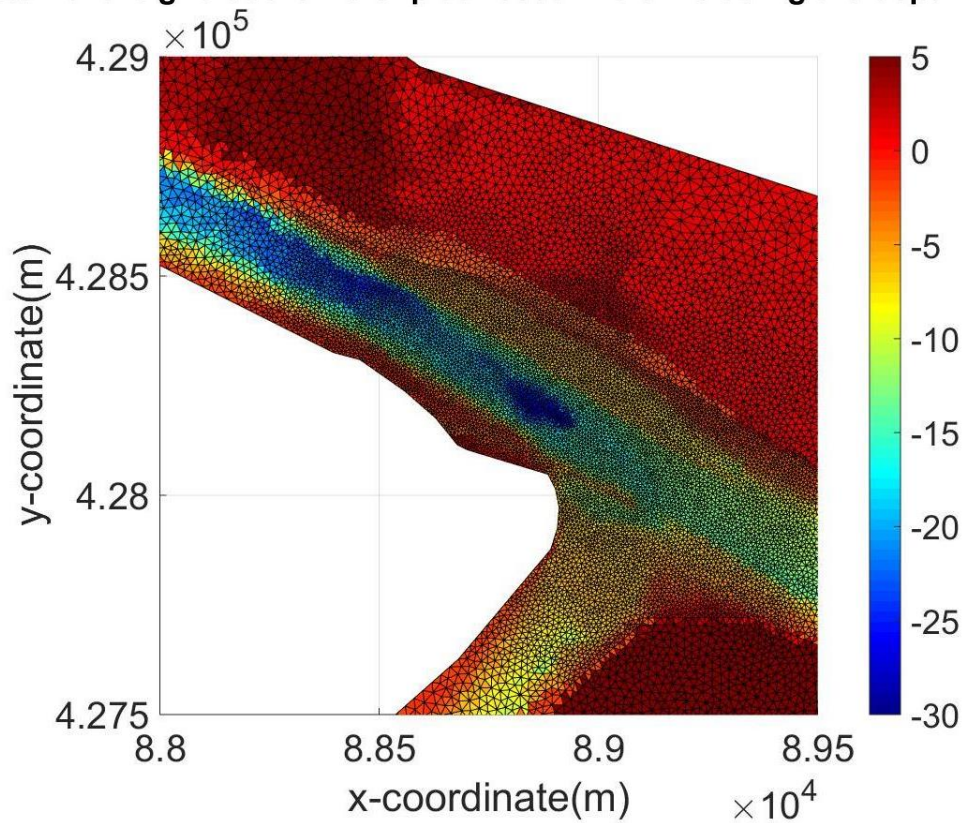


Figure G.1: Top view of the Berenplaat Scour Hole.

In Figure G.2 shows the top view of the scour hole including the locations of the cross sections.

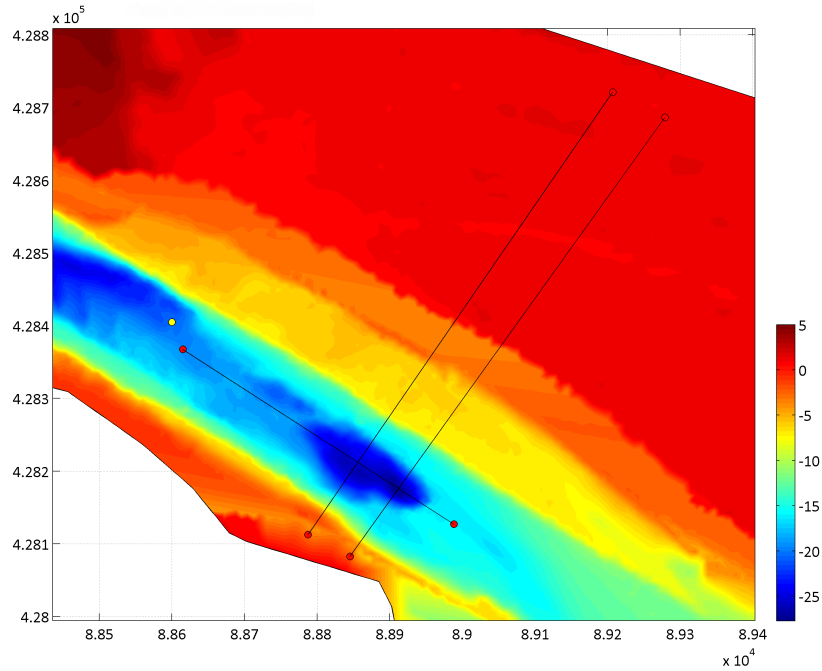


Figure G.2: Top view of the Berenplaat Scour Hole with the cross sections.

Figure G.3 shows the grid at the longitudinal cross-section.

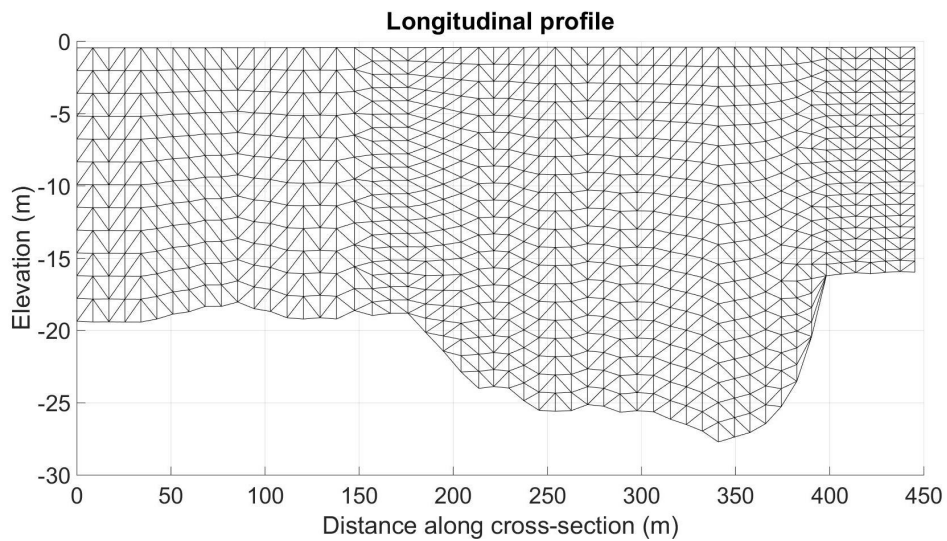


Figure G.3: Computational grid of the longitudinal profile of the Berenplaat Scour Hole.

A top view of the scour holes Schuddebeursedijk and Poortugaal is shown in Figures G.4 and G.5.

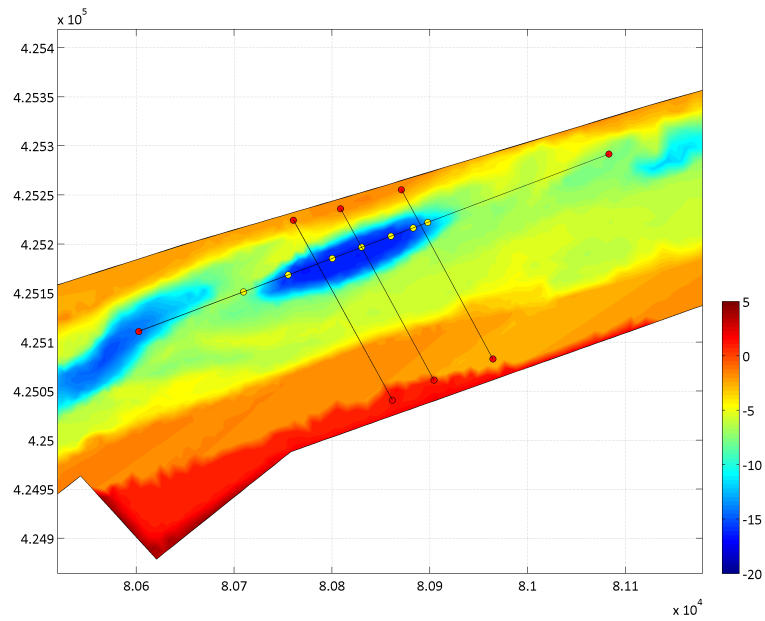


Figure G.4: Top view of the Schuddebeursedijk Scour Hole with the cross sections.

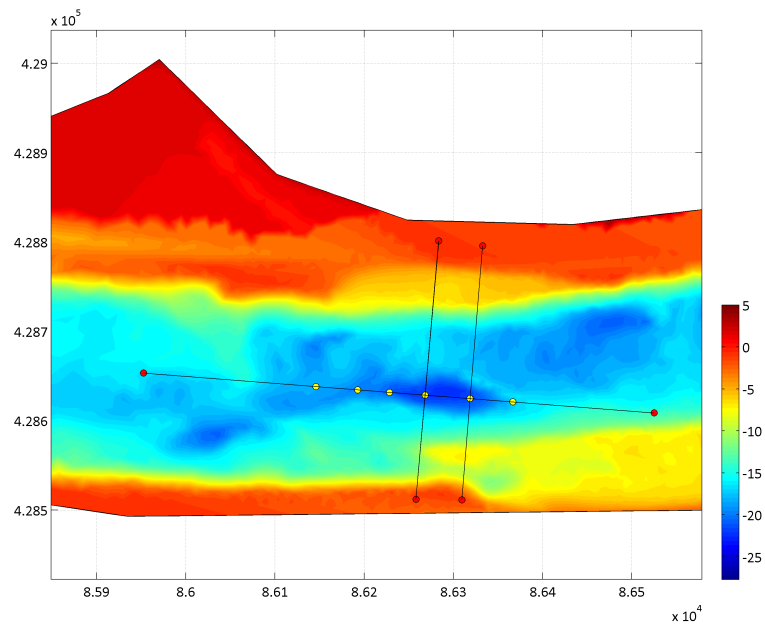


Figure G.5: Top view of the Poortugaal Scour Hole with the cross sections.

Cross-sections of the Berenplaat Scour Hole

The flow velocity over the longitudinal cross section of the Berenplaat Scour hole determined with the $k - L$ model is shown in Figure G.6.

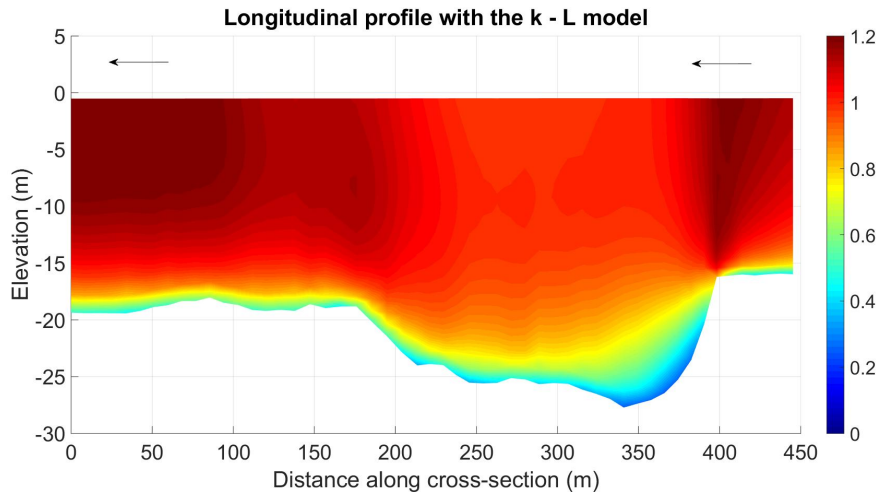


Figure G.6: Longitudinal velocity profile of the Berenplaat Scour Hole ebb (m/s).

Figure G.7 shows the velocity determined with the $k - \epsilon$ model.

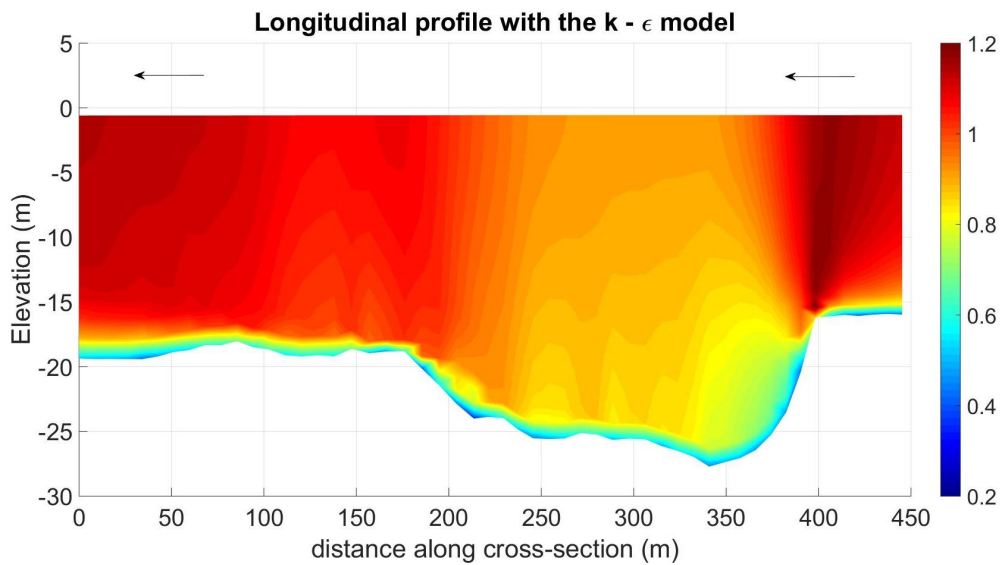


Figure G.7: Longitudinal velocity profile of the Berenplaat Scour Hole during ebb (m/s).

Figures G.8, G.9 and G.10 show the flow velocity over the cross section. The highest velocity peak is at the right side of the deepest point. This is caused by the bend of the confluence at the Spui River. The flow velocity in at the right slope of the scour hole is shows a stepwise increase in the velocity. This is caused by the model. A higher grid accuracy should increase the graphical output.

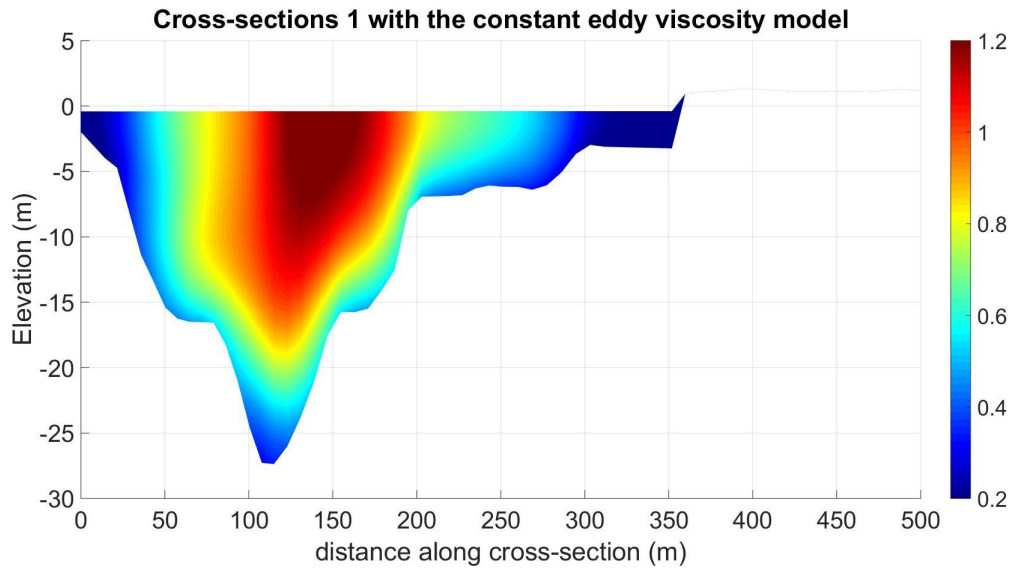


Figure G.8: Cross-section with flow velocities along the Berenplaat Scour Hole ebb (m/s).

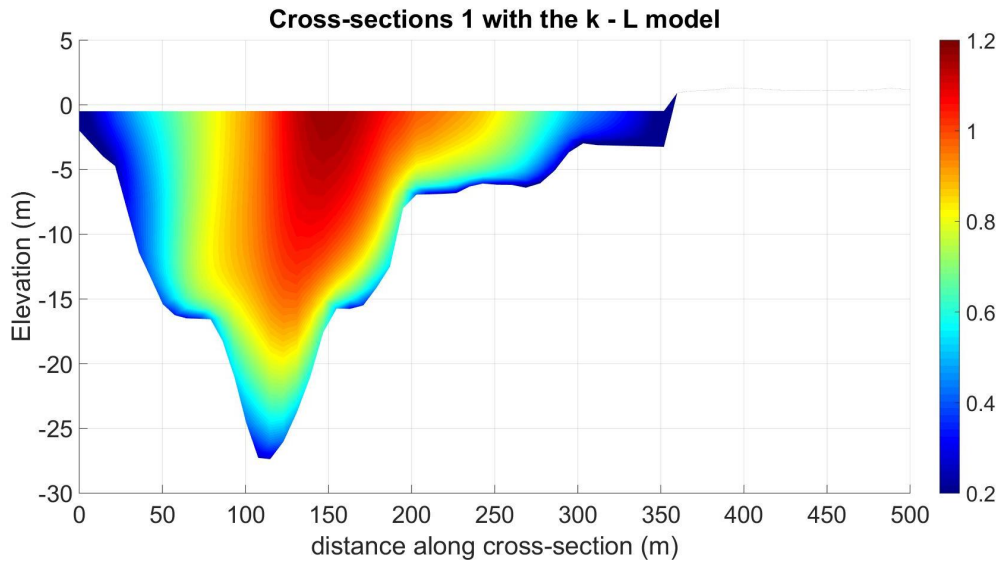


Figure G.9: Cross-section with flow velocities along the Berenplaat Scour Hole ebb (m/s).

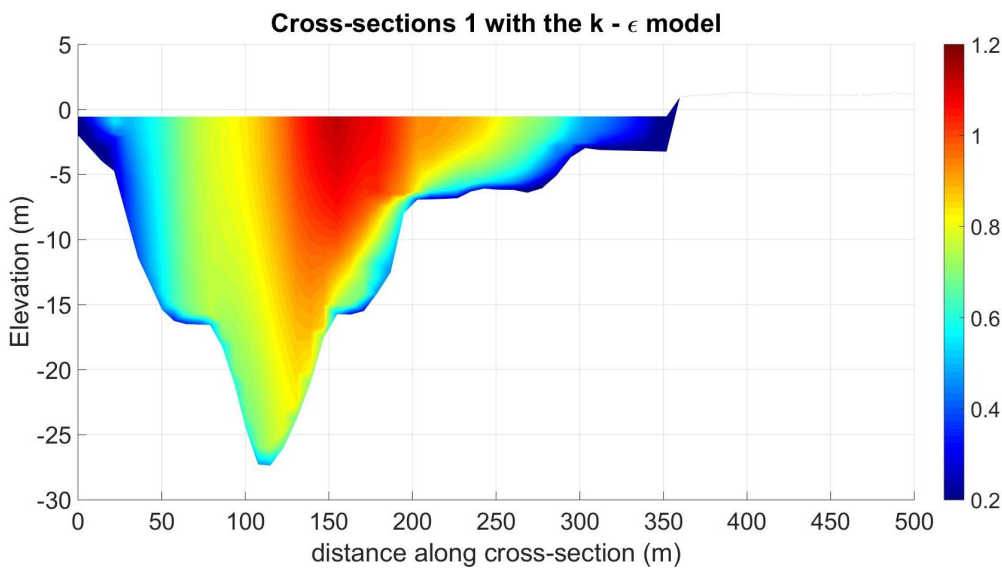


Figure G.10: Cross-section with flow velocities along the Berenplaat Scour Hole during ebb(m/s).

Longitudinal velocity profile Spui Scour Hole

Figure G.11 shows the flow velocity in the Spui Scour Hole modelled with the constant eddy viscosity. The vertical eddy viscosity is $0.0437 \text{ m}^2/\text{s}$.

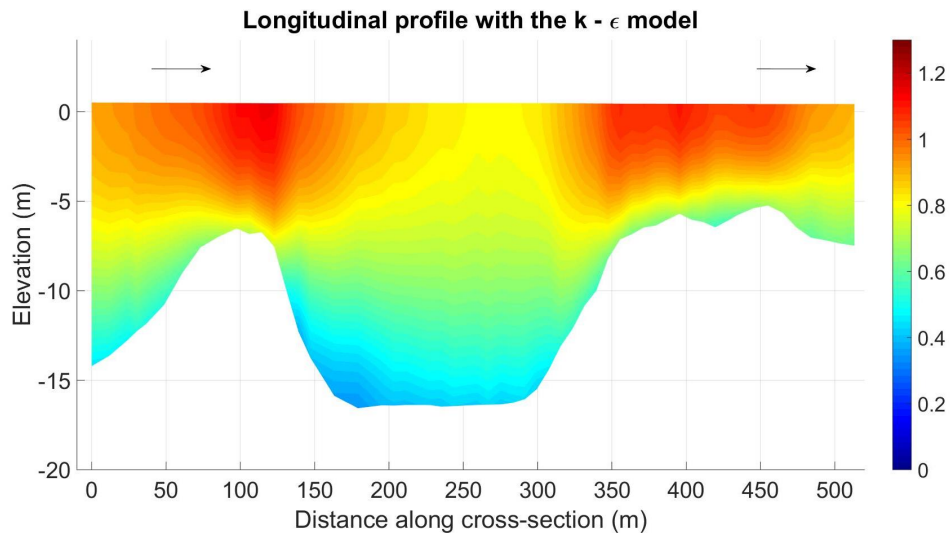


Figure G.11: Longitudinal velocity profile of the Schuddebeursdijk Scour Hole during ebb (m/s).

Figure G.12 shows the flow velocity in the Spui Scour Hole modelled with the $k - L$ model.

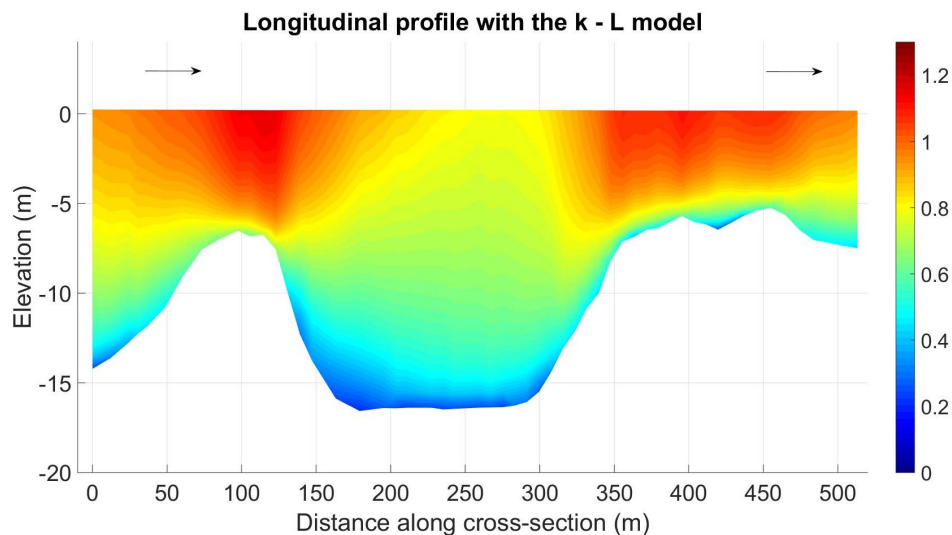


Figure G.12: Longitudinal velocity profile of the Schuddebeursdijk Scour Hole during ebb (m/s).

Figure G.13 shows the flow velocity in the Spui Scour Hole modelled with the $k - \epsilon$ model.

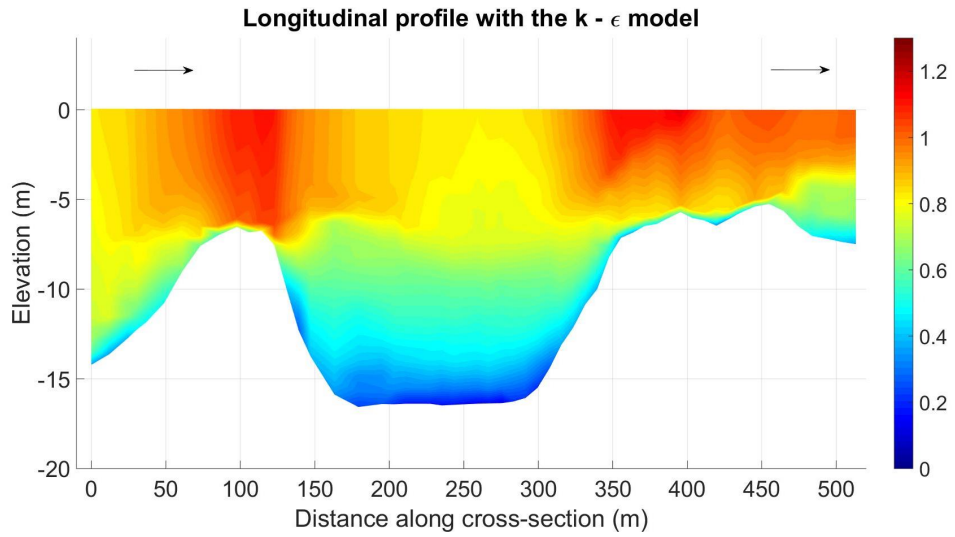


Figure G.13: Longitudinal velocity profile of the Schuddebeursedijk Scour Hole during ebb (m/s).

Shear stress in the Spui and Poortugaal Scour Holes.

Bed shear stress Schuddebeursedijk with constant eddy viscosity (N/m^2)

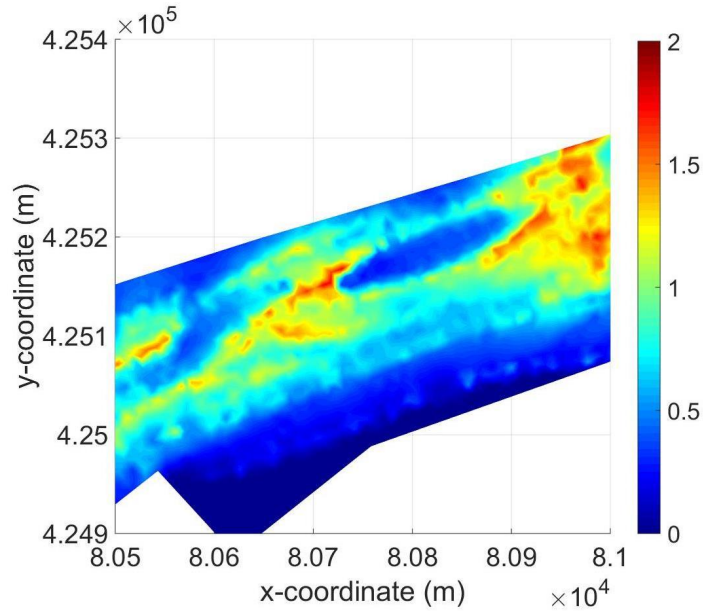


Figure G.14: Cross-section with flow velocities (m/s) along the scour hole during ebb (flow from bottom left to top right).

Bed shear stress Poortugaal Scour Hole with constant eddy viscosity (N/m^2)

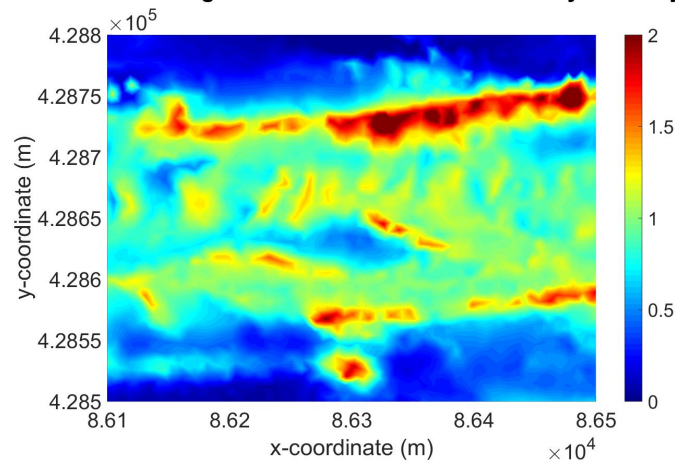


Figure G.15: Cross-section with flow velocities (m/s) along the scour hole during ebb (flow from right to left).

Development of scour in non-cohesive sediments under a poorly erodible top layer

J. A. van Zuylen¹, and C.J. Sloff²

¹ Delft University of Technology, The Netherlands. j.a.vanzuylen@gmail.com

² Deltares and Delft University of Technology, The Netherlands. kees.sloff@deltares.nl

1. Introduction

This study deals with the development of deep scour holes in the river bed of the Dutch Rhine delta in the Netherlands. Assessment of multi-beam surveys, laboratory-flume experiments, and 3D numerical modelling, shows how fast this type of scour holes grows in depth and width. These typical scour holes are found in the tidal deltaic rivers that experience a general incision. This erosion decreases the thickness of the erosion resistant clay/peat layer that is covering and protecting the underlying Holocene and Pleistocene sand (Sloff et al, 2012). Consequently, when this layer breaks, deep scour holes are formed where easily erodible sand is exposed. These scour holes pose risks to the stability of nearby embankments and structures.

Laboratory experiments were designed on basis of the field observations, showing rapid deepening, and only slow growth in horizontal dimension. Subsequently, the findings of the flume experiments were used to study and understand the flow in the scour holes in more detail, using a numerical model, and introducing different flow conditions and calculating the shear stresses.

2. Field observations

Relatively new scour holes have been selected from series of annual multi-beam measurements in the Rhine-Meuse delta in the period 2005-2014. Several of these scour holes have reached depths of about 20 m relative to the original bed, and at some locations where these holes are located in the vicinity of river banks, expensive reinforcements have been implemented to prevent failure of embankments (most critical mechanism for failure is flow slides). The areas protected by these embankments are heavily populated and occupied, and have a very high protection level (up to 1:10,000-year).

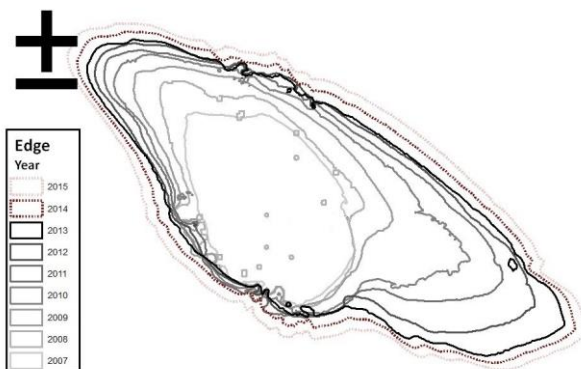


Figure 1: Contours in subsequent years for scour hole in Oude Maas, flow is from bottom right to top left.

Figure 1 shows the contours of a scour hole in the Oude Maas River, based on subsequent annual surveys. The length of the hole is about 200 m, and its depth about 28 m-MSL. The figure shows that the hole is growing 'rapidly' in longitudinal direction (10 to 60 m per year) by crumbling of the clay layer on top, but only slowly in transverse direction. The maximum depth remains more or less constant. Generally these scour holes initially show a rapid deepening, followed by a slow gradual growing in longitudinal and transverse direction with more or less stable depth. The shape of the scour-hole contour is variable, and determined by the strength and thickness of the remaining clay layer around the hole, and by the hydraulic conditions.

3. Laboratory experiments

2DV mobile bed experiments were carried out at the laboratory of Fluid Mechanics of Delft University of Technology to study this scour process. Steel plates with an added roughness were placed on top of a sand bed. The flume width is 0.4 m. A local opening between the steel plates, with varying lengths of 0.1, 0.2, 0.5 and 1.0 m, represented the broken resistant top layer. See Figure 2.



Figure 2: Flume experiment with scour hole. Flow is from right to left

The scour hole initially developed in correspondence with the known theories for scour behind a structure or revetment. However, once the scour hole extended to the edge of the downstream top layer, this layer was undermined. As a result, the sediment was only able to leave the scour hole by transport in suspension. And, although the turbulence within the scour hole was increasing, the rate of scour decreased. With the steel plates remaining at a fixed location, the scour hole approached an equilibrium depth. However, this

extensive undermining of the top layer has never been observed. The erosion of the sediment below the resistant clay layer would lead to failure and crumbling of this layer: block-failure at the edges occurs (blocks of clay can be seen in the multi-beam soundings of these holes). Deformation of the erosion resistant layer may even stabilize the slopes like a falling apron.

Note that due to the 2DV character of the flume experiment, the influence of the shape of the scour hole (planview) could not be investigated. The ellipsoidal shape of the scour hole may lead to attraction of flow from its neighbourhood, and lead to converging flow lines within the hole causing the hole to remain deep.

4. Computational model experiments

It is difficult to identify all relevant phenomena from the small-scale flume experiments. Adaptations of the laboratory experiments to investigate different parameters, geometry, etc. are time consuming and result in high costs. Therefore a 2DV and 3D computational modelling study was made, to see whether the relevant features can be simulated with 3D computational models, and subsequently whether they can be scaled up to prototype conditions. The finite-element solver FINEL3D (Svašek Hydraulics) has been used for these simulations. The results were compared with the experiments.

4.1 2DV model

The results of the laboratory experiments were tested for different turbulence models:

- Constant eddy viscosity
- Bakhmetev mixing length
- k-L model
- k-epsilon model

The simulations have shown large differences in flow velocities along the longitudinal profile. The results of the Bakhmetev and k-L model gave a good indication of the flow velocities. However, the 'simple' constant eddy viscosity model appeared to be more accurate. Furthermore, the k-epsilon model, which is often applied for large river models, was very diffusive and too much dependent on the grid definition. An example of the flow velocity in the scour hole is shown in Figure 3.

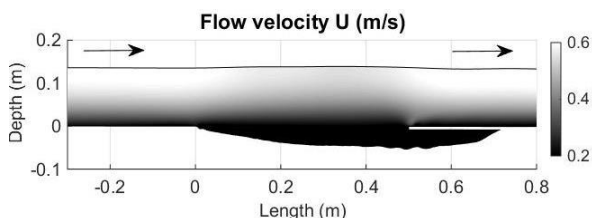


Figure 3: The flow velocity along the longitudinal profile, calculated with a constant eddy viscosity.

One of the problems with verifying these 2DV models was the three-dimensional motion of the flow in the experiments, specifically at the lower edge of the scour hole in the flume (vortex development during undercutting).

4.2 3D model

A next step was made by implementing the obtained results into a 3D model of the Rhine delta branches (prototype scale with realistically shaped scour holes). The model shows a similar distribution of flow velocities at the scour holes as the 2DV flume model. Furthermore, it shows the highest bed shear stresses at the sides of the scour hole, see Figure 4. The scour hole is shown by a lighter ellipse in the centre of the figure. The straight lighter lines were formed by a decrease of cells over the depth, which raised the velocity in the cells.

The high shear stresses at the slopes of the scour hole support the assumption that by deformation of the erosion resistant layer (after undercutting). The shear stresses are higher than the critical shear stress of the sand layer (τ_c 0.30 N/m²), indicating that the slopes of the scour hole are covered and stabilised by this erosion resistant material.

Bed shear stress Berenplaat with constant eddy viscosity (N/m²)

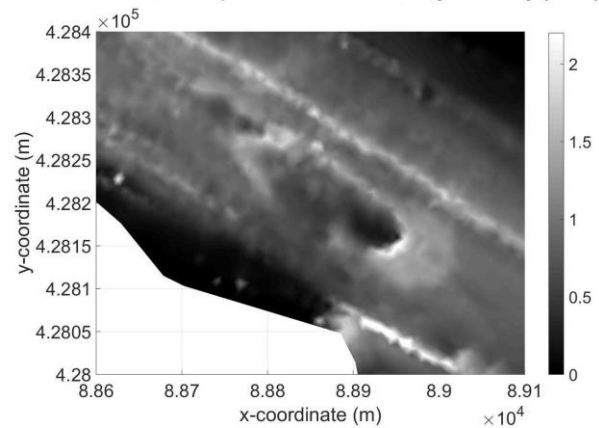


Figure 4: The Shear stresses at the scour hole, the flow is from bottom right to top left.

5. Conclusions

Subsequent surveys in the Dutch Rhine delta show that deep scour holes occur when a clay/peat layer breaks, and underlying sand is exposed. Initially they show rapid deepening (more than 15 m), followed by a growth in plan form. The increase in depth in this stage is rather small.

In flume experiments the erosion resistant layer was represented by a steel plate, which was apparently too stiff to represent reality. The observed undermining at the downstream edge of the scour hole will not occur in the prototype. Undermining apparently causes the erosion resistant layer to deform and function as a falling apron. Furthermore, the failure of the poorly erodible layer by breaking of blocks of clay lead to subsequent growth of the scour hole.

Computations with several turbulence models showed high shear stresses at the edges of the scour hole. This supports the proposition that the material from the crumbling edges is protecting the slopes. Further research to the behaviour of this erosion resistant layer should be carried out to validate the assumed process.

Furthermore, the models show that the complex 2DV and even 3D flow patterns in the scour hole cannot be reproduced easily with classical turbulence models. It is necessary to make more detailed field measurements of flow fields and sediment transport in prototype conditions. Note that the actual conditions in the Rhine-Meuse delta are even more complicated, because of flow reversal due to tidal flows.

Acknowledgments

This research was carried out within the master thesis by Jos van Zuylen and was part of the KPP program of Deltares. Contributions of Prof. Dr. W.S.J. Uijtewaal, Mr. M. van der Wal, Dr. Y. Huisman, Dr. R.J. Labeur, Dr. H. Talstra and Mr. J.R.M. Muller to this project are greatly acknowledged.

References

Sloff, C.J., Van Spijk, A., Stouthamer, E. and Sieben, A. (2012). Understanding and managing the morphology of branches incising into sand-clay deposits in the Dutch Rhine Delta. *International Journal of Sediment Research*, 28 (2013) 127-138.